TUNNEL PILE INTERACTION IN CLAY

RAN XIA

National University of Singapore

2004

TUNNEL PILE INTERACTION IN CLAY

RAN XIA

B. Eng. (Civil Engineering)

A thesis submitted for the degree of

Masters of Engineering

Department of Civil Engineering

National University of Singapore

2004

ACKNOWLEDGEMENTS

It is a great pleasure to thank many people who made this thesis possible.

First and foremost, I would like to express my heartfelt gratitude to my supervisors, Associate Professor Leung Chun Fai and Professor Chow Yean Khow for their continuous guidance and support throughout this project. The encouragement they provided to follow my research project is also greatly appreciated.

I am grateful to Dr G. R. Dasari for sharing his valuable knowledge and time during the group meetings.

For the kindness and patience, I wish to thank the staff of the Geotechincal Centrifuge Lab: Mr. Wong Chew Yuen, Mr. Tan Lye Heng, and Mr. Shen Rui Fu, who lent me their time to talk through my ideas with great benefit to my clarity of mind in centrifuge work.

I am indebted to my many student colleagues for providing a stimulating and fun environment in which to learn and grow. I am especially grateful to Ong Ek Leong, Lee Cheh Hsien, Cheang Wai Lum, Cheng Ch'ng Yih, Zhang xiying, etc. at NUS.

Last but not least, I wish to thank my beloved family and friends for their endless support and caring. I dedicate this thesis to them.

TABLE OF CONTENT

SUMMARY

A centrifuge model study has been conducted to study the effects of tunneling induced soil movements on a single pile in clay. Three test series are performed to evaluate the effects of distance between pile and tunnel, pile length and ground loss on pile responses due to tunnel excavation. The results reveal that both maximum induced pile bending moment and axial force take place at the tunnel spring elevation and around the pile tip for a long pile and a short pile, respectively. In addition, the induced pile movement and deflection continue to increase for some time after the completion of tunnel excavation. It is observed that the maximum induced pile bending moment, head deflection and axial force decrease exponentially with an increasing distance of pile from tunnel, while the pile vertical settlement and base load decrease approximately linearly with an increasing pile-to-tunnel distance.

It is found that the induced pile bending moment, lateral deflection and axial force profiles in clay are similar to those in sand obtained from an earlier study at the National University of Singapore. However, the induced pile responses in clay are observed to be time-dependent whereas the pile responses in sand remain essentially unchanged in the post-excavation period. Moreover, it is noted that the induced pile bending moment and axial force in sand are considerably larger than those in clay under similar pile-to-tunnel distance and ground loss.

A numerical model developed at the National University of Singapore is employed to back analyze the measured pile lateral responses. The model is found to give a fair prediction of the general trend of the induced pile bending moment and lateral deflection profiles. However, the model slightly over-predicts the magnitudes of pile lateral responses which may be attributed to the soil strength reduction due to stress relief caused by tunnel excavation.

The measured pile settlement is back-analyzed using an analytical elastic solution proposed by Poulos and Davis. It is found that for the long and short piles within a ground loss of 4.2%, the pile settlements can be reasonably predicted. However, for the very short pile and long pile in the case of tunnel collapse, the pile settlements are underestimated by the elastic solution due to significant soil plasticity.

Key words: Centrifuge modeling, tunnel, pile, soil movement, bending moment, deflection, axial force, settlement.

LIST OF FIGURES

LIST OF TABLES

LIST OF NOTATIONS AND ABBREVEATIONS

V Tunnel volume loss

i Trough width parameter

S_{max} Maximum ground surface settlement

S Surface settlement,

z_0 Tunnel depth

z Depth below ground surface

x Distance from tunnel centre-line

D Tunnel diameter

S_h Horizontal ground movement

K_0 Ratio of soil horizontal stress versus vertical stress

N Centrifugal gravity

LVDT Linear Vertical Displacement Transducer

PPT Pore Pressure Transducer

C Depth of tunnel cover

EI Bending rigidity of tunnel lining

C_u Undrained soil shear strength at pile base,

A_b Area of pile base

σ'_m Mean effective vertical stress between ground surface and pile tip;

c_m Average soil undrained shear strength along pile;

A_s Pile surface area;

λ Dimensionless coefficient.

K_h Lateral soil stiffness

p_y Limiting soil pressure

E_s Soil stiffness

d Pile diameter.

L Pile length

d_b Pile base diameter

ν_s Soil Poisson's ratio

I_0 Settlement-influence factor

R_k Correction factor for pile compressibility

R_v Correction factor for soil Poisson's ratio

R_h Correction factor for finite depth of layer on a rigid base

CHAPTER ONE

INTRODUCTION

1.1 Background

Scarcity of land and rapid increasing population have led to frequent exploitation of underground space in dense urban areas. Tunnels are often constructed to accommodate the transportation, water supply and drainage systems. As such areas are often heavily occupied by buildings and infrastructures, many tunnels are inevitably constructed underneath or near existing structures. However, large ground movements are usually observed in tunnel excavation in soft ground, even though close face tunneling has been widely employed. It is therefore important to assess the impact of these tunneling-induced ground deformations on structures in close proximity to ensure that the integrity and serviceability of these structures can be maintained.

The effect of tunneling induced ground movements on piles has recently received considerable attention attributing to the fact that tunnel excavation are often carried out close to existing piles in urban environment. Furthermore, some field case studies (Lee et al., 1994, Coutts and Wang, 2000, Tham and Deutscher, 2000) revealed that significant lateral and vertical forces could be induced on piles due to nearby tunnel excavations resulting in failure of the deep foundation.

At present, many research studies have been devoted to examine the tunneling-induced ground movements and many empirical, analytical and numerical prediction methods have been established (e.g. Peck, 1969 and Mair et al, 1993 (empirical methods); Verrujit et al, 1996 and Loganathan et al, 1998 (analytical methods); Rowe et al, 1983

and Gunn, 1993 (numerical methods)). However, relatively few research works associated with tunnel-soil-pile interaction have been published and the understanding regarding this problem is still limited. In practice, it may not be economically viable to conduct large-scale instrumentation and monitoring programs just to study the pile responses due to tunnel excavation. An alternative is to conduct centrifuge model experiments whereby artificial gravitational field is employed to subject the model to stress levels similar to those experienced in the field. Under a well-controlled environment, centrifuge experiments provide the flexibility and repeatability that cannot be achieved in field tests.

In recent years, centrifuge model tests have emerged as a powerful tool to assess tunnel excavation in different types of ground and many major improvements in understanding the tunneling-induced ground behaviour have been obtained using data from centrifuge models (e.g. Mair, 1994 and Taylor, 1997). Subsequent researchers have taken advantage of these modeling methods to evaluate the tunnel-soil-pile interaction problem (e.g. Hegarden et al, 1996, Loganathan et al, 2000 and Jacobsz et al, 2001). The tunnel-to-pile distance and the elevation of the pile tip relatively to the tunnel are found to be the most important factors influencing the pile responses due to a nearby tunnel construction. However, as all the forgoing researchers only focused on one factor in their respective studies and most importantly, their tests were conducted in different soil types, these test results can hardly be compared and some discrepancies are also noted among these studies.

In view of this, Feng (2003) performed centrifuge tests to investigate the pile behaviours subjected to tunneling-induced soil movements in sand at the National University of Singapore (NUS). The experiments covered both the abovementioned

important factors and hence provided a fundamental insight into the pile behaviours due to tunnel excavation in sand.

1.2 Objective of Study

As soft clay is the major soil formation in Singapore and its characteristics are very different from those of sand, the earlier studies on pile behavior due to tunneling-induced soil movements in sand at NUS has been extended to that in clay in the present study. The objectives of the present study are as follows:

a) To investigate and interpret the effects of distance of pile from tunnel, pile length and ground loss on pile responses due to tunnel excavation.

b) To compare the centrifuge test results in clay with previous test results in sand.

c) To back analyse the lateral response of pile using a numerical model developed at NUS and to analyse the measured pile settlement using an analytical solution proposed by Poulos and Davis (1980).

1.3 Organization of Thesis

Chapter 2 presents an overview of the literature relevant to tunnel-soil-pile interaction. This review covers the various tunnel deformation patterns observed in the field, existing prediction methods in tunneling induced ground movements and the usability and limitation associated with each method. Other research studies on tunnel/pile interaction are also reviewed.

Chapter 3 highlights the centrifuge experimental set-up and procedure. Some new instrumentation techniques such as the hydraulic-driven valve for releasing Acetone in-flight are described in detail. The acquisition and processing of images from the tests are also discussed.

Chapter 4 presents the centrifuge test results of the behaviour of a free-headed single pile due to tunnel excavation. Particular emphasis is put on the effects of distance of pile from tunnel, pile length and ground loss on the axial and lateral responses of piles due to tunnel excavation.

Chapter 5 compares the centrifuge test results in clay with those in clay from a previous study in sand. The major similarities and differences in the ground deformation and pile responses due to tunnel excavation are discussed in detail. In addition, the comparisons between the measured test results and theoretical predictions are also presented.

Chapter 6 summarizes the conclusions of findings presented in this thesis along with suggestions for further studies.

CHAPTER TWO

LITERATURE REVIEW

2.1 Introduction

Tunnel construction would cause soil movements that may induce additional axial loads, bending moments and deformations on adjacent pile foundations. If these tunneling-induced pile responses are not taken account in the design, the structural integrity and serviceability of the piles may be compromised. Therefore, it is of great importance to understand the effects of tunneling-induced soil movements on piles. This problem generally involves the studies of deformation of tunnels, induced ground movements and tunnel-soil-pile interaction. Hence, the objective of this chapter covers three aspects:

1. To review the field case studies of deformations of tunnels and briefly examine the causes of various deformation patterns.
2. To examine existing field, laboratory and theoretical studies of tunneling-induced ground movements and briefly assess their usability and applicability under various circumstances.
3. To review the field, laboratory and theoretical studies regarding the pile responses due to an adjacent tunnel construction and extract valuable insight for the present study.

2.2 Deformations of tunnels

As discussed by Verrujit et al. (1996) and Strack et al. (2000), the two basic deformation patterns of a tunnel cavity are in forms of contraction and ovalisation (see Figure 2.1). Contraction is often directly referred to the physical clearance between the excavated tunnel boundaries and linings, whereas ovalisation can be due to uneven soil stresses, tunnel lining deflections, or other reasons such as different support conditions at the crown and sides, or unmatched excavated boundary and lining etc.

2.2.1 Contraction

Contracted deformation is often observed in tunneling operations especially when shield tunneling technique is employed. As concluded by Mair et al. (1997) based on numerous field observations, it is mainly due to:

1. Most boring beads of shield machines overcut the tunnel boundary to accommodate the passage and steering of the shields, which results a void between the periphery of the shield and surrounding soil, see Figure 2.2.

2. Linings are erected inside the edge of shield machines, which leads to a gap between the tailskins of the shields and linings, see Figure 2.2.

Both factors lead to a tendency for the surrounding soil radially moving into the gap between the excavated boundary and lining, see Figure 2.3.

2.2.2 Ovalisation

Ovalisation of a tunnel is not as often observed as contracted deformation in tunneling practice. However, some field cases of ovalisation have been reported by various authors.

George (1981) reported a field case where significant lining ovalisation (Figure 2.4) was induced because of poor ground water condition and laggard grouting. It is noted that, despite the tunnel was shallow (4.5 m below the ground surface), the impact of the contact force between the soil and lining was very large that it forced the liner plate down at the crown nearly 0.5 m and to extrude out at the spring line, forming an ellipse.

Leblais et al., (1991) presented three scenarios in the Villejust tunnel project where oval displacements of the tunnel could be induced:

1. The tunnel rings do not fit in the excavated tunnel boundary precisely because of the construction void between the shield sleeve and gravity effect. Figure 2.5 shows an example for a theoretical diameter of the tunnel ring of Ø, the real horizontal axis is Ø+30mm long and the vertical one is Ø-22 mm, resulting in an oval ring shape.

2. Deformations of the established tunnel rings induced by the thrust of the shield through the jacks which are applied between the shield and rings to push the cutter forward during boring. However, such oval deformations are normally very small.

3. Soil/lining interaction after the shield has passed, see Table 2.1.

Leblais et al., et al. (1991) observed that for the four lining rings in a particular case study, the initial ovalisation is horizontal and very pronounced for ring C. The ovalisation increases with time for rings A and D but decreases for rings B and C.

Table 2.1 Lining ring deformation (Leblais et al., 1991)

Section	A	B	C	D
Short term				
horizontally (mm)	+0,4	-	+15,8	+0,3
vertically (mm)	-0,9	-	-29,4	-1,5
Long term				
horizontally (mm)	+2,3	-4,5	+ 7,8	+3,8
vertically (mm)	-5,3	+4,5	-26,4	-6,2
Stabilization delay (day)	180	>500	80	>500

Vertical lining ovalisation was also reported by Lee (2002) in the London Dockland light railway Lewissham extension twin tunneling project. Two distinguished patterns of lining ovalisation were observed (similar patterns were also reported by Doran et al. 2000, see Figure 2.6). The lining rings were first found "squatted" vertically (i.e. the vertical diameter shortens and the horizontal diameter elongates) during the grouting episode and finally "squeezed" horizontally due to the overconsolidated nature of London clay where the horizontal stress is higher than the vertical stress.

In addition, the failure and deformation patterns of poly-material linings are illustrated in Figure 2.7 extracted from the handbook of Plastic Pipe Institute (2003). It can be seen that the buckling or collapse of the ring exhibits somewhat a 'heart' shape and the ring deformation under service load shows a horizontal-oval shape.

It is evident from the above reviews that both contraction and ovalisation tunnel deformation patterns can occur in the field. Contracted deformation is mainly due to overexcavation of tunnels whilst oval deformation is largely attributed to the tunnel lining deformation. Although tunnel ovalisation is less commonly observed in tunnel excavation than contracted deformation, it can be very significant as reported by George (1981) and Leblais et al. (1991). Furthermore, as a matter of fact, large deformations experienced by some lining tunnel rings are often encountered in tunneling projects, if not all, despite all tunnel linings are supposed to be sufficiently rigid. As the two deformation patterns may cause different ground movements, it is important to study the effects of both tunnel contraction and ovalisation on the ground.

2.3 Tunneling-induced soil movements

2.3.1 Field studies

For the case of a single tunnel excavation in "green field" conditions, Peck (1969) and subsequently many other researchers have shown that the transverse settlement trough in the field immediately following tunnel construction can be well-described by a Gaussian distribution curve (Figure 2.8). The method needs an estimate of volume loss (V) and the trough width parameter (i) to obtain the maximum ground surface settlement (S_{max}) and subsequently the surface settlement profile. Settlements are generally negligible beyond an offset of $3i$ from the tunnel centerline for Peck's proposed curve. The surface settlement, S, and volume loss, V, is approximated by the following equations:

$$S = S_{\max} \exp\left(-\frac{x^2}{2i^2}\right) \tag{2.1}$$

$$V = \sqrt{2\pi} i S_{\max} \tag{2.2}$$

where x is the offset to the tunnel vertical centre-line.

Peck (1969) suggested a relationship between the parameter i, tunnel depth Z_0 and tunnel diameter D that depends on the soil conditions. O'Reilly et al. (1982) showed that i is an approximately linear function of Z_0, and is broadly independent of tunnel construction methods and of D (except for very shallow tunnels with C/D ratio less than one, C is the depth of tunnel cover). A simple approximate relationship can be obtained as:

$$i = Kz_o \tag{2.3}$$

where K=0.4 to 0.6 for clays and K=0.25 to 0.45 for sands and gravels (after Rankin, 1988)

Lake et al. (1992) presented measured data of i in clays and sands shown in Figures 2.9 and 2.10, respectively.

Subsurface settlement profiles can also be approximated by a Gaussian distribution curve in the same way as surface settlements. Based on measured data from many field studies (Figure 2.11), Mair et al. (1993) proposed that at a depth *z* below the ground surface, above a tunnel depth of Z_0, the trough width parameter i for tunnels constructed in clays can be expressed as

$$i = K(z_o - z) \tag{2.4}$$

$$\text{where } K = \frac{0.175 + 0.325\left(1 - z/z_o\right)}{\left(1 - z/z_o\right)} \tag{2.5}$$

Similar patterns of increase in *K* values was observed in studies by Moh et al. (1996) and Dyer et al. (1996) irrespective of the soil conditions encountered. Centrifuge model studies by Grant et al. (2000) show that the proposed variation of *K* with depth for clays by Mair et al. (1993) provide a good fit to their centrifuge test data obtained from tests as shown in Figure 2.12.

Horizontal movements S_h can be predicted by assuming a particular focus point along the tunnel vertical centre line. Attewell (1978) and O'Reilly et al. (1982) proposed a convergence point at the tunnel centre for tunnels in clays while Taylor (1995) demonstrated that for constant volume conditions, the application of Equation 2.4 to represent the variation of K with depth would yield a convergence point $\frac{0.175}{0.325} z_o$ below the tunnel axis level.

For the case of convergence point at tunnel centre

$$S_h = \frac{x}{z_o} S_v$$

$$S_h = 1.65 S_{h\max} \frac{x}{i} \exp\left(-\frac{x^2}{2i^2}\right) \tag{2.6}$$

For the case of convergence point at $\frac{0.175}{0.325} z_o$ below the tunnel axis level

$$S_h = 0.65 \frac{x}{z_o} S_v$$

$$S_h = 1.07 S_{h\max} \frac{x}{i} \exp\left(-\frac{x^2}{2i^2}\right) \tag{2.7}$$

As far as the Author is aware, there are no reported field cases regarding the difference between the soil settlements induced by contracted and oval deformations of tunnels. This suggests that the soil settlements induced by both tunnel deformation patterns may be approximately depicted by Gaussian curves. However, as will be revealed in the theoretical studies section, the surface settlement troughs due to the two distinct tunnel deformations can be dissimilar should serious tunnel ovalisation occurs.

Long-term ground movement can be significant especially in the case of tunneling in soft compressible clays. A comprehensive review of field data of post-construction settlements above tunnels in soft clays by Shirlaw (1995) concluded that the increase in settlement over the long term is typically of the order of 30-90% of the total settlement, and that in many cases a widened settlement trough develops.

The long-term ground surface settlement troughs for tunnels in soft clay can be classified into two distinct patterns, as shown in Figure 2.13 (Shirlaw, 1995). Mair et al. (1997) concluded that the long-term settlement troughs are similar to the classical Gaussian curve associated with short-term settlement when positive excess pore pressures are generated during tunnel excavation such as the overpressurizing of tunnel faces; whereas wider post-construction settlements are related with tunnel lining acting as drain and the development of steady state seepage towards the tunnel.

Analyses of measured field pore pressures induced around tunnels in clays where there is unloading (e.g. Clough et al. 1981; Schmidt 1989; Mair et al. 1993) show that the distribution and magnitude of the excess pore pressures depend on the degree of

unloading and the strength and stress history of the clay. In overcosolidated clays, the excess pore pressures are generally always negative when ground unloading occurs. However, in normally consolidated clays, significant zones of positive excess pore pressures can be induced even for a tunnel where unloading takes place, as reported by Schimdt (1989).

2.3.2 Laboratory studies

The development of laboratory modeling especially geotechnical centrifuge modeling has offered great advantages of well-controlled soil condition and extensive data monitoring in the study of tunneling. Significant improvements in tunnel modeling methods have been made. These enabled an in-depth understanding into the mechanism of ground responses associated with tunnel construction in terms of surface and subsurface soil movements, as well as soil stresses. Some widely used simulation methods and major findings in case of both contracted and oval tunnel deformations are discussed in this section.

Grant et al. (2000) carried out a series of centrifuge tests to investigate tunneling-induced ground movements in clay. The tunneling simulation method in their studies was proposed by Potts (1976), where the radial tunnel deformation is achieved by reducing the compressed air pressure in a model tunnel lined with a latex membrane, see Figure 2.14. Using this method, they have successfully evaluated that Equation 2.4 proposed by Mair (1993) is appropriate.

Kuwano et al. (1998) also used the same simulation method in the centrifuge to examine soil nailing in tunneling in clay. It is observed that soil nails installed in the

region of 30° to 60° extending from tunnel spring line are the most effective in stabilizing the ground and reducing the surface settlement (Figure 2.15). This is coincident with the vector map of the minor principal strains of the ground, where the concentration area of the large strains are primarily in the region of 30° and 60° from the tunnel spring horizontal. Kuwano et al. (1998) concluded that this phenomenon is largely due to the soil above the tunnel moving to the tunnel cavity as a block and the region of 30° and 60° behaves like shear zones as predicted in the numerical analysis by Grant (2000), see Figure 2.16.

Alternative methods using liquid pressure using the same principle as the air pressure tunnel were adopted by subsequent researchers, of which the latest and most sophisticated model was proposed by Loganathan (2000). The tunnel excavation was simulated by pumping certain amount of silicon oil out of a model tunnel in-flight to impose desired ground losses. Figure 2.17 shows the cross-section of the model tunnel. The advantage of this method lies in the control of the tunneling process and the convenience of imposing various volume losses. Using this method, Loganathan compared the ground settlement troughs with his analytical prediction (Loganathan et al. 1998, see Figure 2.18) and investigated the tunneling-induced pile behaviours (to be reviewed in Section 2.4.2).

An in-flight shield model machine was developed by Yasuhiro et al. (1998) to study the tunneling-induced ground movement in both sand and clay. The shield model machine consists of steel rings and a wedge shaped shaft, which are able to simulate the tail void and backfill grouting in-flight by contraction and expansion of the shield model rings controlled by a motor, see Figure 2.19. Figure 2.20 shows the measured surface and subsurface soil movements in their tests. From subsequent analysis of the

shear strain, Yasuhiro et al. (1998) concluded that the maximum shear strain extents from the side wall of the tunnel to the upper layer of the ground with a value of over 10% in both sandy and clay grounds, see Figure 2.21. It is interesting to note that the large shear strains in his study were also concentrated in the region described by Kuwano et al. (1998).

Hegarden et al. (1996) developed a tunnel simulation method at the Delft Geotechnics centrifuge. The tunnel excavation was simulated by a customized instrument that is able to vary in diameter. Tests were carried out to examine tunneling induced ground movements on end-bearing piles at 40g. Detailed test results will be reviewed in Section 2.4.2.

Sharma et al. (2001) developed a different approach to simulate tunnel excavation in the centrifuge. This technique is based on polystyrene foam being dissolved quickly by an organic solvent. The polystyrene foam core was placed tightly inside the model tunnel lining, which was made by wrapping a brass foil around the foam core and soldering the lap joint with the help of tin solder and an electronic gun (Figure 2.22). The flow of this liquid into the polystyrene foam to simulate tunnel excavation is controlled by using solenoid manifold and solvent reservoir. The stiffness of the filled tunnel can approximately be made to simulate the parent soil. The stiffness of the lining is correctly left in place when the foam core has been dissolved. As the brass foil lining is 'ready-in-place' before the tunnel excavation, the tunnel deformation essentially comes from the lining deflection. Therefore, this method actually aims to simulate a tailless tunneling method or a NATM construction procedure. Moreover, it may well-serve as a means to study the ground stability associated with lining stiffness as well as ground movement due to lining deflection. Another advantage of this

technique is that three-dimensional tunnel construction can be modeled by dissolving the foam in the model tunnel segmentally. Figure 2.23 shows the propagation of settlement trough in the longitudinal direction.

Atkinson et al. (1975) reported a laboratory study on the behaviour of a lined tunnel in clay. The tunnel lining was made of aluminum and supported by internal air pressure. Tunneling process was simulated by decreasing the tunnel pressure and increasing the surface pressure of the clay. Both lining behavior under collapse and small deflections were studied. Figure 2.24 shows the collapse of the lined tunnel and Figure 2.25 shows the soil displacements when lining was under small deflection. The displacements of the soil around the tunnel indicated that the invert remained almost stationary while the tunnel crown descended and the springs separated during tunneling. In addition, comparison of the mean hoop thrust with the stress difference integrated over the horizontal area shows that approximately 90 per cent of the vertical loads are taken by the lining and the remainder to the surrounding soil, reflecting a very limited soil arching effect.

Kongpathomporn (2002) reported a series of centrifuge test results of a flexible lining behaviour in clay. The flexible lining was simulated using an aluminum hollow tube with 60 mm diameter and 0.65 mm thickness. Figure 2.26 shows the configuration of the tunnel model and test set-up. Figure 2.27 shows the distribution of the induced lining bending moment and ground surface settlement. Although lining deformation was not directly measured in these tests, the distribution of the lining bending moment suggests that the tunnel would deform into an oval shape. Moreover, it is also noted that the lining deformation and ground movement continue to increase with time.

It is noted from Figure 2.20 and 2.25 that the lateral soil movements are markedly different in the contracted and oval tunnel deformations. Soil moves horizontally towards the tunnel in case of contracted deformation, while the lateral soil movements are away from the tunnel side as a consequence of ovalisation effect. Therefore, it should be noted that the soil movements induced by the two deformation patterns could have different impacts on adjacent structures.

2.3.3 Theoretical studies

Loganathan et al. (1998) presented a quasi-analytical method to predict tunneling induced ground movements. Although the method has been successfully used to back analyze some case histories in clay, calculated results have to be treated with caution as the method consistently yields smaller settlement trough volumes than the prescribed input tunnel face loss, which does not satisfy volumetric constancy for undrained conditions. This is due to the assumed empirical distribution of ground loss with horizontal and vertical distance $\epsilon_{x,z}$ from tunnel center as given below:

$$\varepsilon_{x,z} = \varepsilon_0 \exp\left\{\left[\frac{1.38x^2}{(H+R)^2} + \frac{0.69z^2}{H^2}\right]\right\} \tag{2.8}$$

where ϵ_0 is the ground loss ratio, H is the tunnel depth, z is the depth below ground surface and x is the lateral distance from tunnel centre-line.

The assumed ground loss distribution as shown in Equation 2.8 attempts to indirectly model the effect of nonuniform soil convergence around a deforming tunnel shown in Figure 2.28.

Verrujit et al. (1996) developed an analytical solution to account for the ground loss and ovalisation of an excavated tunnel boundary in an elastic half plane, see Figure 2.1. Two cases with K_0 =1 and 0 were studiesd respectively, see Figure 2.29. The results reveal that a narrower trough width would be caused by the significant ovalisation effect due to the zero K_0 condition. However, the zero K_0 condition is very unlikely to occur in reality as most soils have horizontal stresses. On the contrary, Verrujit et al. (1998) presented the comparison between the ovalisation-induced surface settlement troughs and Gaussian curves (Figure 2.30). The results yield nearly identical trough shapes and widths in the two cases even when relatively large ovalisation factors are used. Furthermore, Verrujit et al. (1998) reported a case study (Figure 2.31) where a large ovalisation parameter was incorporated with ground loss parameters. The computed results show fairly good agreements with both measured surface settlement trough and the empirical formula by Peck (1969). Although the stresses accommodating the ovalisation of a shallow tunnel without lining may not be realistic as pointed out by Strack et al. (2000), the soil deformation profile of the tunnel ovalisation in this approach provided a good indicator for future studies.

Rowe et al. (1983) proposed the 'gap' parameter to depict the ground deflections that should be prescribed in a 2-D FE analysis prior to installing the lining, as illustrated in Figure 2.32. The gap represents the physical clearance between the tailskin of the shield and the lining plus an allowance for the out-of-plane (3-D) ground movements, together with an allowance for workmanship. Lee et al. (1992) used 3-D elastoplastic FE analysis to develop a means of quantifying the gap parameter for use in 2D. However, although this method shows a reasonable prediction of field observation in the closed face tunneling when the gap parameter is simply the physical clearance

between the outer skin of the shield and lining, it should be used with caution in open face tunneling where stress relief occurs.

Gunn (1993) found that isotropic non-linear elastic perfectly plastic 'small-strain' stiffness soil models (Simpson, 1979; Jardine et al., 1986) improved the 2-D FE predictions for tunnels in heavily overconsolidated London clay as compared with linear elastic-perfectly plastic models, but even these predicted wider settlement troughs than those observed in practice. In contrast, Simpson et al. (1996) reported 2-D FE predictions for a tunnel in London clay showing the shape of the settlement trough to be little influenced by non-linearity but substantially influenced by shear modulus anisotropy. Subsequent the results of the bender element tests on undisturbed London clay samples and in-situ shear wave tests supported the above findings.

Although attractive as predictive methods, significant limitations of theoretical analysis associated with tunneling still prevail. The well-known problems with these analysis are: (1) They tend to predict higher displacements than field observations, even with 'correct' material models and 'appropriate' parameters. (2) They tend to predict higher far-field surface settlements. Clough et al. (1989) and Chen (2002) acknowledged that both sophisticated soil models and improved simulation methods are required to achieve realistic predictions of tunneling-induced ground movements. However, the tunnel construction process is extremely complex, particularly if shield tunneling is involved and tunneling modeling represents a great challenge in geotechnical analyses.

2.4 Tunnel-soil-pile interaction

2.4.1 Field studies

Lee et al. (1994) reported the field data obtained from a tunnel constructed beneath a seven-story building supported by pile foundation in London. The piles were sleeved with slip coating and taken through 28-m of London clay to found in the underlying Woolwich and Reading Beds. The tunnel was excavated using hand tools in two stages; a pilot tunnel of 4.5 m diameter and a subsequent enlargement to a maximum diameter of 8.25 m. The center line of the nearest piles was only 1.6 m from the tunnel periphery. Figure 2.33 shows the configuration of the site condition. The data suggested that the ground loss was approximately 1.5% for the pilot tunnel and an additional 0.5% for the tunnel enlargement (Mair, 1993). Inclinometers were installed in piles and various locations of the soil to measure the pile lateral deflection and soil movements respectively. Figure 2.34 shows the measured horizontal ground movement and pile lateral deflection. From the comparison of the profiles of inclinometers in the ground and in piles, it was concluded that the piles acted as slender members and generally deformed in the same manner as the surrounding soil. It was also found that the settlement of building supported by the piles since the commencement of tunneling was very small, typically only 1 mm or 2 mm. The maximum settlement recorded was 5 mm.

Teunissen et al. (1998) reported the results of a pile test project during the construction of a large diameter bored tunnel in Netherlands. In the full scale test, a total of 36 timber piles, 18 concrete piles, 156 surface settlement points, 29 subsurface points were continuously monitored. The monitoring process covered the entire testing period

of 2 years. To determine the effects of tunneling on piles, three different and independent monitoring principles were used, namely:

1. Pile, surface and subsurface settlement,
2. Static pile ultimate bearing tests,
3. Soil investigation.

Particular attention was paid to the pile settlements and their relationships to soil movements. Figure 2.35 shows the variation of pile settlement versus time. The pile settlement versus surface and subsurface settlement are illustrated in Figure 2.36.

Based on the field data, the following conclusions were drawn:

1. The piles founded above and close to the tunnel have a vertical displacement slightly more than the measured ground settlement. The piles founded under and beside the horizontal tunnel axis show smaller vertical displacement than at the ground level.
2. Stress relief due to tunneling is almost negligible.
3. Long-term pile settlements are about 15% of the total pile settlements.

Coutts and Wang (2000) instrumented 1200-mm diameter bored piles supporting a vehicle viaduct to measure the pile responses when the tunnel boring machine (TBM) approached or moved away from the instrumented piles. The piles for the viaduct were already constructed before the start of the tunneling process. The location of the instruments is shown in Figure 2.37. Anticipating that ground deformation surrounding the tunnel would occur, the bored piles were heavily reinforced to increase their bending moment and tension capacities. Typical reinforcement consisted of 20 T25

longitudinal bars with T16 link at 175 mm centers. Reinforcement was used over the top 20 to 30 m of the piles. The tunnels with an excavated diameter of 6.4 m closely follow the alignment of the viaducts on opposing sides. Tunnel boring proceeded within a close distance of $0.855D_t$ (tunnel to pile center) to the pile at an average axis depth of 20 m. Field data revealed that maximum forces and stresses were recorded when the TBM was directly adjacent to the piles as well as maximum bending moments were recorded at invert and crown levels. The test results revealed that significant bending moments (59% of design working moment) and axial forces (91% of design working load) were induced in the piles for moderate volume losses of 1 to 2%. This could be due to the stiff weathered granite soil encountered at the site.

Published field case histories of tunnel-soil-pile interaction are sparse as it is difficult to predict when such a situation may arise unless prior planning and arrangements are made to instrument the pile. Moreover, nearly all existing field cases are limited in several aspects of measurements, which may be due to either the deficiency of instrumentation planning or the difficulty of collecting field data. Thus, laboratory testing especially centrifuge tests were employed as an alternative method to study the tunnel-soil-pile interaction problem.

2.4.2 Laboratory studies

Morton et al. (1979) carried out laboratory tests to study the effects of tunneling induced ground movements on piled foundations. The tests were carried out in a mixture of coarse silt and sand under 1g thus neglecting the effects of confining stress on pile behaviour. Constant load was maintained on the piles during the tunneling process. It was concluded that a critical, triangular boundary exists (Figure 2.38)

within which pile would experience high settlements. It was also observed that short piles embedded entirely within the large settlement zone could be greatly affected. Furthermore, the settlement of friction piles is controlled mostly by the ground deformation that is induced at or close to the pile tip location by the tunneling operation and the prime factor to induce geotechnical failure of piles is dilatancy of the sandy soil near the pile tips. Although limited in scope and information regarding the magnitude of induced forces on the piles, the tests provided useful insight into the settlement behaviour of piles with tip levels above the tunnel crown level.

Hegarden et al. (1996) carried out centrifuge tests on the Delft Geotechnics centrifuge to study the effects of tunneling induced ground movement on end-bearing piles. Tests were carried out with clay overlaying sand at 40g. The model tunnel had a prototype diameter of 7 m and the setup can impose volume losses ranging 0 to 10%. The model piles were installed using loading frame in-flight and loaded up to 70% of the ultimate bearing capacity. The test results showed that the decompression of the sand layer caused by tunneling has a significant influence on the settlement and bearing capacity of adjacent end bearing piles. Moreover, parametric study of tunnel/pile distance showed piles at a distance of 2 tunnel diameters from the edge of the tunnel are unaffected. At distance in the range 0.25 to 1 time tunnel diameter, the pile settlements varied in proportion to the volume loss, and closer than 0.25 times tunnel diameter, severe pile settlement occurs. These effects, together with the reduction in pile resistance, are illustrated by Figure 2.39 derived from similar tests by Bezuijen et al. (1994). From the parametric study of the pile tip location below, at and above tunnel spring line, it was found that the pile settlement was the largest when the tunnel spring was at the pile tip level and the pile settlement was the smallest when the tunnel spring was above the pile tip level. They also pointed out there were three stages of

development of pile skin friction. When the pile tip was above tunnel spring level, negative skin friction was induced on the pile in small volume losses (less than 1%). Positive skin friction was mobilized along the pile shaft when the volume loss ranged from 1% to 6% due to the large increasing displacement of the pile tip and skin friction changed its sign to negative again when the volume loss reached around 10%.

Loganathan et al. (2000) reported the first centrifuge model study on both induced pile bending moments and axial forces due to tunnel excavation in overconslolidated clay**.** The scope of the study was focused on friction piles (single pile and a 2x2 pile group). The effects of pile tip level relative to tunnel axis level and volume loss on the displacements and performance of piles were investigated to gain valuable insight into the interaction problem. The relative position of the piles in various tests is shown in Figure 2.40. Three tests were performed with tunnel located above, at and below the pie tip level. The induced bending moment and axial force profiles at a volume loss of 1% are presented in Figures 2.41 and 2.42 respectively. It is observed that both the induced maximum bending moment and axial force occurred at approximately at the tunnel spring level in a long pile case where the pile tip below the tunnel spring line. The maximum bending moments occurred just above the pile tips and axial force increased from the pile heads to the pile tips in a short pile case with pile tip at or above the tunnel spring level. The comparison of the three tests showed that for single piles, the maximum bending moment was the largest when the pile tip was located at the tunnel spring elevation, whilst the maximum axial force was the largest when the pile tip was above the tunnel spring line. Comparisons of pile deflection and soil lateral soil movement are illustrated in Figure 2.43. It can be seen that the magnitude of pile lateral deflection is very similar to the soil lateral movement at the same offset. This

shows that the piles apparently behaved as a flexible member and deformed with soil. Table 2.2 displays the pile head settlements and deflections in the three tests.

Table 2.2 Measured pile displacements in centrifuge tests (Loganathan et al. 2000)

Test No.	Settlement: mm		Lateral deflection: mm	
	Single pile	Pile group	Single pile	Pile group
1	10·5	6·6	2·0	3·7
2	11·8	12·2	4·4	5.7
3	11·6	7·6	6·4	5·3

It can be seen that the largest pile settlement occurred when the pile tip was at the tunnel spring elevation and the largest pile head deflection occurred when the tunnel was below the pile tip. Figure 2.44 shows the tunneling-induced maximum bending moments for varying ground loss values. It was concluded that the maximum measured bending moments vary almost linearly with ground loss values below 5%. As such, it was postulated that an elastic analysis may be performed to predict tunneling-induced pile behaviour if the ground loss value was less than 5%.

Jacobsz et al. (2001) presented centrifuge test data on the effects of tunneling in dry sand, focusing on the axial response and vertical pile head settlement of single piles. The experiment was performed at a *C/D* ratio of 4.25 with a *D* of 4.5m in 75g. The results showed that a triangular zone can be formulated (Figure 2.45) due to the deforming tunnel which could induce large pile settlements should a pile tip be located within this zone and subjected to volume losses exceeding 1.5%. This zone was further sub-divided according to the amount of settlement that the piles underwent at 1.5% volume loss compared to the surface settlement. A pile with its tip located in zone D, settled less than the ground surface. A pile with its tip located in zone B settled more

than the surface. In zones A and C, the pile and surface settlements were very similar. Table 2.3 shows the pile settlement versus surface settlement in the four zones.

Table 2.3 Pile settlement versus surface settlement (after Jacobsz et al. 2001)

Pile no	Settlement (mm at prototype scale)	
	Pile	Surface
1 (Zone A)	15	16.5
2(Zone B)	38.6	13.5
3(Zone C)	9.4	8.3
4(Zone D)	2.0	6.6

It is noted that the pile settlement in Zone B is nearly 2.5 times the pile settlement in Zone A although the surface settlement in Zone A is larger than that in Zone B. This implies that the pile at Zone B is much more critical than the pile in Zone A in terms of settlement.

However, the test data revealed that for piles located in the large deformation zone, the skin friction was constantly positive up to a volume loss of 10%. They attributed this to the rapid reduction of the pile base resistance due to the sand dilation near the pile base during tunneling.

Feng (2003) performed a series of centrifuge tests to investigate the pile responses associated with a lined tunnel in dry sand at NUS. The simulation method of tunnel excavation proposed by Sharma et al. (2001) was adopted in the tests. Figure 2.46 shows a typical configuration of the tests. Two major series of tests were reported regarding the effects of stiffness of tunnel lining and pile-to-tunnel distance, as well as

on the effects of pile length. The test results will be compared in Chapter 5 with the present study in clay.

Various experimental studies regarding tunnel-soil-pile interaction have been performed to provide a better understanding of pile responses due to the contracted tunnel deformation. However, no research works regarding the pile behaviours associated with the tunnel ovalisation exist in published literatures as far as the Author is aware. As the lateral soil movements in the two deformation patterns are markedly different, the pile responses are expected to be different as well. Therefore, it remains of interests to study the pile responses due to tunnel ovalisation. Besides, two effects associated with pile-to-tunnel distance and pile tip locations relative to tunnel have been addressed by earlier researchers as the most prominent factors influencing pile behaviours due to adjacent tunneling. Thus, these two factors will be examined in the present study.

2.4.3 Theoretical studies

Chen et al. (1999) presented a simple approach to assess tunneling induced pile responses where a two-stage uncoupled method was introduced. In the proposed method, greenfield tunneling induced ground movements at the pile location is first approximated based on the quasi-analytical method proposed by Loganathan et al (1998), subsequently applying the movements on soil elements surrounding the pile using separate numerical programs (PALLAS and PIES) to assess the lateral and vertical pile responses. The approach started with a basic problem as illustrated in Figure 2.47 where an existing single pile is situated adjacent to a tunnel under construction. The induced pile responses together with the greenfield soil movement of

the basic problem are shown in Figure 2.48. Subsequent parametric studies provided valuable insight into the various factors affecting pile performance, in particular the variation of maximum induced bending moment and axial force with pile-to-tunnel distance and relative position of pile tip to tunnel axis level. In general, the maximum bending moment and axial force values decrease to insignificant magnitudes (less than 10% of value at X=1D) beyond a respective distance of 2D and 5D from the tunnel centerline. At a given horizontal offset from the tunnel centerline, the pile bending moment is generally the greatest when its tip is below the tunnel axis level, decreasing as the pile tip moves upwards. However, pile horizontal deflection profiles are almost identical in shape and magnitude to the free field soil displacements as shown in Figure 2.49. This is probably due to the flexible lateral rigidity of the pile and the homogenous clay profile with constant C_u and Young's modulus along depth used in the analysis.

In their 3D FE studies, Mroueh and Shahrour (1999) attempted to simulate a sequential shield tunneling process while studying the induced effects on piled foundations. Although three-dimensional heading effects are accounted for in this analysis with the inclusion of lining elements, the Convergence-Confinement method (Panet et al., 1982) was used to control the soil convergence around the tunnel. The soil elements were modeled as linear elastic with Mohr-Coulomb failure criterion while the pile elements are linear elastic with no provision for interface slip between the soil and pile. Computed results from the simulation show pile response to vary realistically with advancement of tunnel face as shown in Figures 2.50 and at the creation of tail void as shown in Figure 2.51. Moreover, the effects of pile tip location relative to tunnel have also been investigated, which is also revealed in Figure 2.51. The term x_p/L_p represents the length along the analysed pile normalized by total pile length.

Free-field displacements are movements of the soil that occur at a distance from the pile such that the displacements are not affected by the presence of the pile. A free-field soil displacement method, in which a pile was represented by beam elements and the soil was idealized using the modulus of subgrade reaction, was proposed by Chow and Yong (1996). The magnitude of soil movement profile serves as input to the method. With this idealization, non-homogeneous soil can be easily treated. This approach requires the knowledge of the pile bending stiffness, distribution of lateral soil stiffness and the correct limiting soil pressure acting on the pile with depth. Comparisons with available well-documented case histories suggest that the method gives reasonable prediction of the general behaviour of pile foundation subjected lateral soil movements.

It is noted that numerical methods still encounter difficulties of realistic prediction of surface settlement and hence the subsurface soil movements. Their usability in tunnel-soil-pile interaction is limited as pile responses may be predicted under inaccurate soil displacement profiles. On the other hand, the free-field displacements based numerical methods seem to be a promising alternative as they incorporate the 'correct' soil movement profiles either from analytical solution or experimental observations with powerful numerical programs to obtain a more realistic prediction of pile behaviours such as those proposed by Chen et al (1999) and Chow and Yong (1996).

2.5 Summary

Two distinct tunnel deformation patterns in the form of contraction and ovalisation are observed in the field. The review of the induced ground movements due to the two deformation patterns reveals that the soil settlements in both cases can be

approximately depicted by Gaussian curves, whereas the lateral soil movements basically have opposite directions. Further examination of the research methods shows that empirical methods are limited to greenfield conditions and hence unable to account for tunnel-soil-pile interaction. Analytical and FE methods still face the deficiencies of soil models and simulation methods in predicting accurate tunneling-induced soil movement. Therefore, centrifuge methods are deemed to be an alternative attractive to understand the tunnel-soil-pile interaction mechanisms and provide preliminary assessment of loads and deformations induced on adjacent piles due to tunneling.

Various methods have been developed by researchers to study the tunneling-induced soil movements as well as their impacts on adjacent pile foundations in the centrifuge. However, little attention has been paid to the pile responses in case of tunnel ovalisation. As the soil movements induced by the two deformation patterns are different, it is important to study the pile behaviours subjected to adjacent tunnel ovalisation.

In addition, the earlier test results pointed out that the pile-to-tunnel distance and the relative pile tip locations to tunnel play the most important roles in characterizing pile responses associated with tunnel construction. Moreover, a large pile settlement zone was also identified for piles whose tips are above the tunnel spring level. However, centrifuge tests have not been conducted to give a comprehensive view of all the above factors in a single type of ground. Therefore, some test results and interpretations seem to be inconsistent probably due to different types of soil used in the tests. As such, centrifuge tests regarding these factors were performed in the present study to gain a better understanding of the behaviour of piles influenced by tunneling excavation.

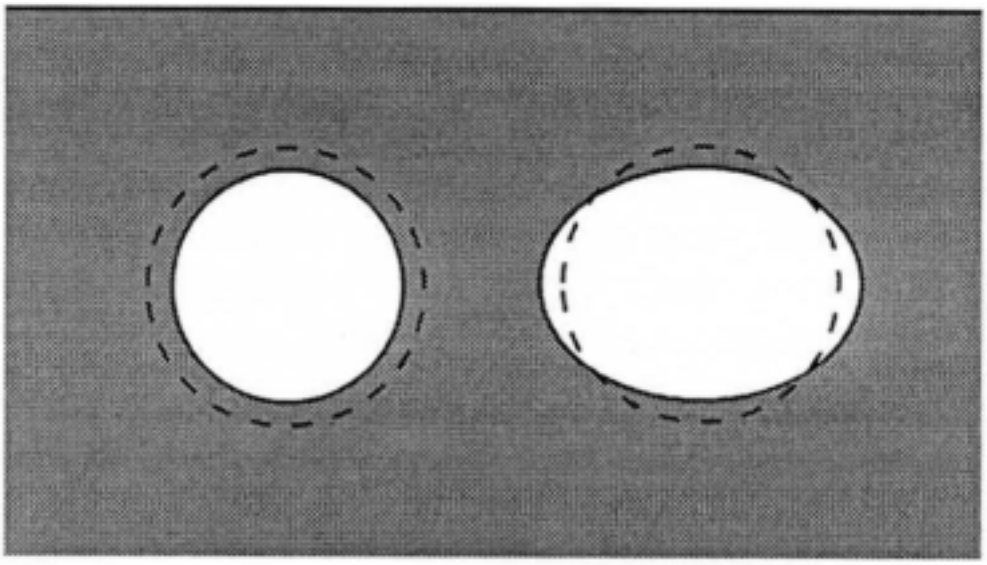

Figure 2.1 Contraction and ovalisation of a tunnel (Verrujit et al. 1996)

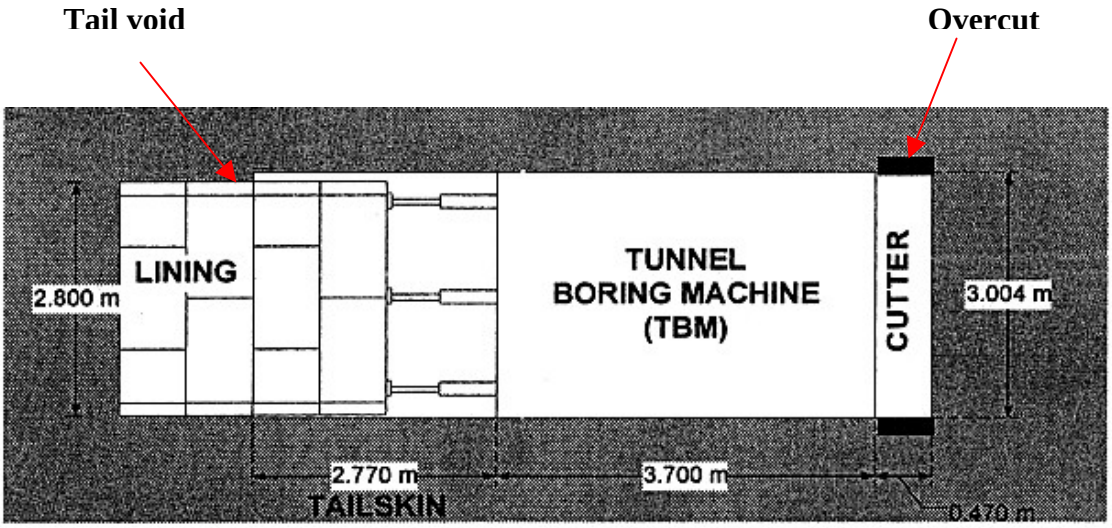

Figure 2.2 Overcut and tail void in shield machine tunneling (Dasari, 2002)

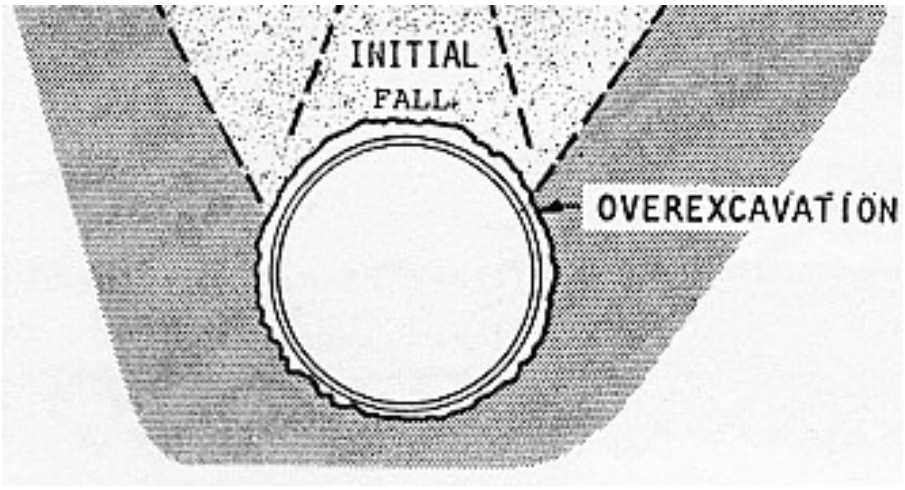

Figure 2.3 Gap between excavated boundary and lining (George, 1981)

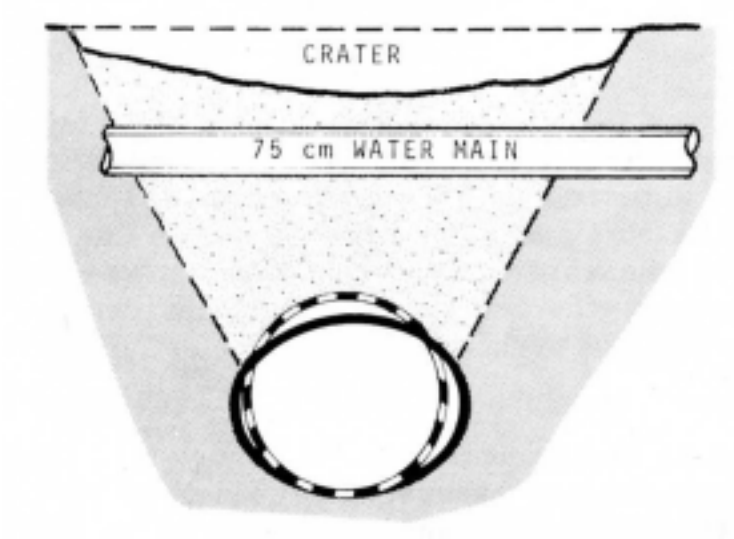

Figure 2.4 Lining ovalisation (George, 1981)

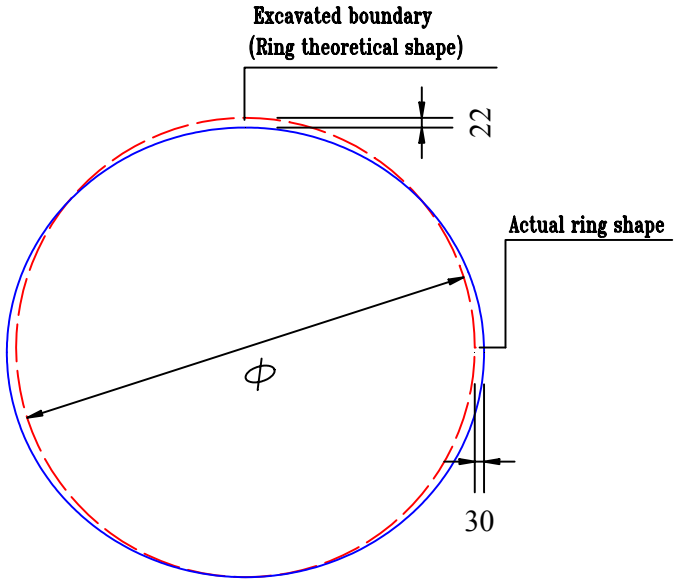

Figure 2.5 Comparison of theoretical ring shape and actual ring shape in the Villejust tunnel project (Leblais et al., 1991)

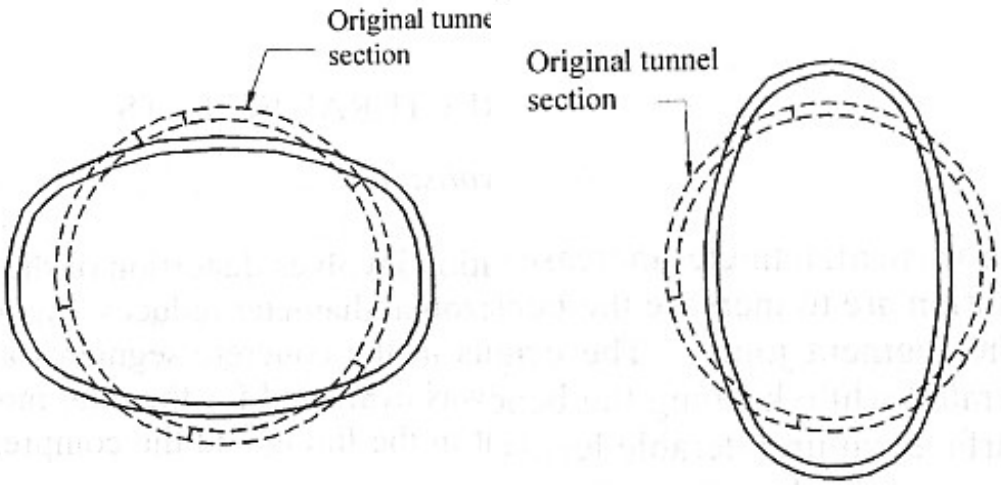

(a) (b)

Figure 2.6 Comparison of (a) horizontal and (b) vertical lining ovalisation (Doran et al, 2000)

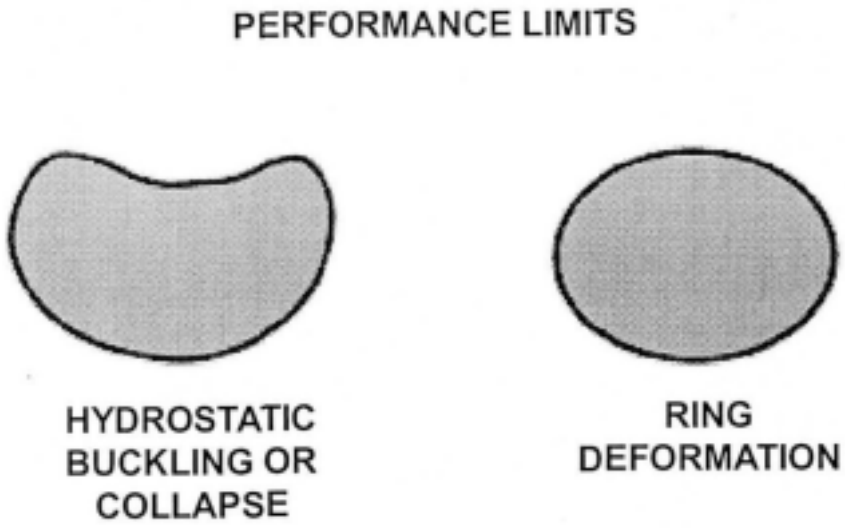

Figure 2.7 Performance of HDD pipe subjected to service load (Handbook, Plastic Pipe Institute, 2003)

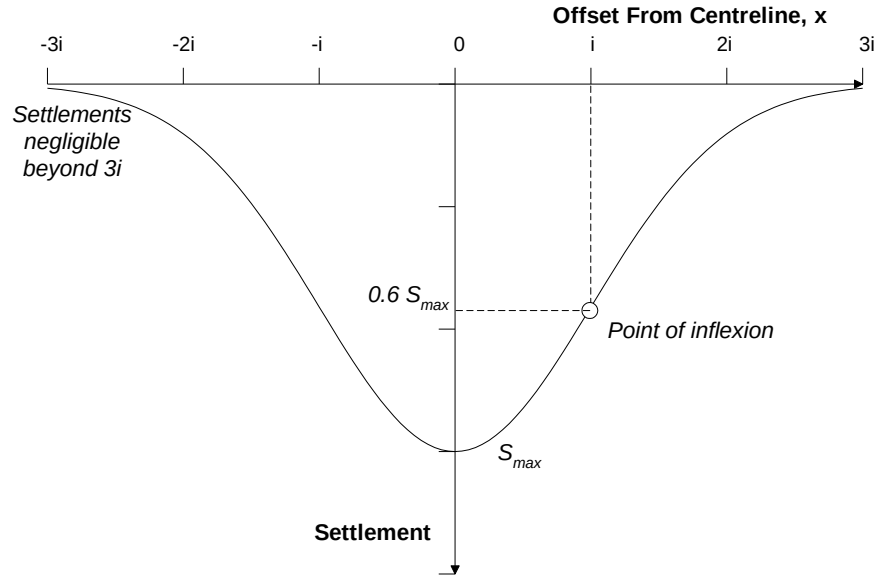

Figure 2.8 Gaussian curve approximating transverse surface settlement trough (Peck, 1969)

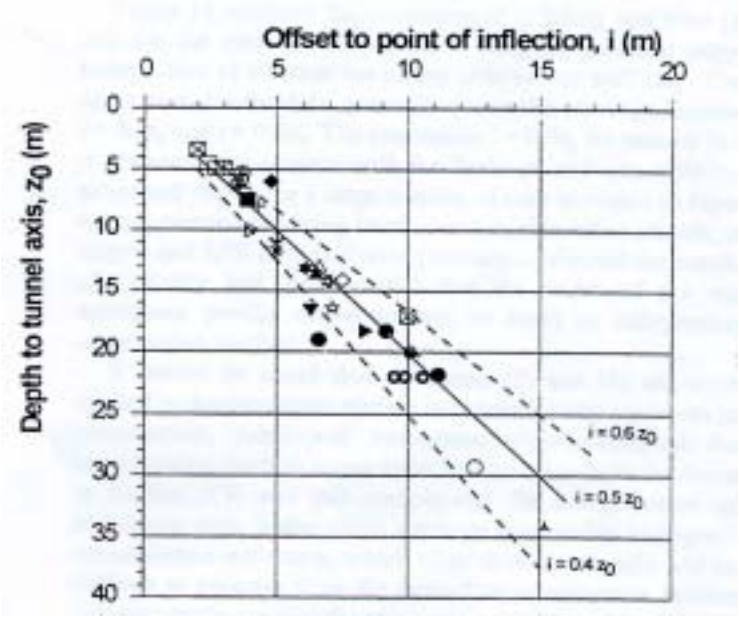

Figure 2.9 Variation of surface settlement trough parameter i with tunnel depth for tunnels in clays (Rankin, 1998)

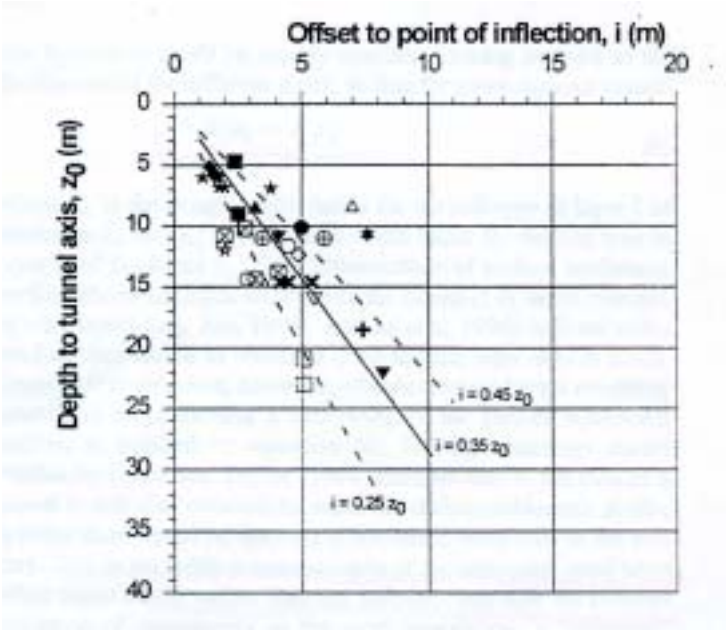

Figure 2.10 Variation of surface settlement trough parameter i with tunnel depth for tunnels in sands and gravels (Rankin, 1998)

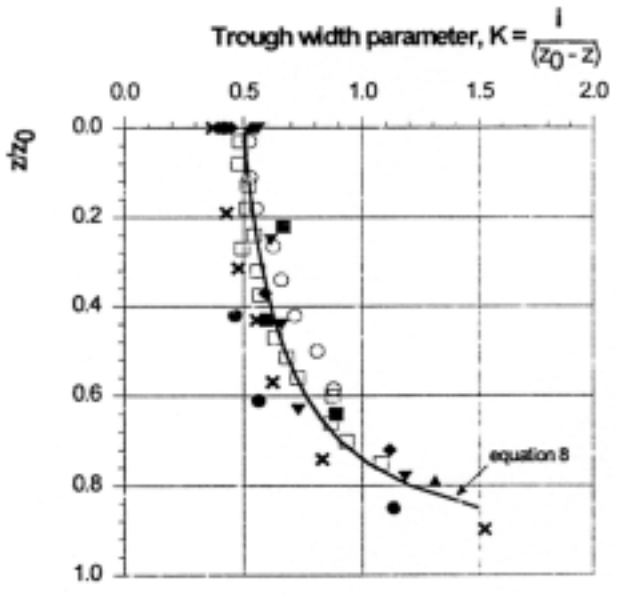

Figure 2.11 Variation of trough width parameter *K* with depth for subsurface settlement profiles above tunnels in clays (Mair et al., 1993)

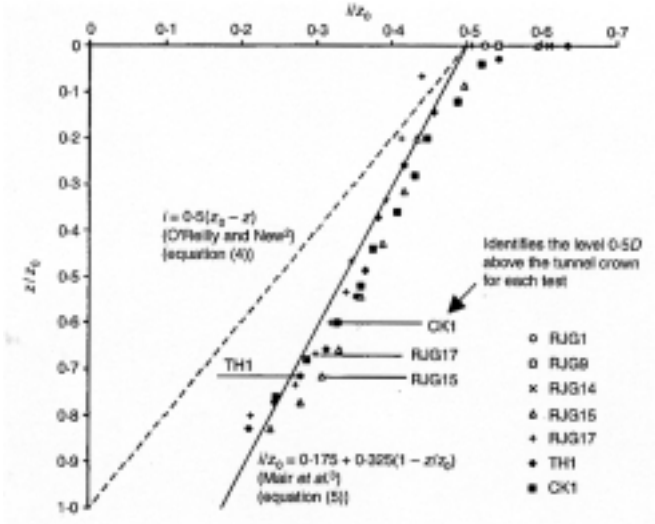

Figure 2.12 Variation of normalized *i* parameter with depth (Grant and Taylor, 2000)

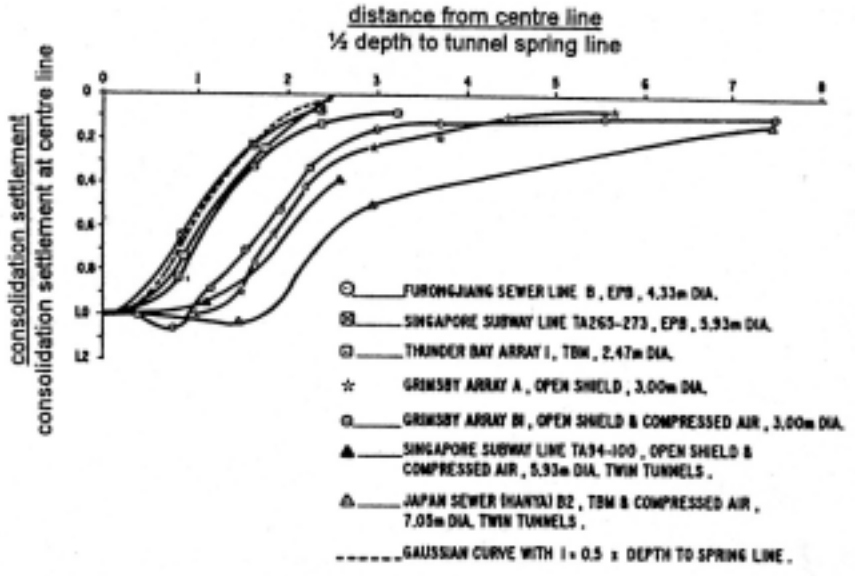

Figure 2.13 Normalized post-construction surface settlement troughs in soft clays (Shirlaw, 1995)

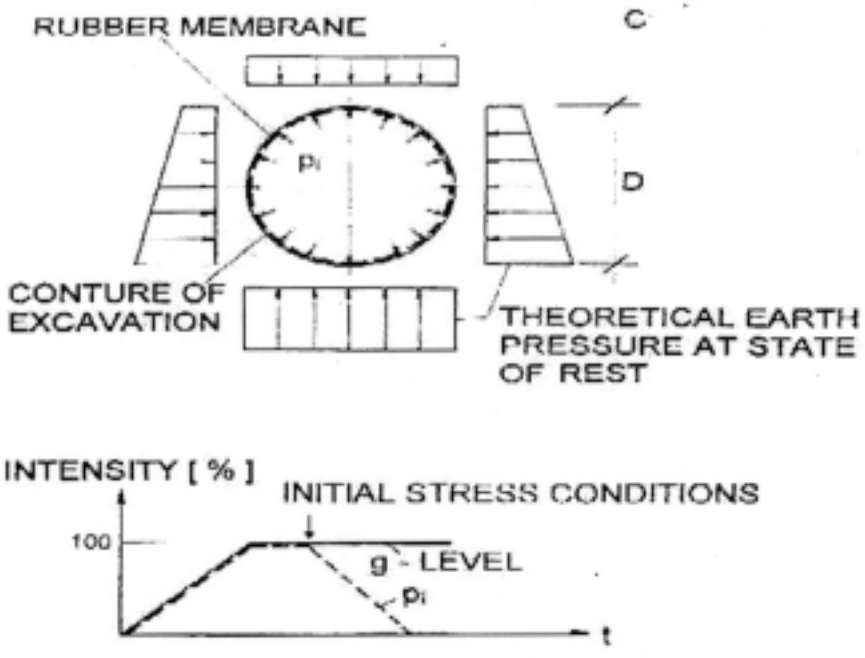

Figure 2.14 Principle of air pressure technique (Potts 1976, Mair et al. 1984)

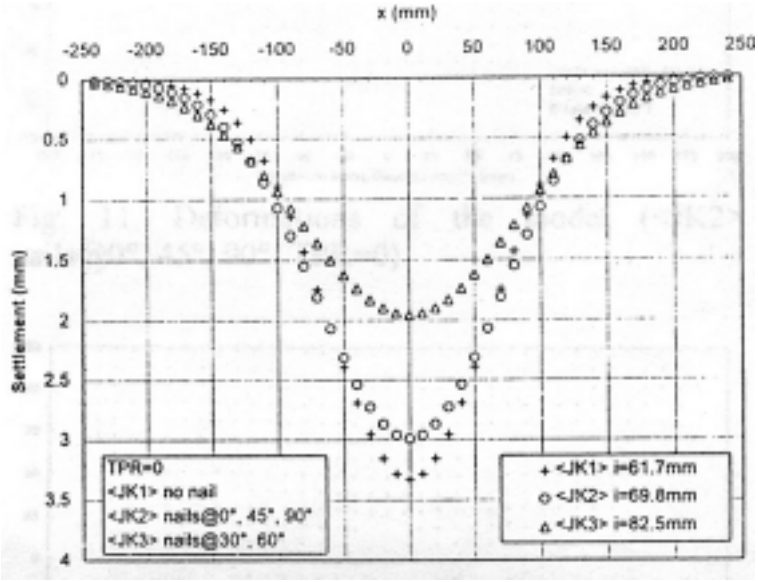

Figure 2.15 Comparisons of ground surface settlement associated with soil nails (Kuwano et al. 1998)

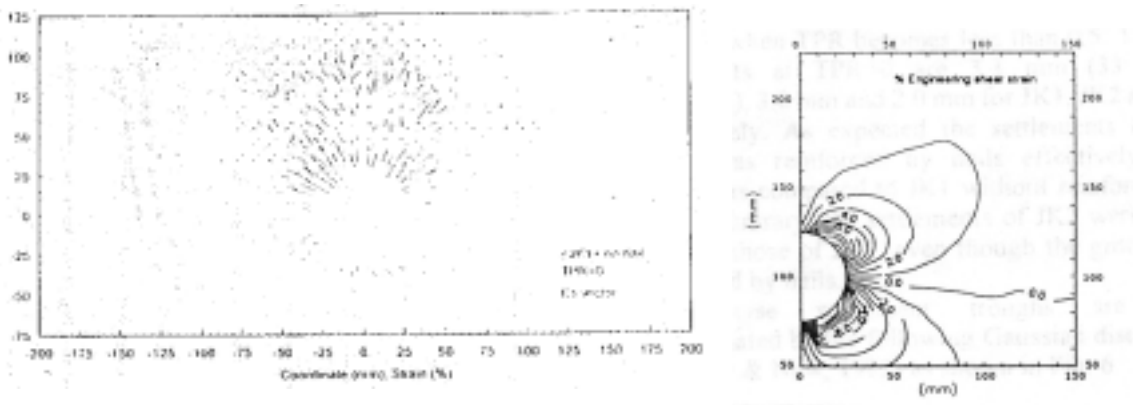

Figure 2.16 Comparisons of measured minor principal strains and numerical prediction (Kuwano et al. 1998)

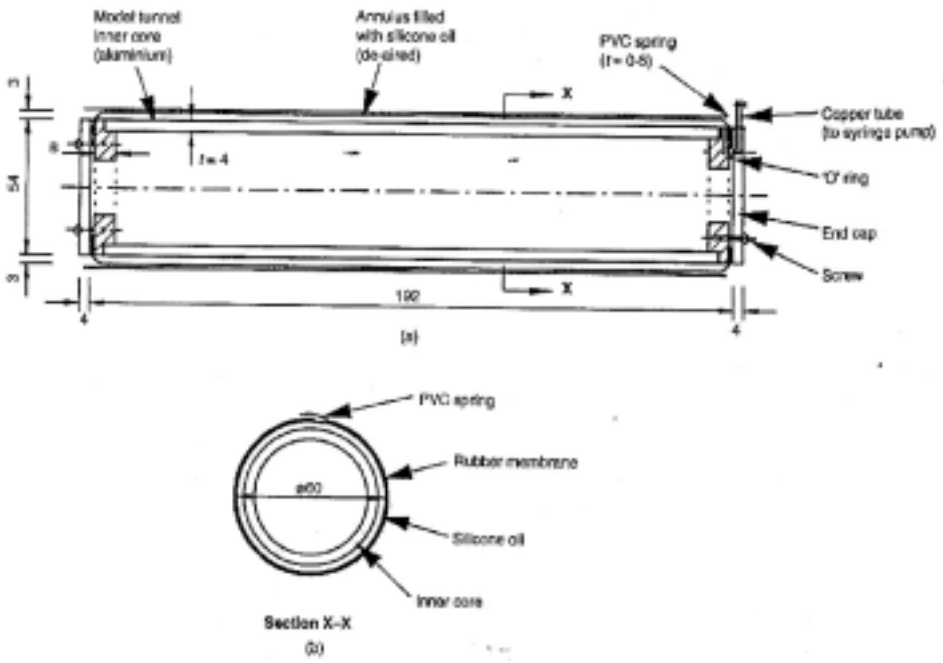

Figure 2.17 Configuration of model tunnel (Loganathan et al. 2000)

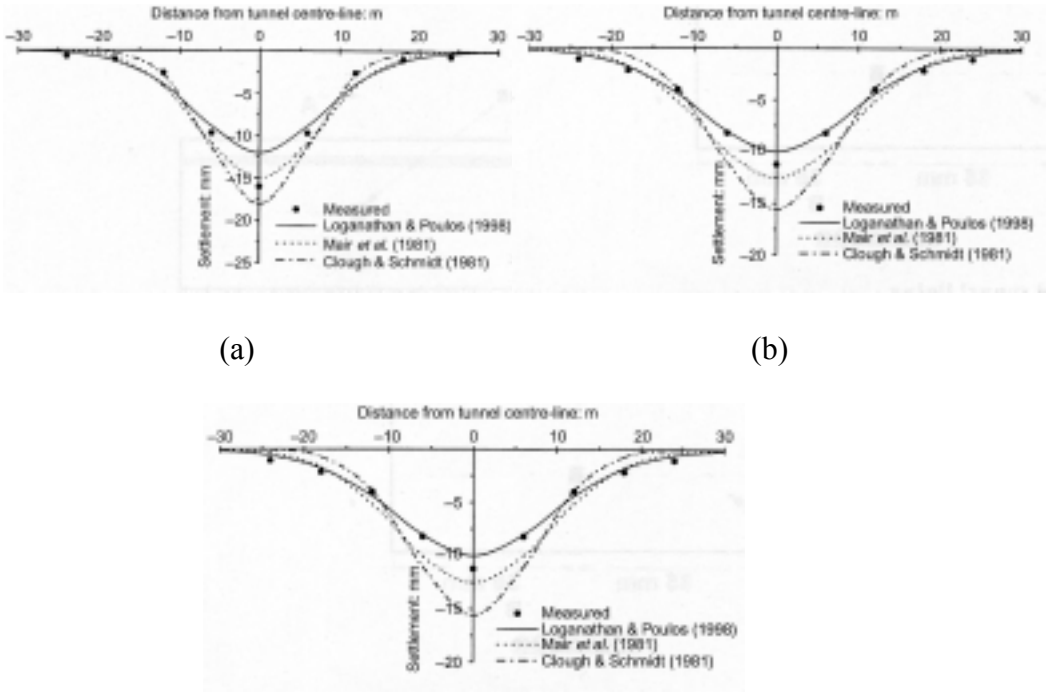

Figure 2.18 Comparisons of measured surface settlement and analytical solutions (a) test1, (b) test 2 and (c) test 3 (Loganathan et al. 2000)

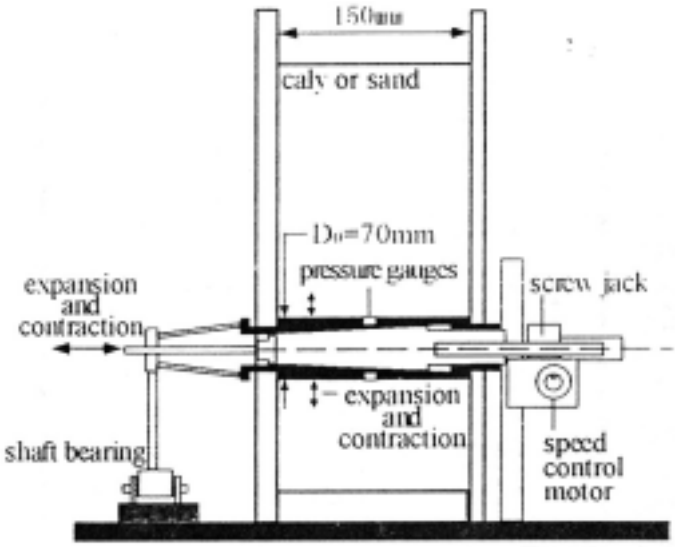

Figure 2.19 Configuration of shield model machine (Yasuhiro et al. 1998)

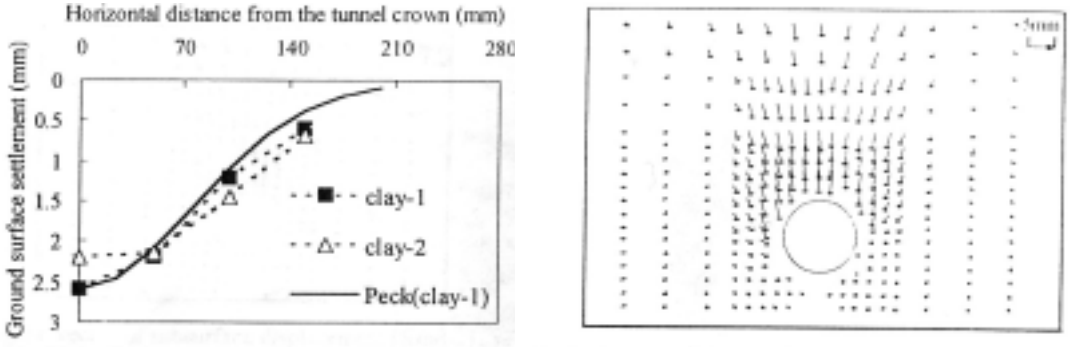

Figure 2.20 Surface and subsurface soil movement (Yasuhiro et al. 1998)

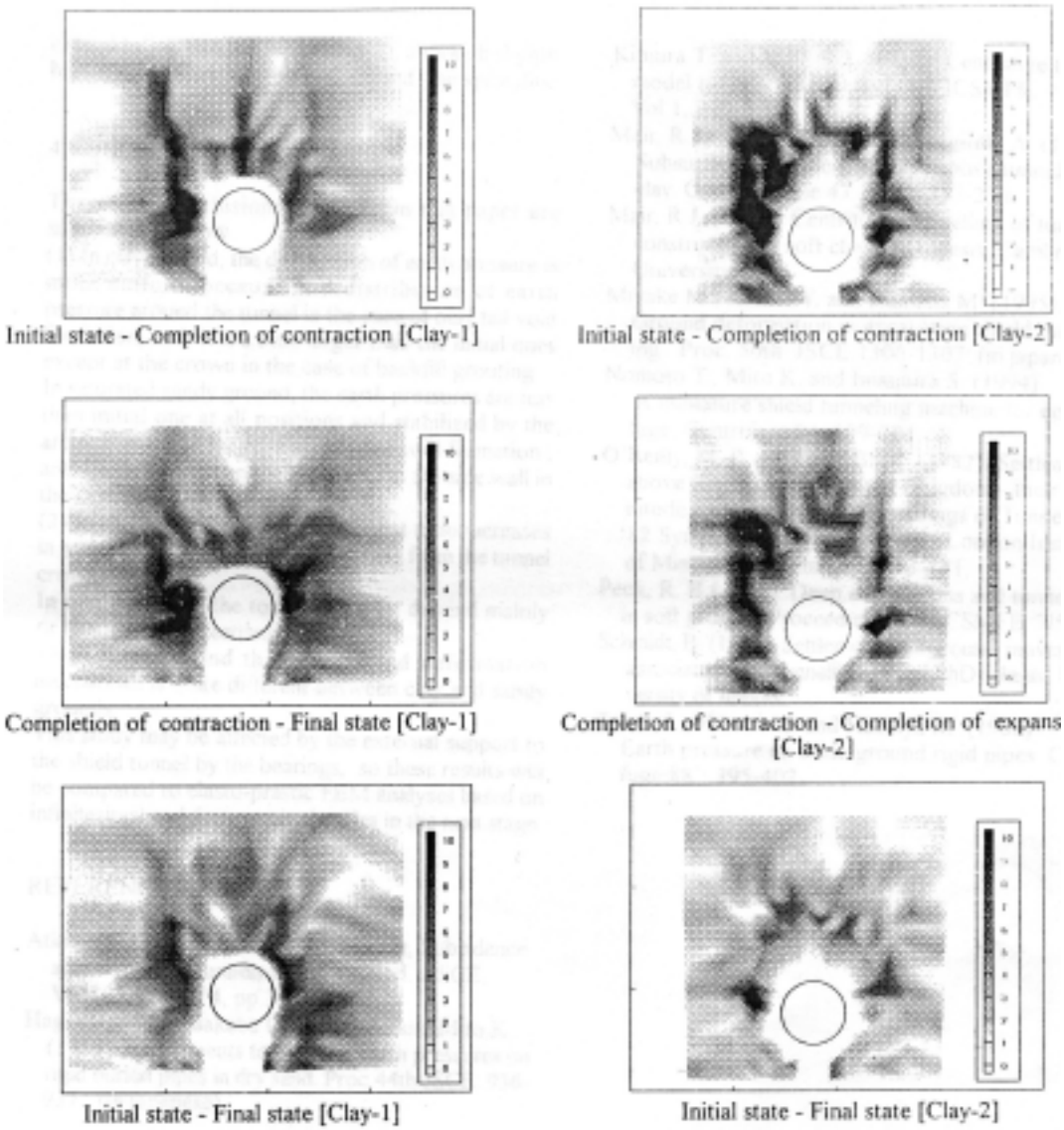

Figure 2.21 Maximum shear strain associated with tunneling (Yasuhiro et al. 1998)

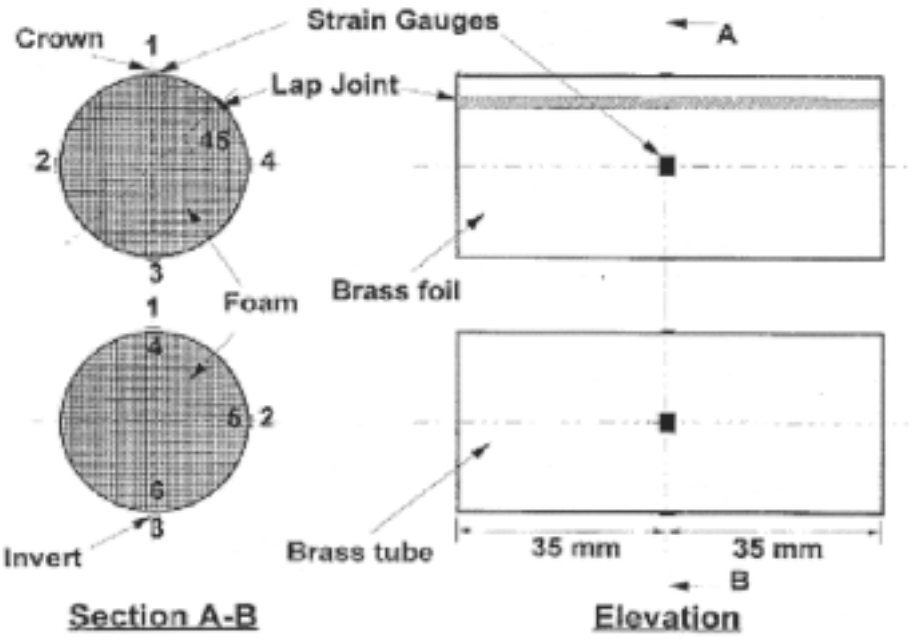

Figure 2.22 Configuration of model tunnel (Sharma et al. 2001)

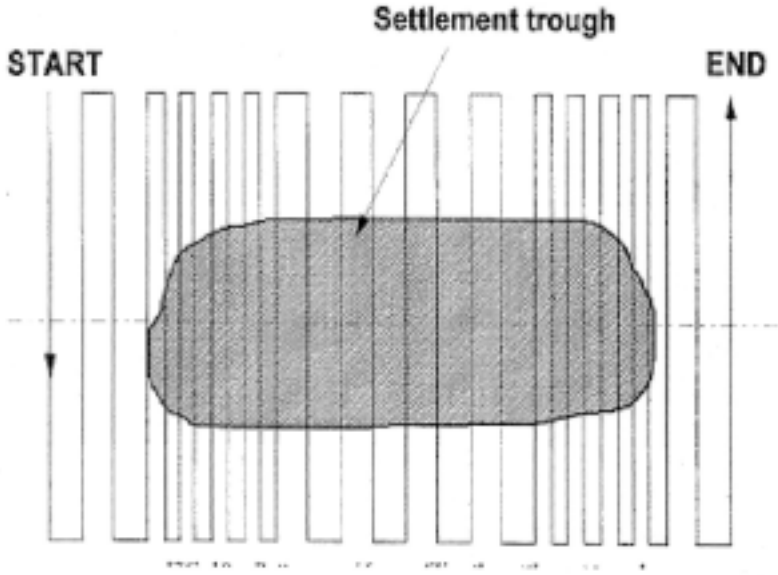

Figure 2.23 Propagation of surface settlement trough (Sharma et al. 2001)

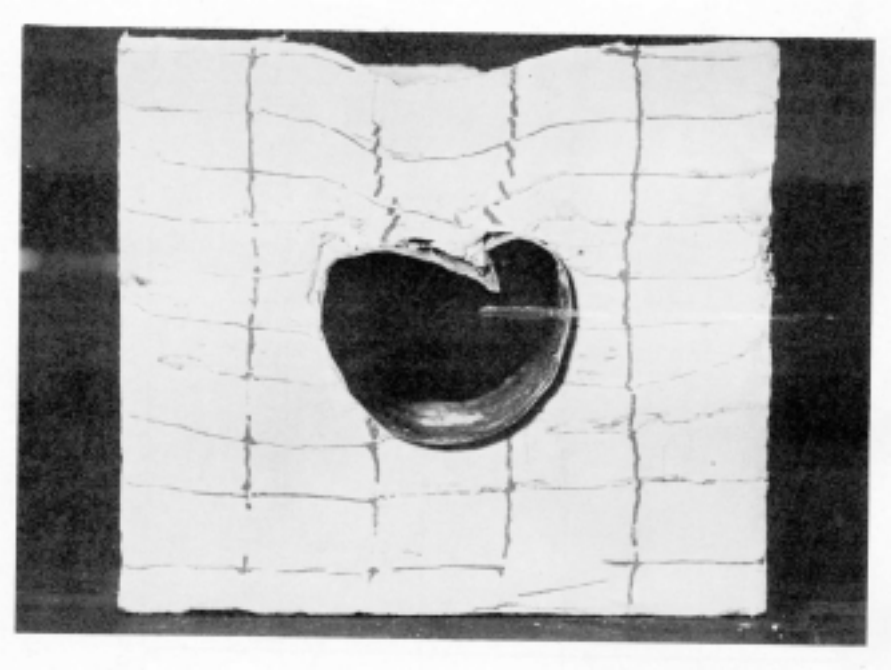

Figure 2.24 Collapse of a lined tunnel in clay (Atkinson et. al 1975)

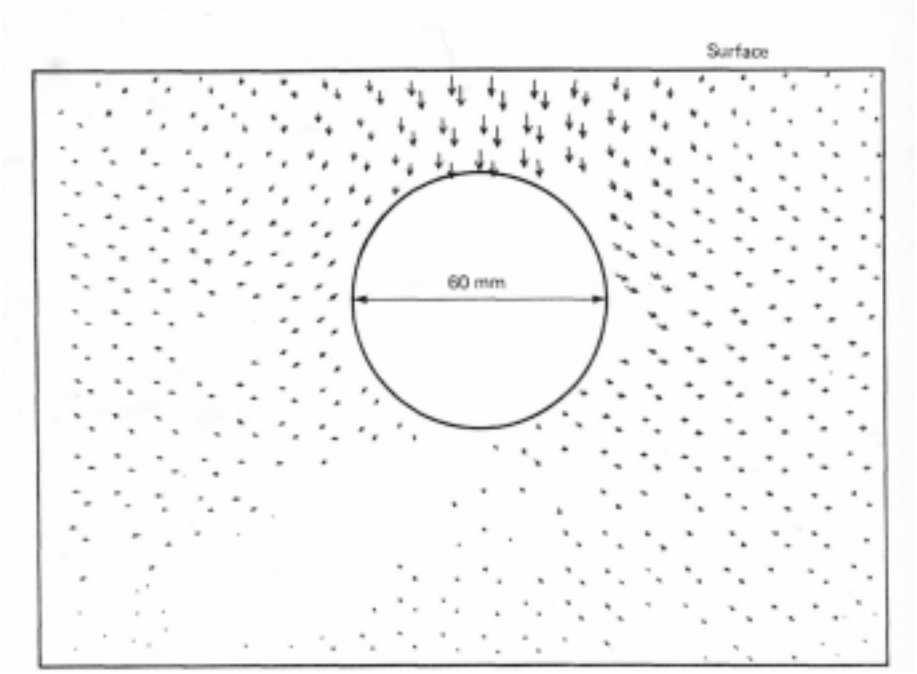

Figure 2.25 Soil displacement associated with lined tunnel (Atkinson et. al 1975)

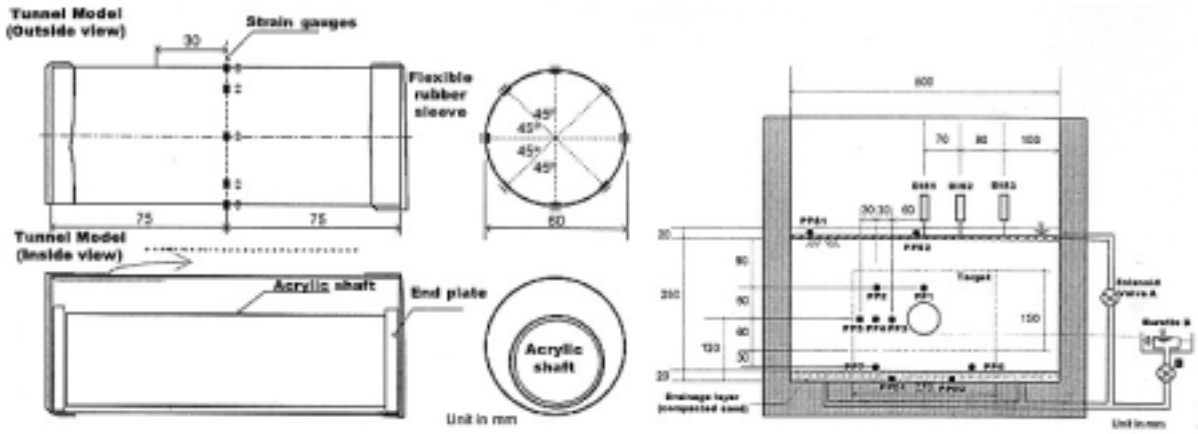

Figure 2.26 Configuration of model lining (Kongpathomporn, 2002)

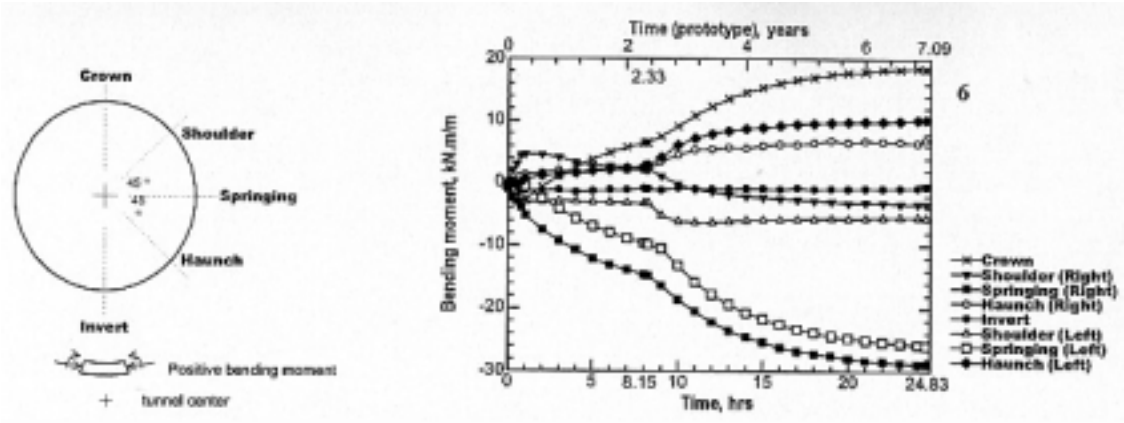

(a)

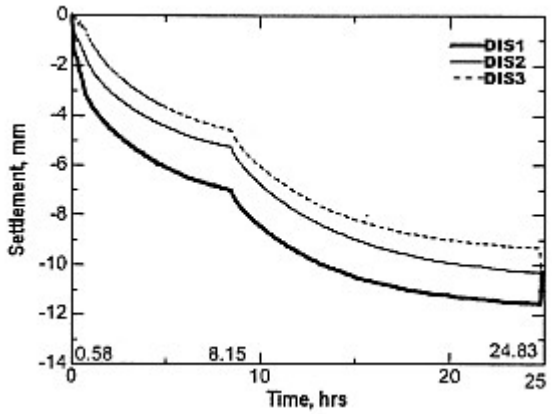

(b)

Figure 2.27 (a) Bending moment distribution and deformation pattern of lining (b) ground surface settlement over time (Kongpathomporn, 2002)

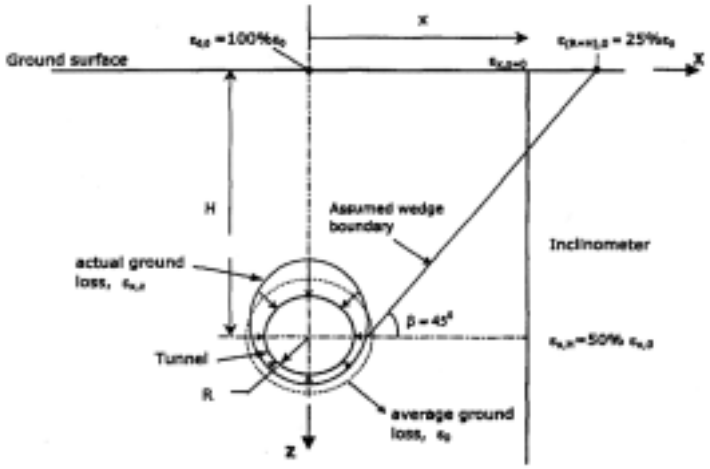

Figure 2.28 Non-uniform soil displacement around tunnel boundary (Loganathan et al, 1998)

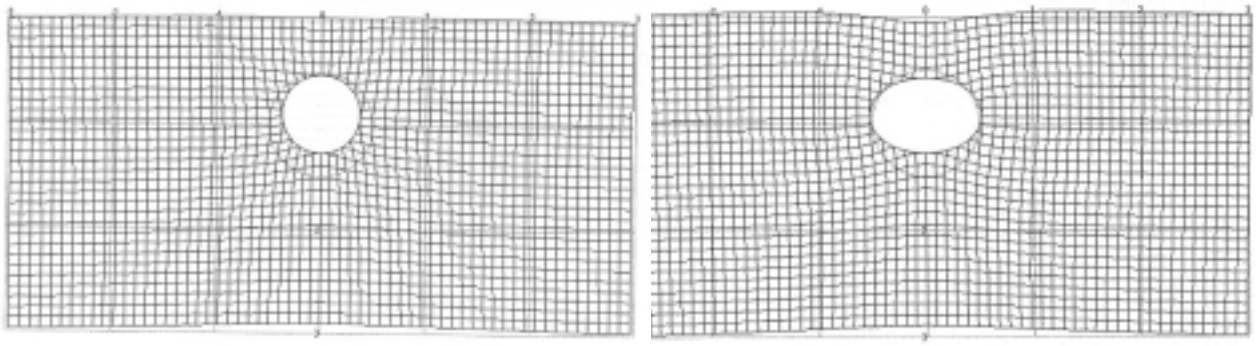

(a) K_0=1 (b) K_0=0

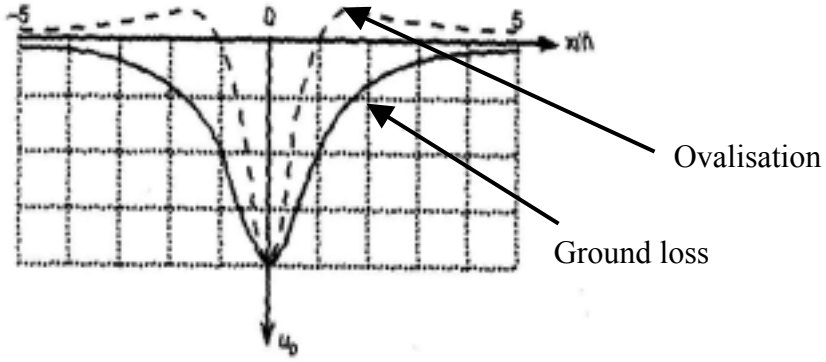

(c)

Figure 2.29 (a) ground loss tunnel deformation, (b) ovalisation tunnel deformation and (c) induced surface settlement troughs. (Verrujit et al, 1996)

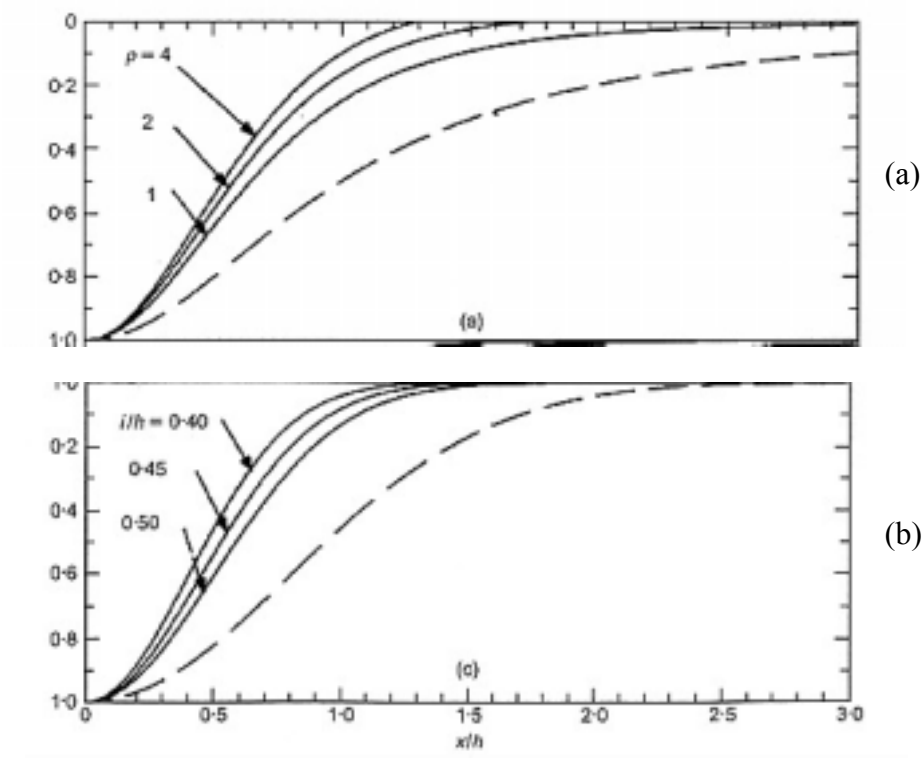

Figure 2.30 Comparisons of (a) ovalisation-induced surface settlement troughs and (b) Gaussian curves (Verrujit et al, 2000 (ρ= ovalisation factor, for ρ>1, tunnel spring expands outwards)

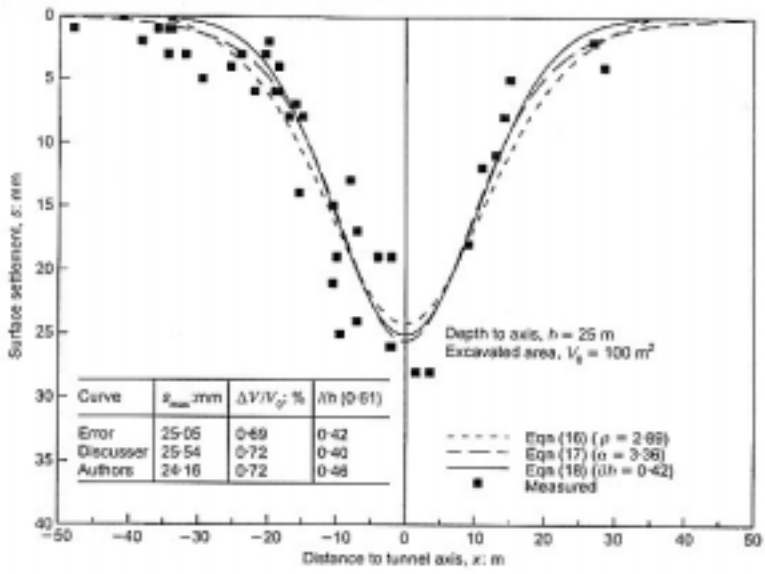

Figure 2.31 Comparisons of (a) ovalisation-induced surface settlement trough and (b) Gaussian curve (Verrujit et al, 2000)

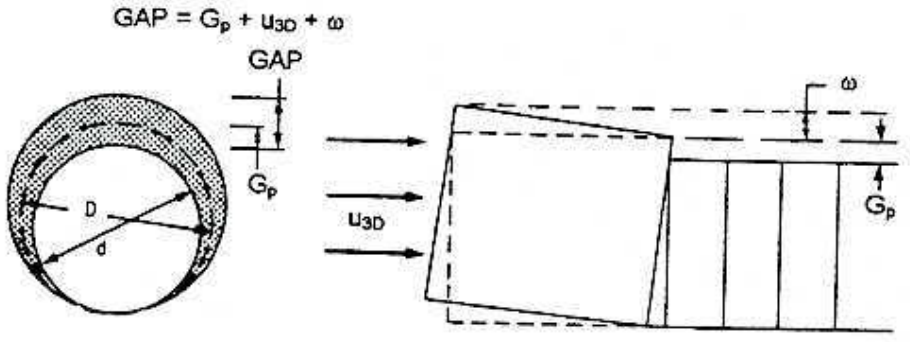

Figure 2.32 Definition of gap parameter (Rowe et al, 1983)

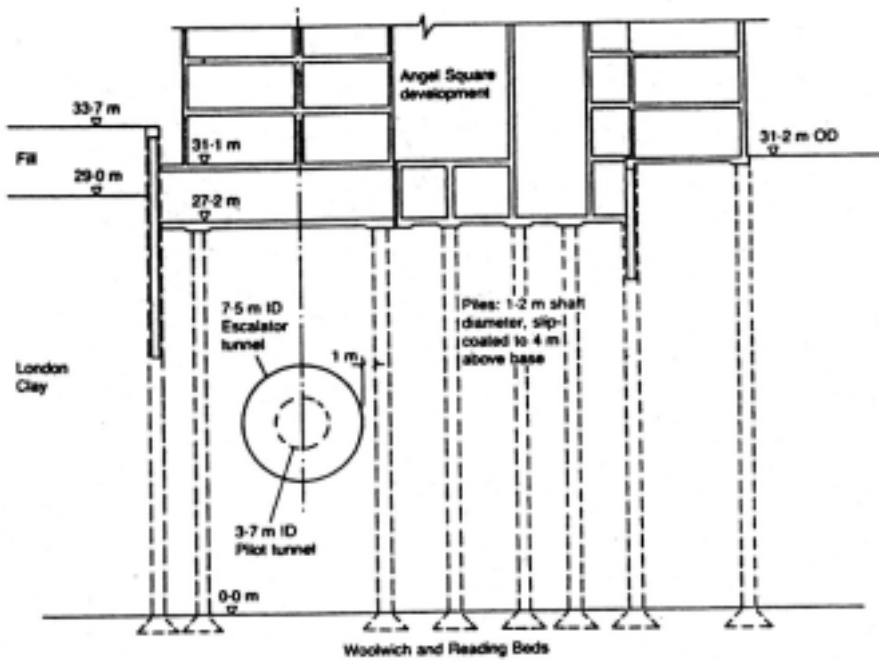

Figure 2.33 Configuration of site condition (Lee et al. 1994)

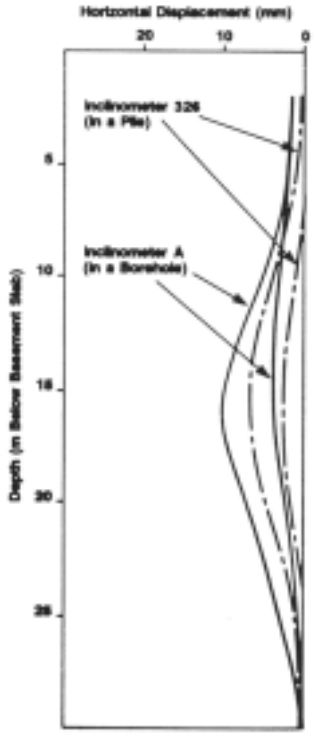

Figure 2.34 Displacement profile of soil and pile with depth (Lee et al., 1994)

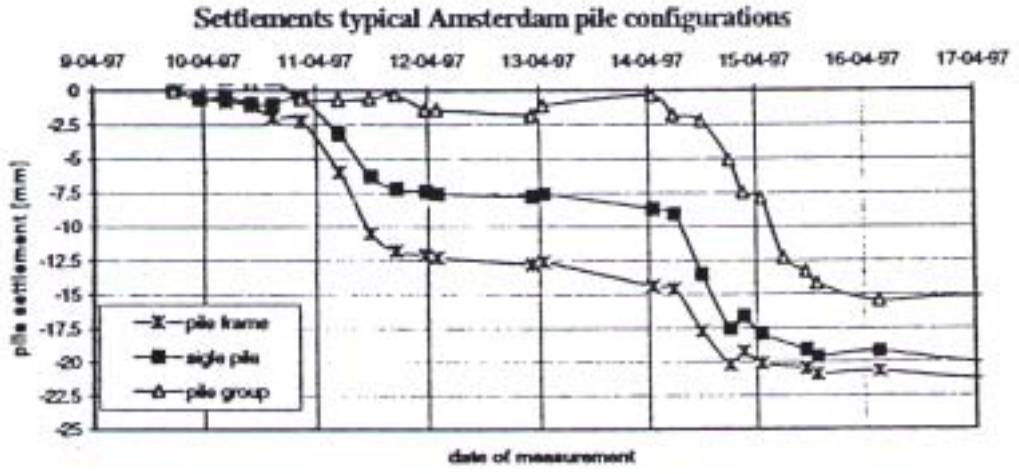

Figure 2.35 Pile Settlement stations versus tunnel excavation time (Teunissen et al., 1998)

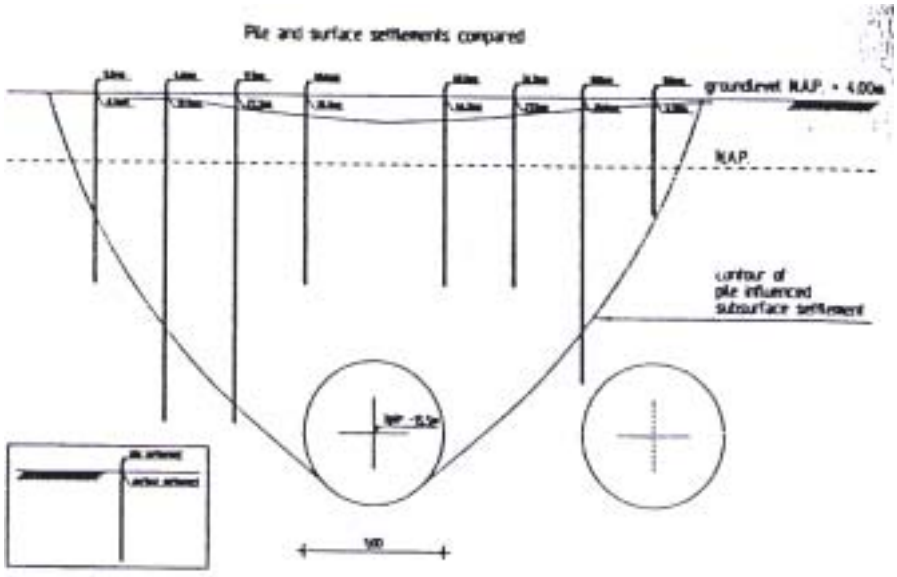

Figure 2.36 Pile Settlement stations vs. surface and subsurface settlement (Teunissen et al., 1998)

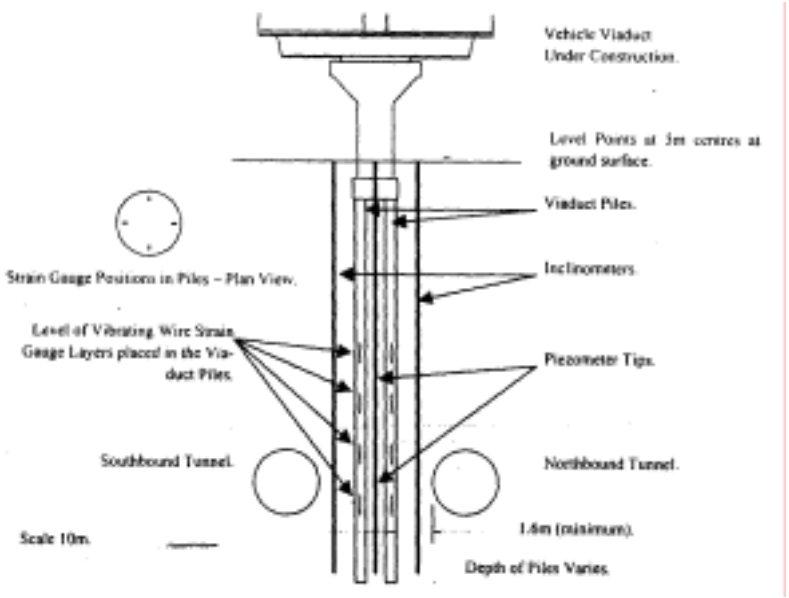

Figure 2.37 Viaduct, pile and tunnel layout (Coutts and Wang, 2000)

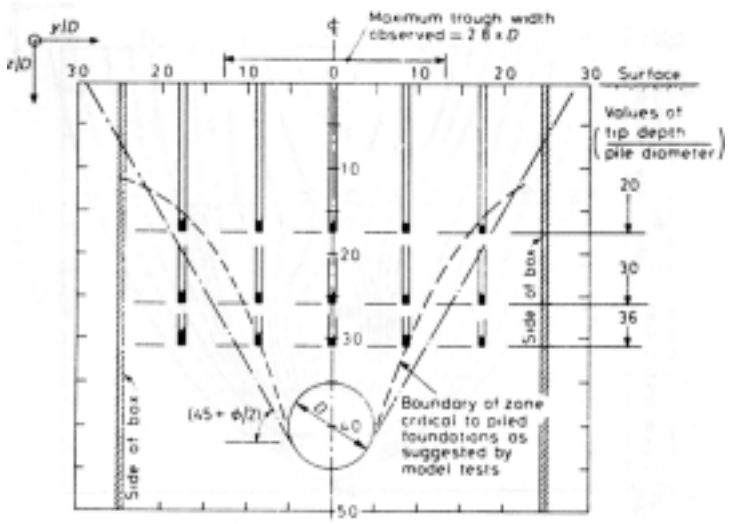

Figure 2.38 Zone of high pile settlements (Morton et al., 1979)

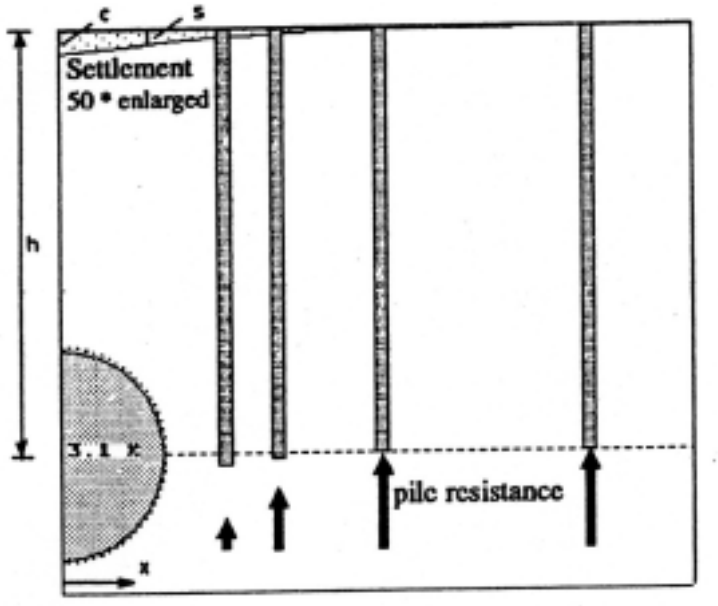

Figure 2.39 Centrifuge modeling of influence of tunnel construction on settlement of adjacent piles (Bezuijen et al.,1994)

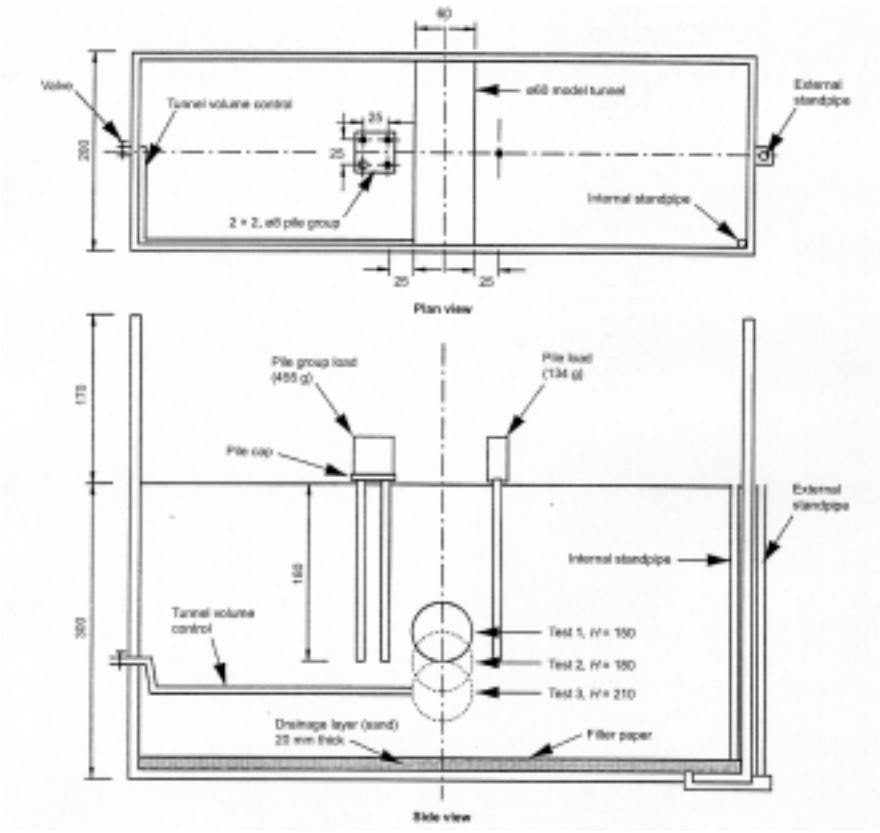

Figure 2.40 Configuration of centrifuge tests (Loganathan et al. 2000)

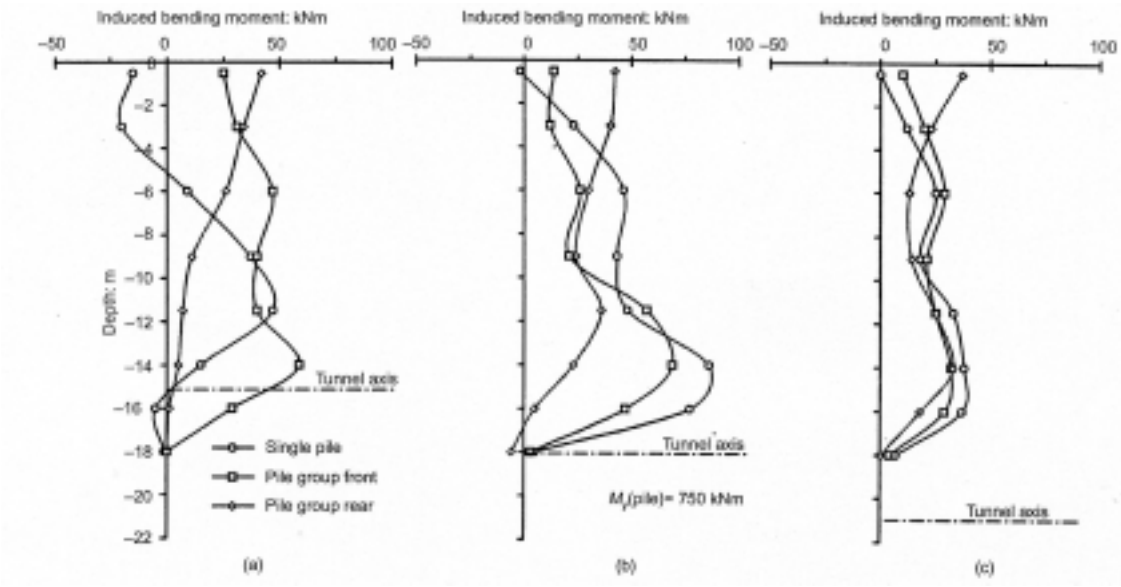

Figure 2.41 Tunneling-induced pile bending moments (Loganathan et al. 2000)

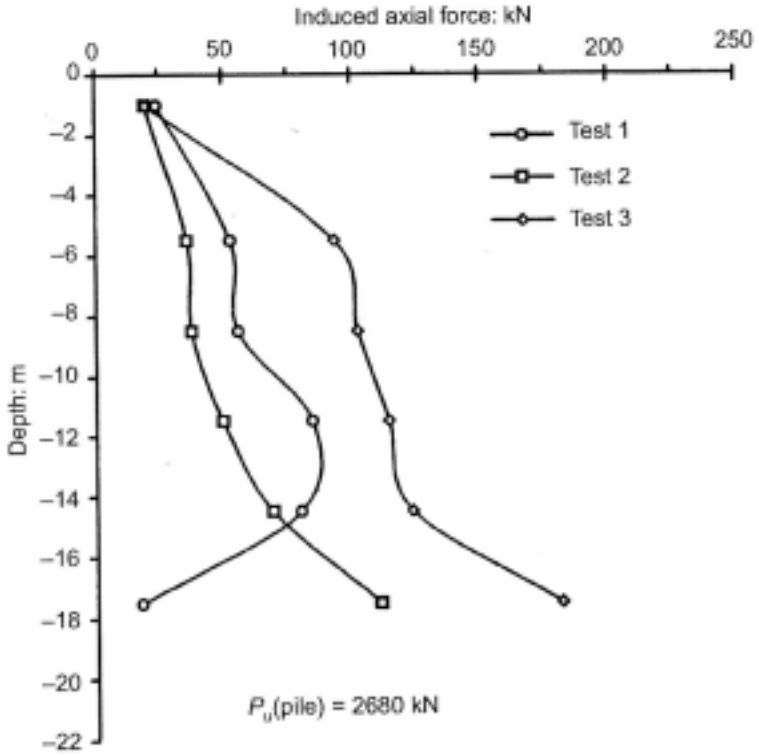

Figure 2.42 Tunneling-induced pile axial loads (Loganathan et al. 2000)

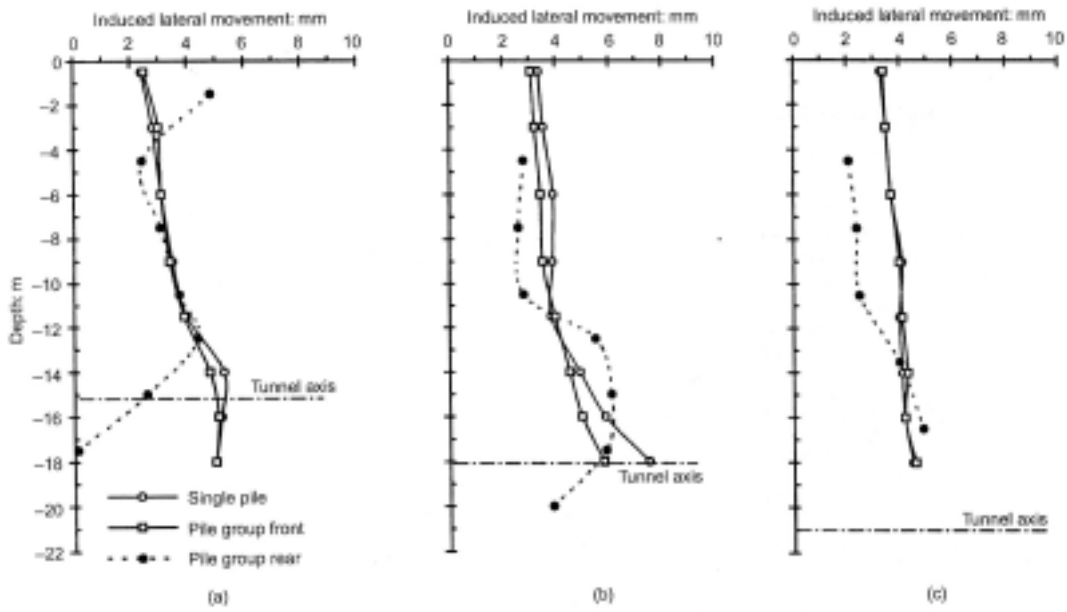

Figure 2.43 Tunneling-induced lateral movements of ground and piles (Loganathan et al. 2000)

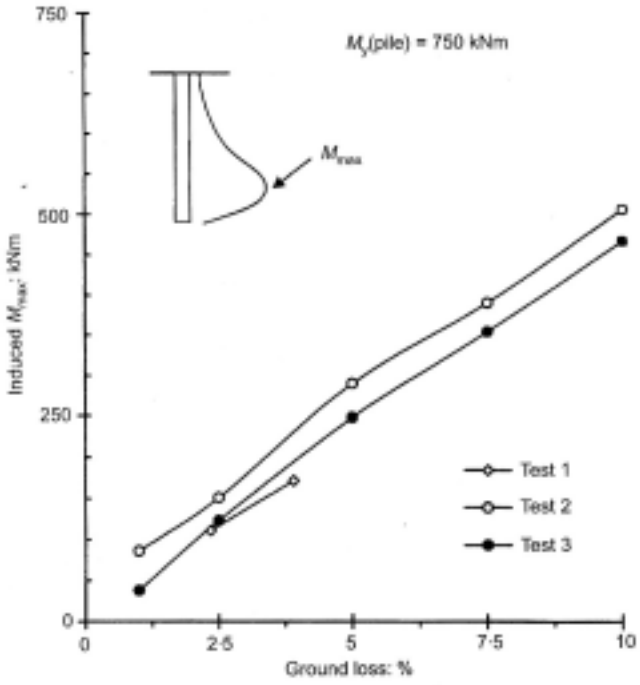

Figure 2.44 Tunneling-induce maximum bending moments for varying ground loss values (Loganathan et al. 2000)

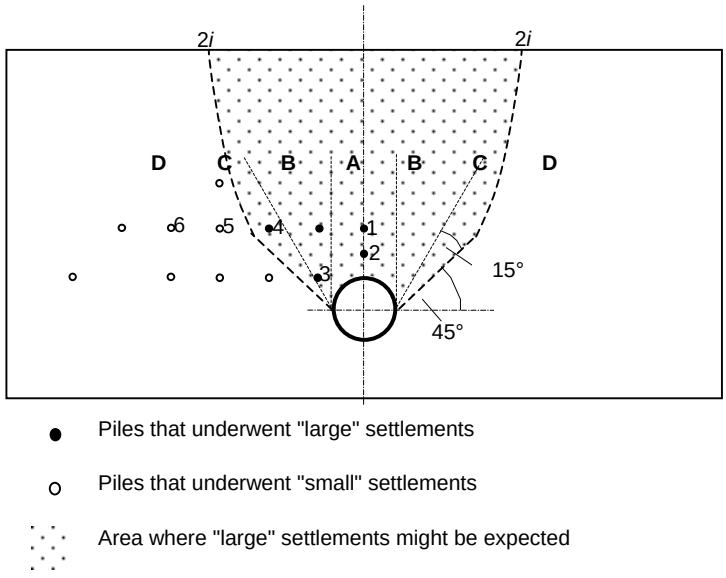

Figure 2.45 Zone of large pile settlements (Jacobsz, 2001)

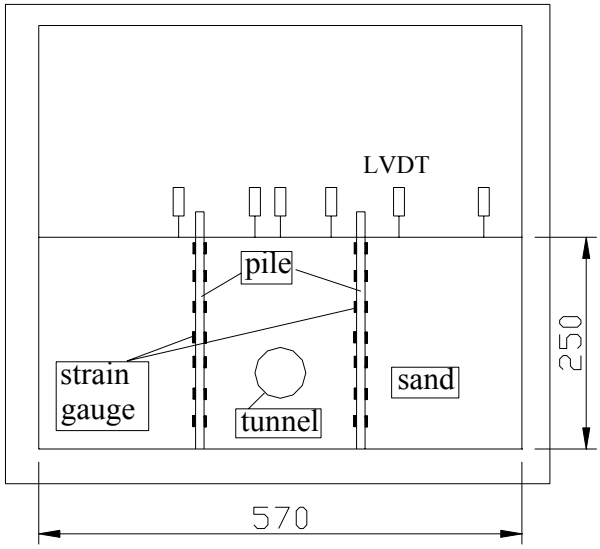

Figure 2.46 Typical configuration of centrifuge tests (Feng, 2003)

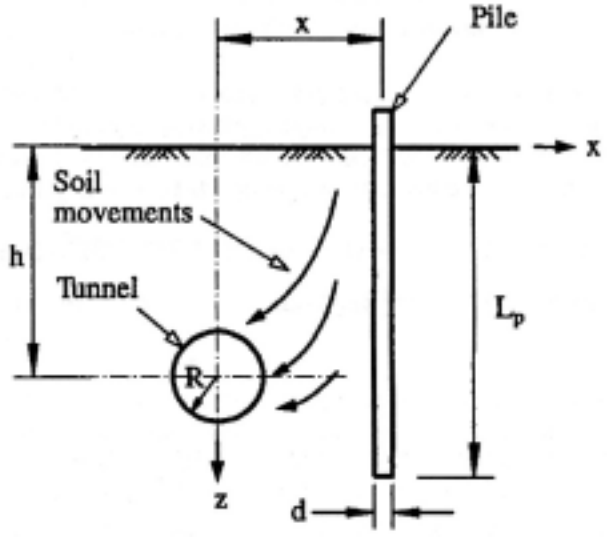

Figure 2.47 Layout of basic problem (Chen et al., 1999)

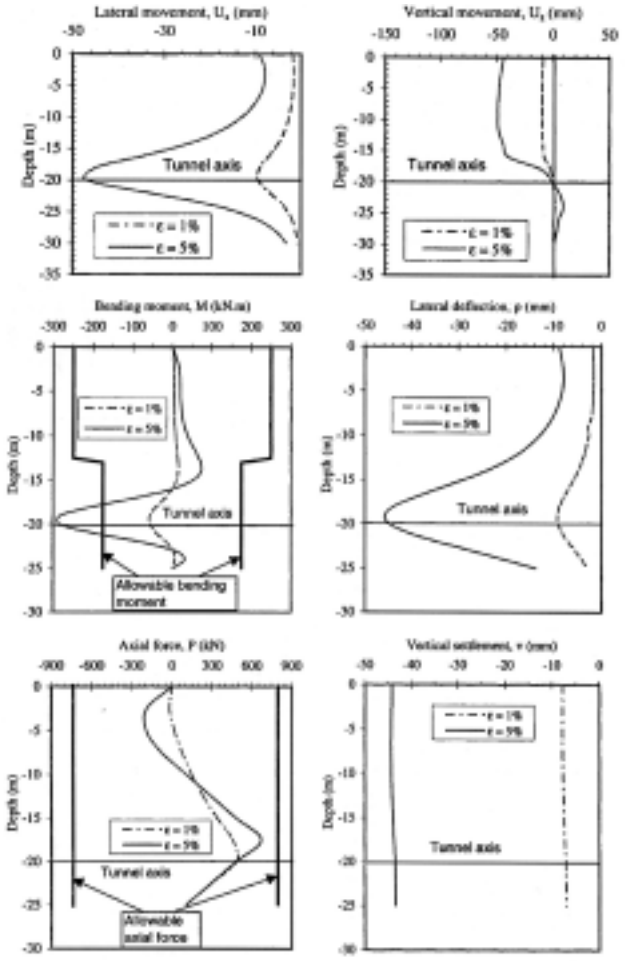

Figure 2.48 Tunneling-induced pile responses and greenfield soil movement (Chen et al., 1999)

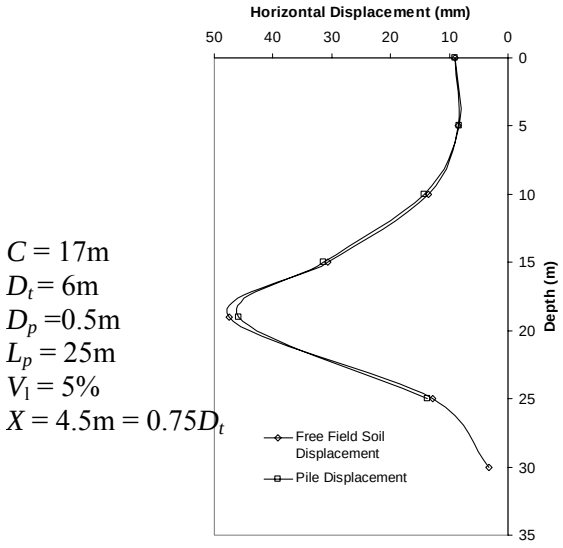

C = 17m
D_t = 6m
D_p =0.5m
L_p = 25m
V_l = 5%
X = 4.5m = 0.75D_t

Figure 2.49 Computed pile horizontal displacement approximately similar in shape and magnitude to imposed free field soil displacement (Chen et al., 1999)

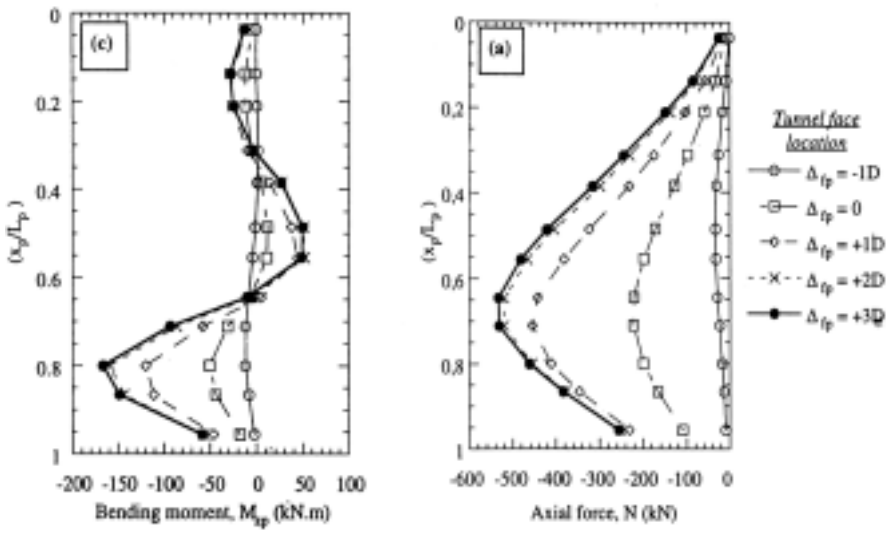

Figure 2.50 Development of pile bending moment and axial forces with advancement of tunnel face (Mroueh and Shahrour, 1999)

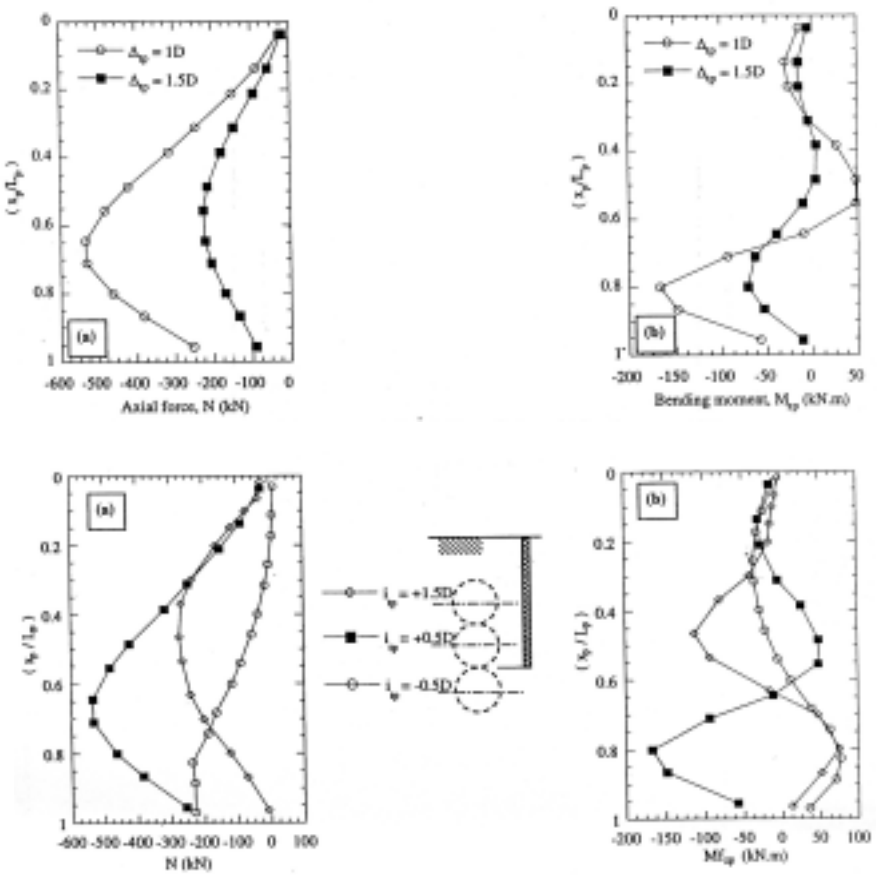

Figure 2.51 Induce pile bending moment and axial forces with various pile-to-tunnel distance and pile tip locations (Mroueh and Shahrour, 1999)

CHAPTER THREE

EXPERIMENTAL SET-UP AND PROCEDURE

3.1 Introduction

This chapter presents the general principle and scaling relationships of geotechnical centrifuge modeling as well as briefly describes the National University of Singapore Geotechnical Centrifuge facility. The preparation of the model ground, fabrication and configuration of the model tunnel and piles are then elaborated. Last but not least, the model set-up and test procedure are described in detail. All the tests were carried out at 100g in the present study.

3.2 Centrifuge modeling technique and scaling relationships

Physical modeling is an attractive alternative to study geotechnical problems as they are less costly and time-consuming to perform as compared to full-scale field tests. Furthermore, as it is normally not feasible to test real-life structures to failure in the field. Conventional small-scale physical models have significant limitations as the mechanical behaviour of soil is highly non-linear and stress-level dependent. However, by subjecting a $1/N^{th}$ scaled model in a geotechnical centrifuge to an enhanced gravitational field N times the earth's gravity, the prototype stress levels can be reproduced in the reduced model. Hence the centrifuge model test results can be used to interpret the prototype behavior in a rational manner.

Over the past 40 years, centrifuge modeling technique has become popular to investigate geotechnical problems such as tunneling, deep-excavation, embankment and soil dynamic studies etc. Its applications include three main aspects: understanding

of the mechanics of geotechnical materials and problems; development or modification of methods of analysis for idealized but realistic geotechnical structures by providing quantitative indications of the effects of various parameters; and the modeling of specific situations to aid in design and project appraisal. Majority of the existing centrifuges are found in universities and research laboratories in United Kingdom, France, the Netherlands, Germany, US, Canada, Australia, China, India, Japan, and Singapore etc.

The scaling relationship between a small-scale model and its prototype counterpart can be derived either by dimensional analysis or by consideration of the governing equations and system mechanics. A list of scaling relations used in the present thesis is shown in Table 3.1. The centrifuge tests results in the present study will be extrapolated to their corresponding prototype magnitudes using the scaling relations shown in the table.

Table 3.1 Scaling relation of centrifuge modeling (modified from Leung et al. 1991)

Parameter	Centrifuge Model / Prototype at Ng
Linear dimension	1/N
Area	$1/N^2$
Volume	$1/N^3$
Density	1
Mass	$1/N^3$
Acceleration	1/N
Velocity	1
Displacement	1/N
Strain	1
Stress	1
Force	$1/N^2$
Time (viscous flow)	1
Time (seepage)	$1/N^2$
Flexural rigidity	$1/N^4$
Axial rigidity	$1/N^2$
Bending moment	$1/N^3$

3.3 NUS geotechnical centrifuge

Being the only geotechnical centrifuge in Southeast Asia, the centrifuge facility at the National University of Singapore (NUS) was established in 1990 and has contributed to various geotechnical studies including land reclamation, deep excavation, tunneling and pile and others.

Figures 3.1 and 3.2 show the NUS geotechnical centrifuge, which consists of a conical case, a drive shaft, a rotating arm, and two swinging platforms. It has a capacity of 40,000-kg and operates up to a maximum g-level of 200g, implying that the allowable payloads at 200g and 100g are 200 kg and 400 kg, respectively. The structure of the centrifuge is based on conventional dual swing platform design. The model package is normally loaded onto one of the swing platforms with the opposing platform counter balanced by either counterweights or another model package with identical weights. When fully spun up during test operation, the distance from the axis of rotation to the base of the platform is 1.871 m. The centrifuge is driven by a hydraulic motor delivering up to about 37 kW power. The swing platform has a working area that measures 750 mm x 700 mm and a headroom of 1180 mm. A stack of electrical slip rings is mounted at the top of the rotor shaft for signals and power transmission between the centrifuge and the control room.

DC voltage is transmitted through the slip rings to the transducers mounted on the centrifuge or the model package from the control room. Similarly, registered signals from the transducers are then transmitted via the slip rings. The signals are first filtered by an amplifier system at 100 Hz cut-off frequency to reduce interference or signal noise pick-up through the slip rings. The amplified signals are then collected by a data acquisition system at a regular interval in the control room. A software called Dasylab

is used to process the signals whereby the signals are smoothened by using a block average. Two closed circuit cameras, which are mounted on the centrifuge, enable the entire in-flight process to be monitored in the control room. Figures 3.3 and 3.4 show the various facilities in the centrifuge control room. The NUS centrifuge is described in detail by Lee at al. (1991) and Lee (1992).

3.4 Centrifuge model

Figures 3.5 and 3.6 show the sketch and photograph of the model package for the present study. The main features of the model are described in this section.

3.4.1 Model container

The container is made of stainless steel alloy and has internal dimensions of 525 mm × 200 mm × 490 mm (length ×width ×height). One sidewall of the container is made of a 75-mm thick transparent Perspex plate, which allows image acquisition by a video camera mounted to the model container. A measuring tape is attached to the Perspex wall to provide reference co-ordinates. Both the front (Perspex plate) and back walls of the container can be removed to facilitate the installation of model tunnel and transducers during the model set-up. A valve designed to drain Acetone via a tube is located at the middle bottom of the back wall. To minimize the soil/container friction, all the inner walls of the container are heavily greased. This would also ensure the deformation of the model ground is under plane strain condition.

3.4.2 Model ground

A 20-mm thick sand layer was first placed at the base of model container to facilitate bottom drainage during the centrifuge tests. A thin geotextile was placed on top of the

sand to separate the sand and clay. Malaysian kaolin clay powder and water were thoroughly mixed at a ratio of 1 to 1.2 by weight in a de-airing mixer. The mixing process lasted for four or five hours until the slurry was free of air-bubbles. The clay slurry was then carefully scooped into the container to a predetermined height. After that, the container was shifted to a pneumatic loading frame and the sample was consolidated under a pressure of 20 kPa for six days. This would result in a thin layer of over-consolidated clay at the top such that the clay is sufficiently stiff and would not heave during subsequent consolidation in the centrifuge. Figure 3.7 shows the photograph of sample preconsolidation in the loading frame.

When the 'preconsolidation' stage was completed, six Linear Vertical Displacement Transducers (LVDTs) were employed to measure the ground settlement and four Pore Pressure Transducers (PPTs) were inserted into the sample to measure the pore water pressure at various locations. The container was placed on the centrifuge platform which was then accelerated to 100g. After the measured ground settlement and pore water pressure readings stablised, the centrifuge was stopped for the next stage of sample preparation.

The measured settlements were analyzed by the hyperbolic method to determine the degree of consolidation. Figure 3.8 shows the typical time/settlement versus time plot during self-weight consolidation. A high degree of consolidation of around 90% can be consistently achieved in the model ground. The minor discrepancies among the individual LVDTs were caused by the variation of centrifugal gravity field on the sample.

The stress history of the model ground was intended to simulate that of a normally consolidation clay deposit with a 4-m thick overconsolidated crust at the top. Tables 3.2 and 3.3 show the physical properties of the clay and sand in the tests.

Table 3.2 Physical properties of Malaysian kaolin clay

Specific gravity	2.65
Liquid limit, LL	80%
Plastic limit, PL	40%
Compression index, C_c	0.65
Swelling index, C_s	0.14
Void ratio at 115 kPa at NC line	1.67
Permeability at 115 kPa at NC line	1.3×10^{-8} m/s

Table 3.3 Physical properties of sand

Mean grain size	0.16 mm
Uniformity coefficient	1.3
Specific gravity	2.65
Friction angle (50-100 kPa)	43°

Tan (2003) reported the in-flight undrained shear strength profile of the Kaolin clay (Figure 3.9) used in NUS obtained using miniature T-bar developed by Stewart and Randolph (1991). The in-flight T-bar tests were conducted at 100g after the soil consolidation ratio reached 90%. The undrained shear strength profile indicates an overconsolidated layer down to 40 mm (4 m in prototype scale), below which the shear strength increases almost linearly with depth, and is consistent with that for normally consolidated clay. The soil sample used by Tan (2003) has an identical preparation procedure and preconsolidation pressure as in the present study.

3.4.3 Model pile

Two instrumented model piles are used in the present study. They are fabricated using square aluminum tubes of 8 mm external width and 6 mm internal width. Both piles are 250 mm in length and the bottom end of each pile was sealed by an end cap of 14 mm width. Ten pairs of strain gauges (Kyowa KFG-1-120-C1-23, resistance: 120 Ω, gauge factor: 2.1) were attached along the pile shafts to measure the bending moments along one pile (termed 'bending' pile) and axial forces along the other pile (termed 'axial pile'). Figures 3.10 and 3.11 show the configuration and photograph of the model pile, respectively. The strain gauges are protected by a thin layer of epoxy resin for waterproofing. The final external width of each pile shaft is 12.6 mm. The strain gauges was wired and then connected to a TDS-300 strain meter mounted on the centrifuge to form a Wheatstone bridge circuit utilizing the dummy strain gauges provided in the strain meter. Figure 3.12 shows the photograph of the connections of the model pile cables in the strain meter. The 'bending' pile and 'axial' pile were connected to the strain meter with half-bridge mode and quarter-bridge mode, respectively. The detailed connection principles and load-output relations have been elaborated by Feng (2003).

'Bending' pile was calibrated by fastening the pile head with a G-clamp and hanging mass centrally at the pile tip, the strain gauge outputs were then related to the applied bending moments. The 'axial' pile was calibrated by applying load on top of the pile that was rested on a digital balance. The corresponding strain gauge outputs were then related to the applied axial force.

Figures 3.13 and 3.14 show the calibration charts for the two instrumented piles. The calibration factors are noted to be 3.8746 Nmm/microstrain for bending moments and a range of -1.4 to -2.0 3.8746 Nmm/microstrain for axial load strain gauges.

The 'axial' pile head was connected with a short wooden extension coated with smooth paint to facilitate the reflection of laser-rays. The wooden extension was chiseled into the pile head tightly to ensure that it deflects with the pile together.

3.4.4 Model Tunnel

In the present study, the method proposed by Sharma et al. (2001) for the simulation of tunnel excavation in centrifuge flight has been adopted and modified. Figures 3.15 and 3.16 show the configuration and photograph of the model tunnel, respectively. The model tunnel core was made of high-density polystyrene foam. A hot heating wire stretched tightly in a U-frame and two coaxial guide plates (made of stainless steel) were used to cut the foam to a 60-mm diameter circular tunnel shape. The lining of the model tunnel was made of brass foil and manufactured by wrapping a rectangular brass foil around a 60-mm diameter cylinder and soldering the joint with tin solder and an electronical soldering gun. The model tunnel has a length of 200 mm, which is the same as the model container width. At 100g, it represents a 6 m diameter and 20 m long tunnel. Two tubes were inserted to the core foam for subsequent supply and drainage of acetone respectively. The tubes were bound together with the 'supply' tube right below the 'drainage' tube in order to speed up the drainage flows during the in-flight tunnel excavation. To achieve a top-to-bottom excavation sequence, the two tubes were placed just under the crown of the model tunnel so that the dissolving of polystyrene foam was in the order of crown-spring-invert.

3.4.5 Hydraulic-driven valve

The hydraulic valve includes a hydraulic cylinder and a hose with one end connected to the model tunnel and the other end to the acetone container, see Figure 3.5. The rod of the hydraulic cylinder could be controlled to move forward and backward according to the input signal from the control room. The hose was tied with a nut, which could be held on the acetone container by a 'keeper' attached to the free end of the rod. When the 'keeper' was driven out of the acetone container boundary by the rod, the nut would bring down the hose due to both centrifugal gravity and normal gravity. Figure 3.17 illustrates the details of the device and its connections. Figure 3.18 shows the photographs of the hydraulic valve in the 'hold' and 'release' phrases.

The function of the valve is to change the potential level of the hose to achieve holding or releasing acetone automatically. During the 'hold' phrase, the hose was retracted by the rod and 'keeper' to a higher potential level than that of acetone in the container. Hence, acetone was stopped by the centrifugal gravity and remained at its original potential level. On the contrary, pushing the rod forward to enable the hose drop to a lower potential level could release the acetone to the model tunnel.

3.5 Transducers

3.5.1 Pore pressure transducers

Druck PDCR81 miniature pore pressure transducers (PPT) were used to monitor the pore water pressures in the soil during the centrifuge tests. Before each test was carried out, the PPTs were carefully de-aired using an electronic vacuum pump to release trapped air bubbles in the PPTs. Each PPT comes with its own manufacturer's

calibration factor and to confirm the factors, a digital air pump and a multimeter were used to calibrate the PPTs. This was achieved by pumping air into the PPTs and recording simultaneously the air pressure as well as the PPTs output voltage readings measured by the multimeter.

3.5.2 Linear vertical displacement transducers

Midori linear vertical displacement transducers (model LP-50F-61) were used to measure the surface settlements and pile head settlements during the tests. This model has a measuring range of 50 mm and an independent linearity of ±0.2%. The working part of the model consists of a resistant and a rod whose stretch can alter the resistance of the resistant and hence the output voltages. The output voltages are then linearly translated to the measured distance. A round plastic plate is attached to the tail end of the rod to prevent it from penetrating into the clay.

3.5.3 Non-contact laser transducers

NAIS micro laser sensors LM10 (model ANR1250) were used to measure the pile head movements during the tests. This model of sensors has a center point distance (distance between sensor and target) of 50 mm and a measurable range of ±10 mm within the center point distance. The light source comes from a laser diode and has a wavelength 685 nm and beam dimension of 0.6 mm x 1.1 mm at the center point distance. It has a linear resolution of 0.5 μm, which translates to a linear error of 0.5 mm in prototype scale.

The laser sensor has three main components; namely, the sensing body, the relay cable and the controller/display unit. The sensing body houses the laser diode and its

function is to emit laser beam upon connected to a power supply of 24V DC. The relay cable connects the sensing body to the DC power supply. The controller/display unit is used to control and set the measuring limit of the sensor.

Calibration was carried out by attaching securely a 100 mm Linear Vertical Displacement Transducer (LVDT) to the sensing body of the laser sensor. The LVDT was connected to a multimeter so that the digital display of the voltage could be displayed. The LVDT could take up to a maximum of 10 V. Hence, a direct relationship between displacement and voltage could be established, i.e. 1 V per 10 mm movement of the LVDT. The laser sensor has a specified optimum range of measurement to ensure accuracy of the readings. However, readings outside this optimum range can still be measured by the laser sensor but to a lower accuracy.

The output voltage reading on the laser sensor display unit varies with the displacement. Each set of readings of the LDVT and the laser sensor were recorded at every specified displacement intervals so that correlation between displacement and voltage could be established. The calibrated charts for the two laser sensors used in the centrifuge tests are shown in Figures 3.19.

3.6 Image acquisition and analysis

Although the measurements of discrete LVDTs could provide valuable information regarding the ground settlement pattern, a comprehensive insight into the pile responses due to tunneling-induced soil movement would not be obtained without examining the overall subsurface deformations of the soil. An advanced technique of image analysis has been developed at NUS as a method of acquiring soil movement

profiles from high-solution photographic images captured in the centrifuge model tests. Black marker beads which have the highest contrast with the white kaolin were placed on the clay in a 20 mm×20 mm grid to trace the subsurface soil movements induced by tunneling. The beads were pushed into the soil by the highly greased Perspex window of the model container. These beads are made of light PVC and have a flat dual-conical shape so that they could move with the soil freely. Two black dots with known center-to-center distance were marked horizontally on the Perspex window in order to provide reference points to subsequent image analysis. A micro closed circuit TV (CCTV) and a CV-M1 2/3" CCD progressive high scan resolution image processing camera were mounted in front of the Perspex window of the model package. The CCTV was channeled to the monitor TV (see Figure 3.4) in the control room to provide instant in-flight observation during tests. The images were captured by the camera and stored in the onboard PC. They could be retrieved after tests and imported into the OPTIMAS computer program for analysis. Figure 3.20 displays the picture captured by the CV-M1 camera. To cope with various requirements of the images (such as capture frequency, picture resolution and format, etc), the software PCAnyWhere was used to remotely control the image acquisition through the Local Area Network (LAN) when the centrifuge was spinning.

In each test, a series of photographs at different stages of tunnel excavation were selected to examine the soil movements. The image analysis in OPTIMAS produces co-ordinates for the centers of the marker beads, direction and magnitude of the beads movements as well as the information of the model tunnel deformation. Then, the software Surfer was used to plot the vectors of the movements using the foregoing direction and magnitude. The vector plots were finalized by another software Grapher for visualization.

3.7 Experimental procedure

After the completion of the self-weight soil consolidation at high g, the centrifuge was stopped. Both the front and back walls of the container were removed and replaced by two wooden walls with 60 mm-diameter circular openings according to the model tunnel position. A stainless steel tube (60 mm in diameter, 0.8 mm wall-thickness) was used to excavate a cylindrical cavity through the two openings. At the same time, the model tunnel was carefully inserted into the cavity manually. The wooded walls were then removed so that the soil movement beads could be placed on the clay, see Figure 3.5. The container walls were fixed back to the model container after lubricated with vacuum silicon grease. A small opening at the center bottom of the container back wall was used to accommodate the drainage hose of the model tunnel. The hose was fitted to the opening with tape sealant to prevent leakage.

During a test, five LVDTs in a transverse row were used to measure the surface settlement trough. Two non-contact laser transducers were used to measure the lateral deflection of the pile head. The pile settlement was measured by one LVDT resting on the pile head. All the transducers were attached to a stainless steel holder, which was mounted tightly on top of the container with screws.

The model container was then ready for the final set-up. The strain meter, onboard PC, power-supply box of the spotlight and acetone container were assembled on the centrifuge arm. All the transducers were channeled to the junction boxes on the centrifuge platform. The junction boxes functioned as power supplies and data interchange stations for the transducers. The measured data were transferred through the junction boxes to a computer in the control room. The software Dasylab was used

to collect the data at frequent intervals and convert them into format which could be recognized by Microsoft EXCEL.

After all the instruments were assembled in the centrifuge, the signals of the transducers as well as the strain gauges of the model piles were synchronized and tested to verify that they function properly. However, although the signal tests could maximize the quality of data at 1g, a small number of transducers were found to be out of order during some tests at 100g.

Since the organic solvent (Acetone) used in the tests is erosive, the solvent contained was only filled with Acetone just prior to the start of the tests for safety reason. In addition, the solvent container was covered by a plastic bag to avoid the volatilization of Acetone during the reconsolidation of clay.

The entire model package was then spun up to 100g for reconsolidation of the clay. The reconsolidation process normally lasted for 4 hours until the pore water pressure and surface settlement readings stablised. The test proper then began with opening the hydraulic-driven valve was then opened to let the organic solvent to flow into the model tunnel. The tunnel excavation process could be observed through the CCTV camera in the control room. The excavation rate was about 290 m^3 per day in prototype scale. After the polystyrene foam was dissolved, only the brass foil was left in place to simulate the situation of the tunnel lining supporting the soil after tunnel excavation.

In order to study the post-excavation ground deformation and pile responses, the centrifuge would be kept at 100g for additional three hours after the completion of tunnel excavation. All instruments were monitored regularly throughout the entire test.

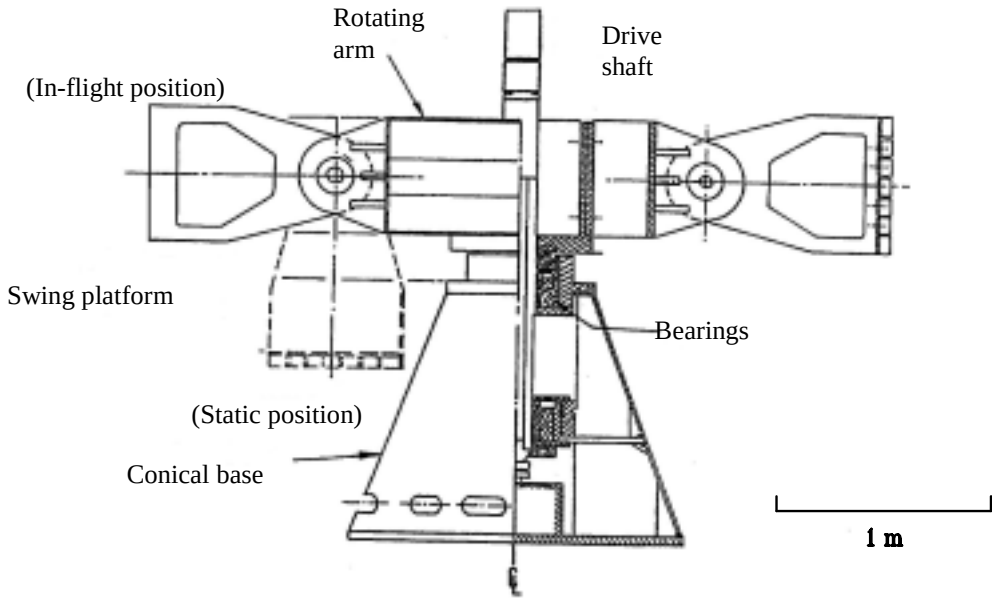

Figure 3.1 Schematic diagram of NUS geotechnical centrifuge

Figure 3.2 Photograph of NUS geotechnical centrifuge

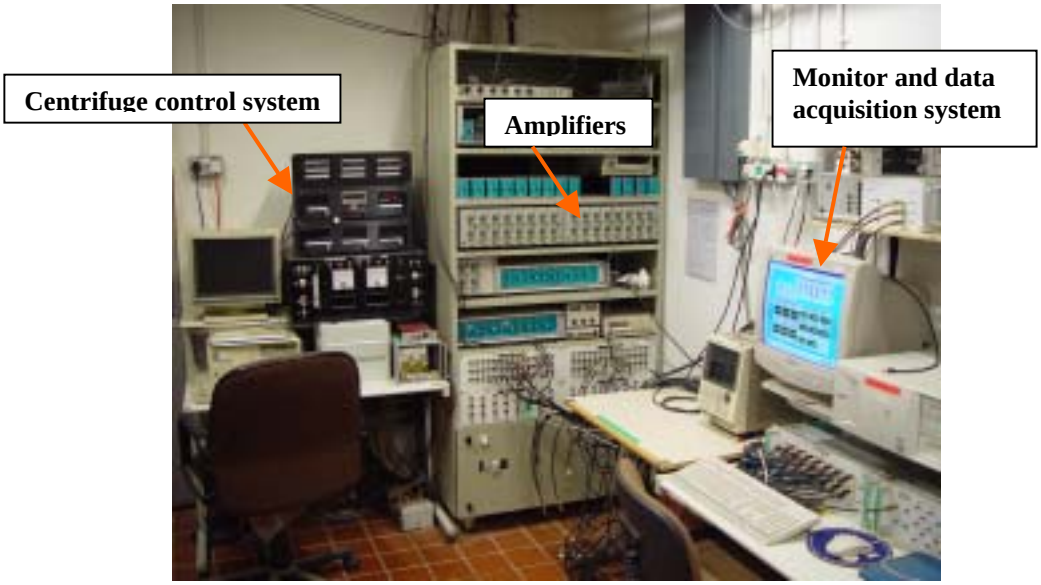

Figure 3.3 Centrifuge control and data acquisition system

Figure 3.4 TV monitors in control room

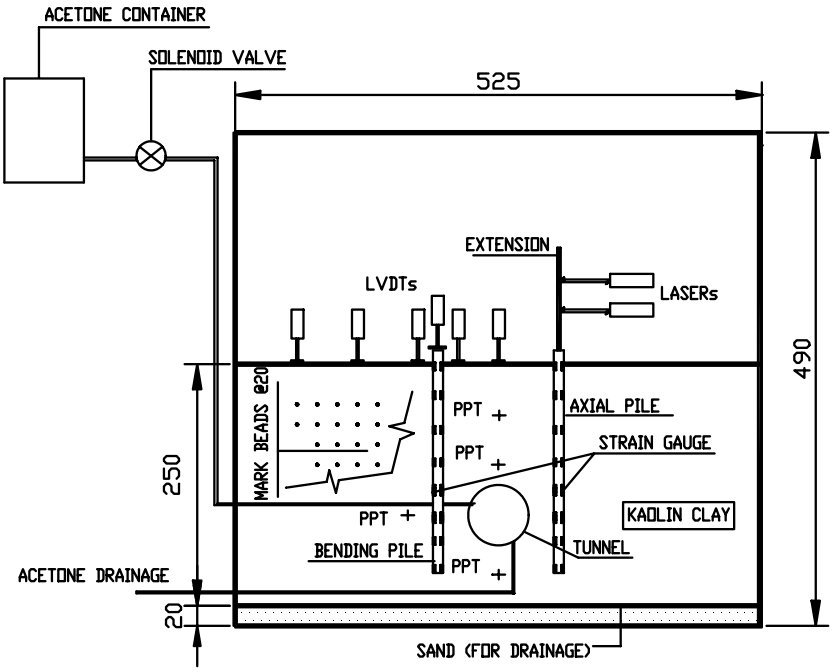

Figure 3.5 Sketch of a typical centrifuge model package (all dimension in mm)

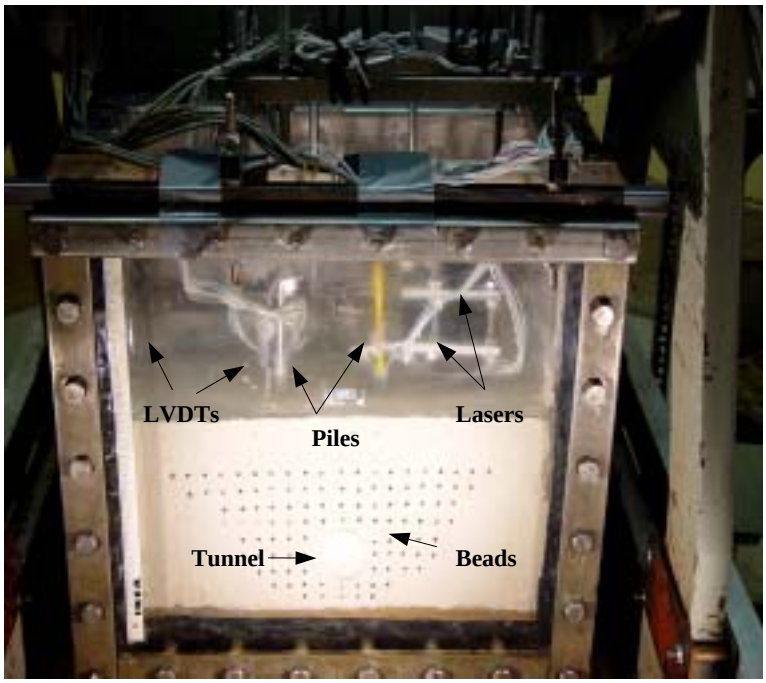

Figure 3.6 Photograph of a typical centrifuge model package

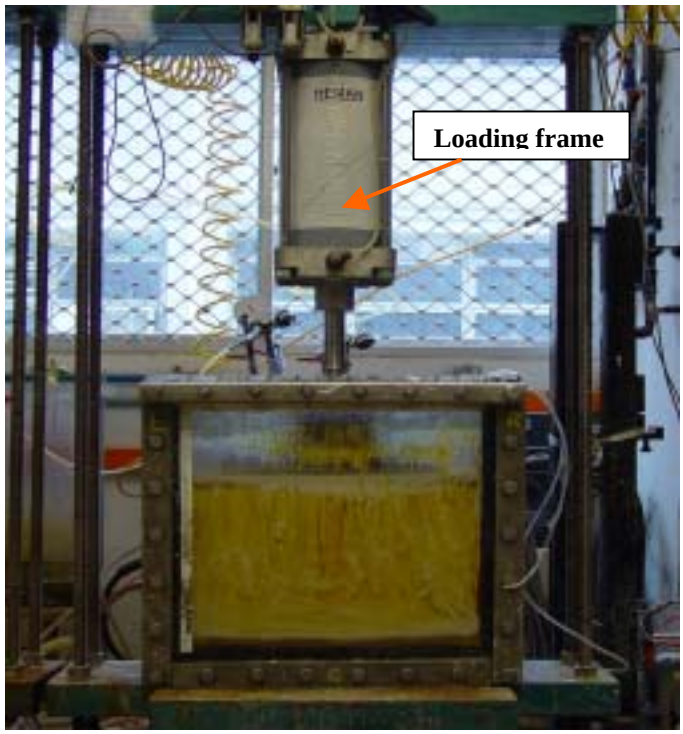

Figure 3.7 Sample preconsolidation in the loading frame

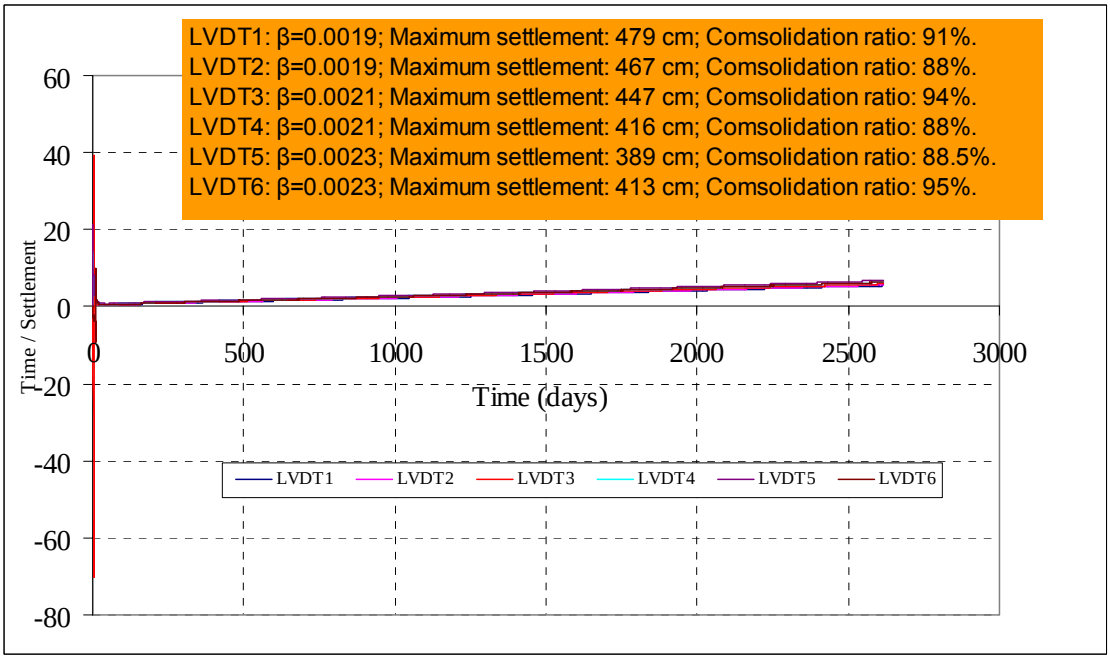

Figure 3.8 Degree of consolidation of model ground at the completion of self-weight consolidation

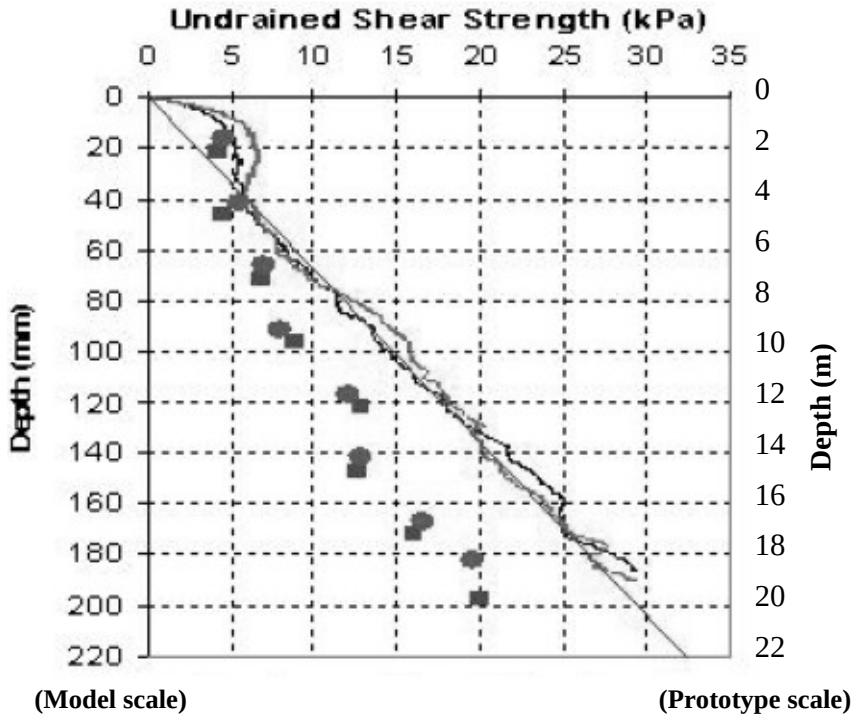

Figure 3.9 In-flight undrained shear strength of clay (Tan 2003)

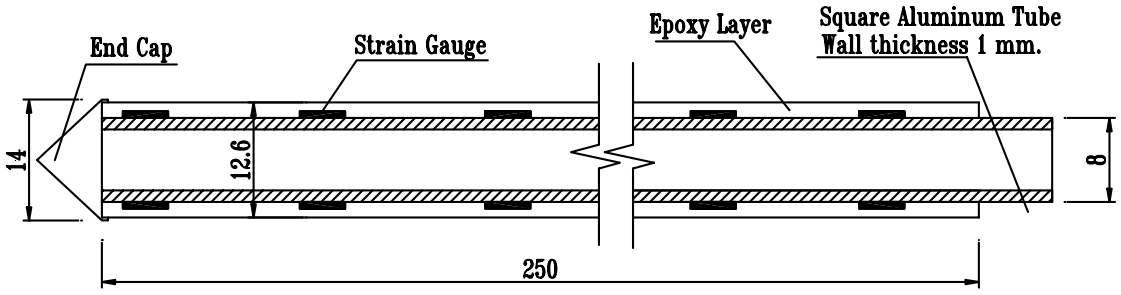

Figure 3.10 Sketch of Instrumented model pile (Dimension in mm)

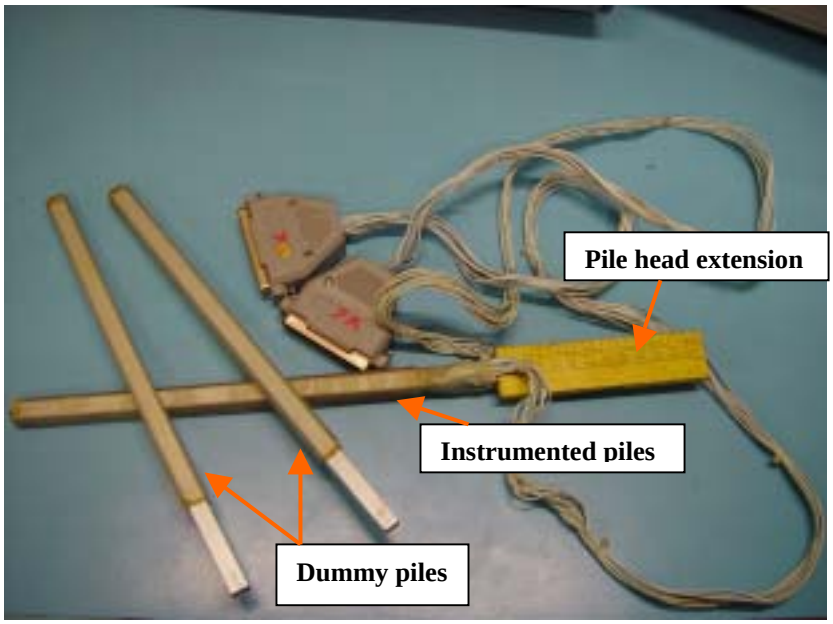

Figure 3.11 Photograph of Instrumented model pile and dummy piles

Figure 3.12 Strain meter connected with model pile cables

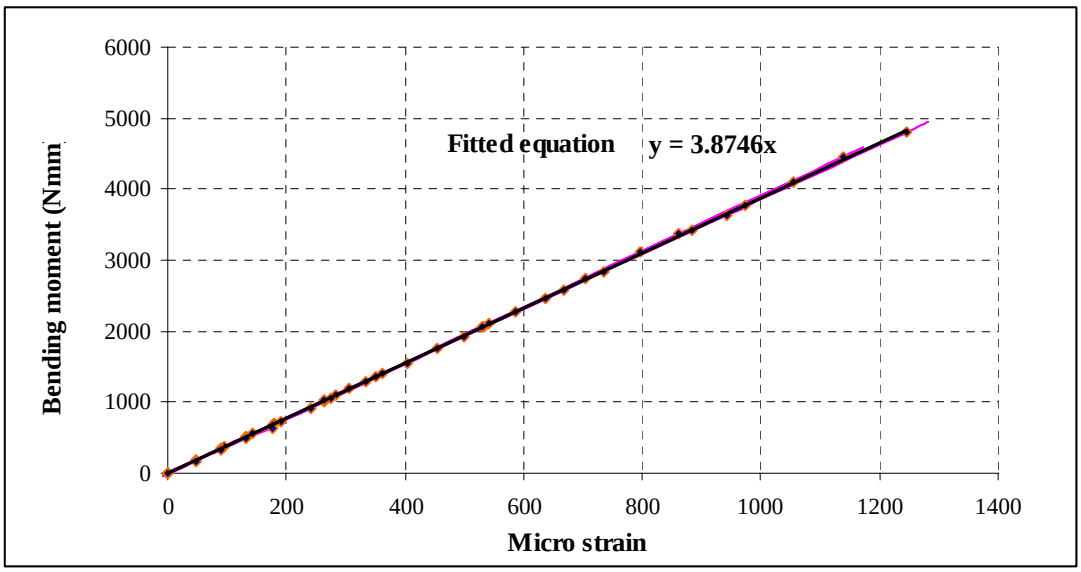

Figure 3.13 Calibration factor of model 'bending' pile

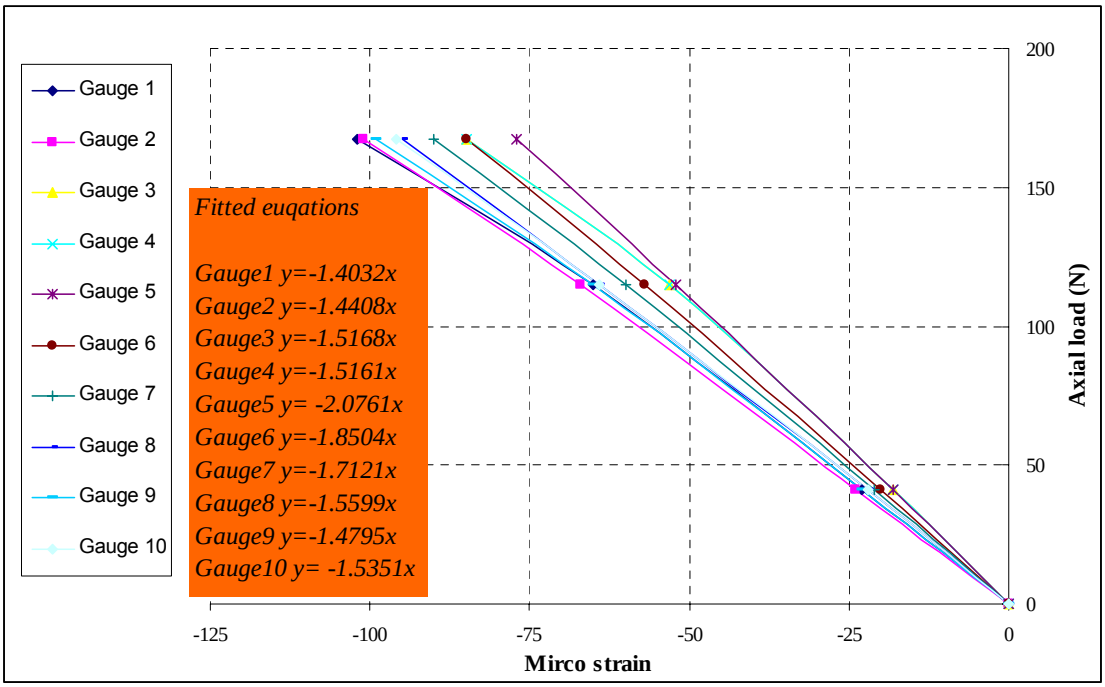

Figure 3.14 Calibration factors of model 'axial' pile

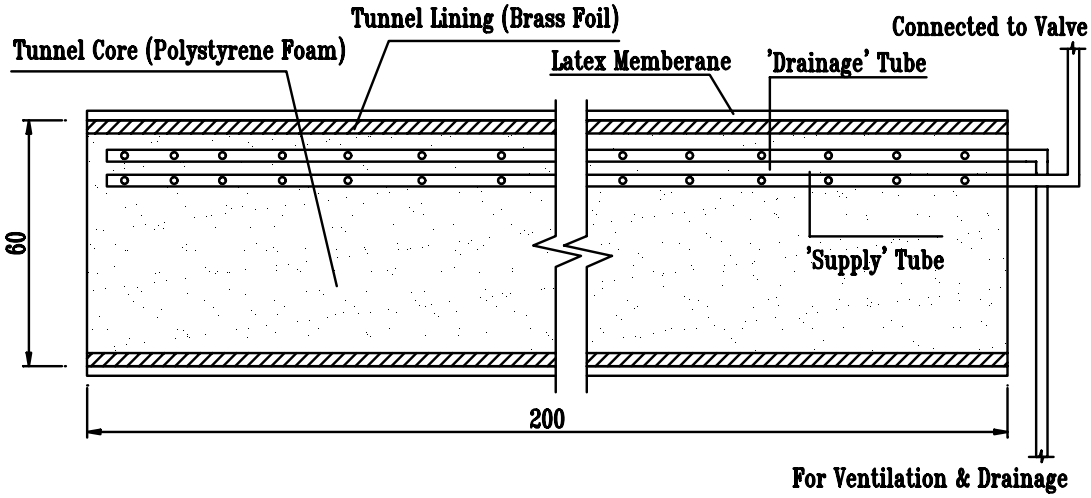

Figure 3.15 Sketch of model tunnel (Dimension in mm)

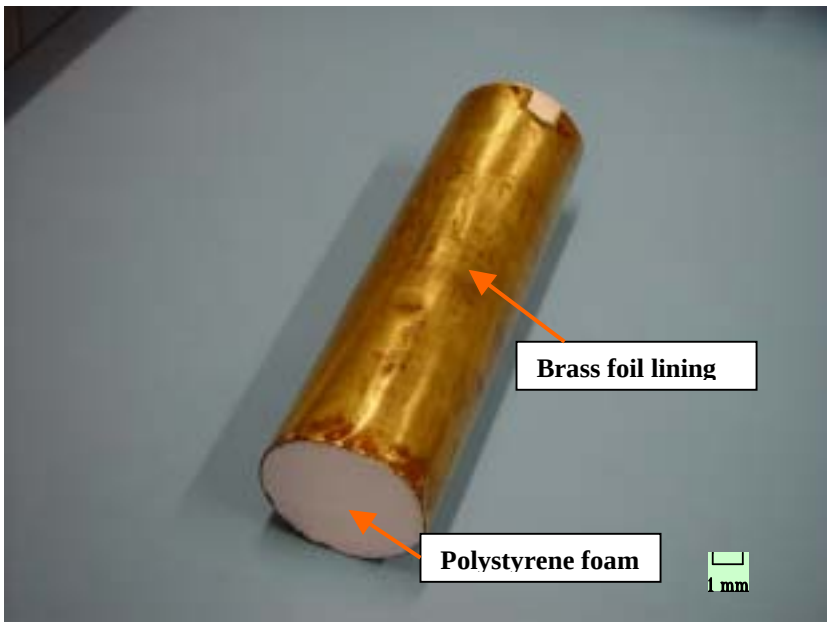

Figure 3.16 Photograph of model tunnel

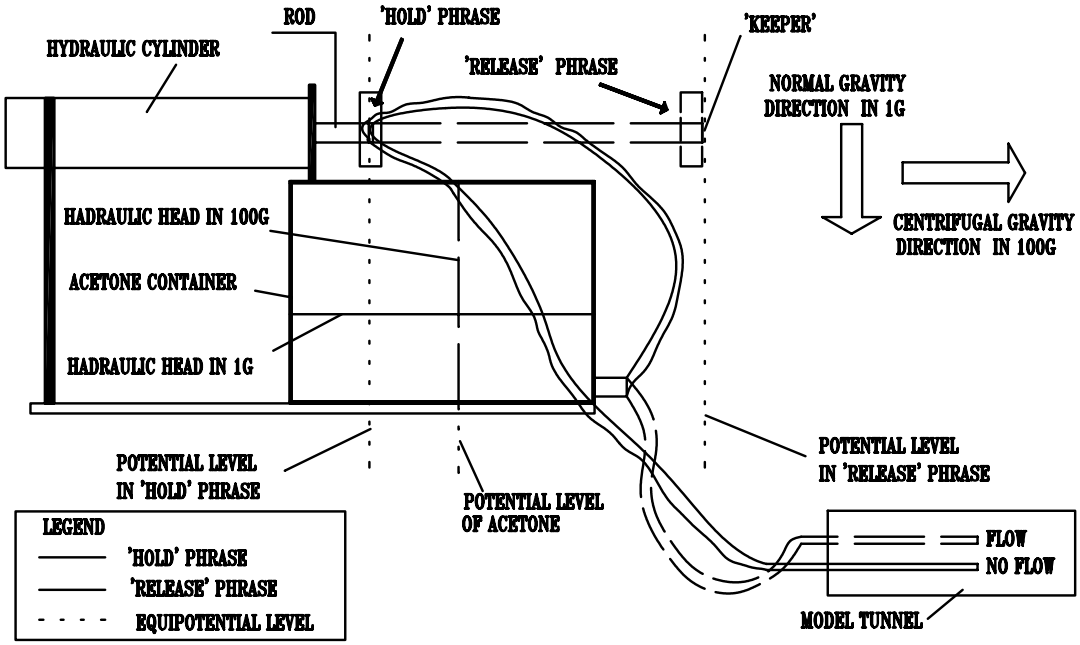

Figure 3.17 Sketch of hydraulic-driven valve

'Hold' phrase 'Release' phrase

Figure 3.18 Photographs of hydraulic-driven valve

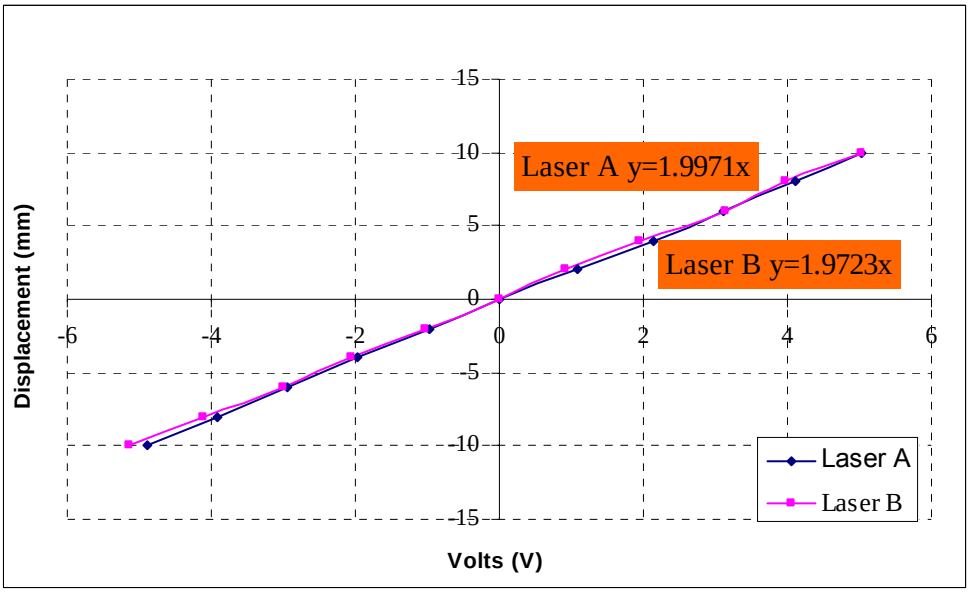

Figure 3.19 Calibration of non-contact laser displacement transducers

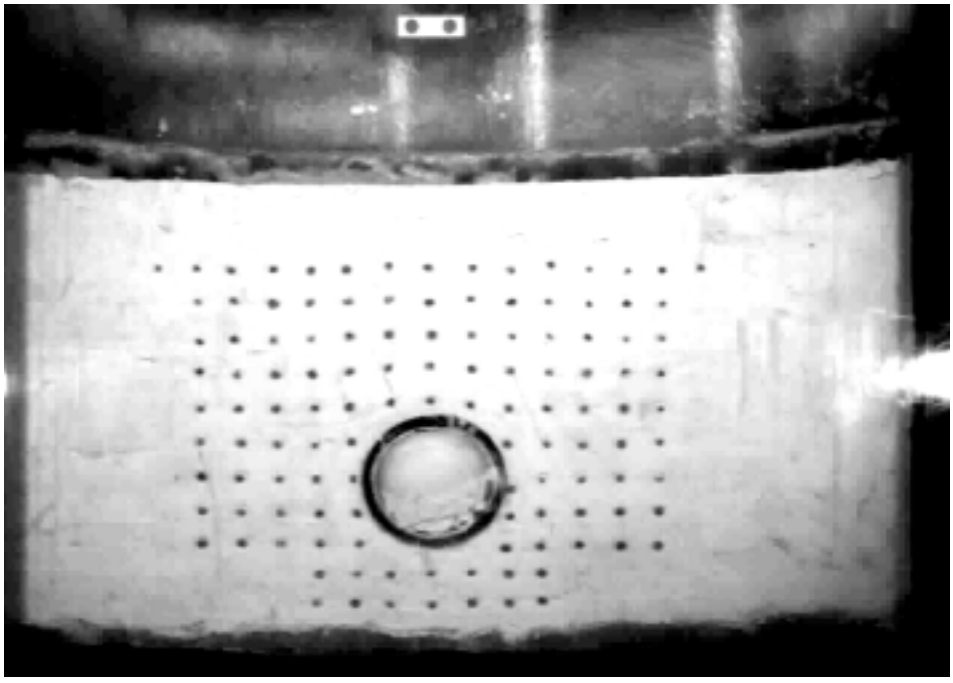

Figure 3.20 Picture captured by CV-M1 2/3" CCD camera

CHAPTER FOUR

TUNNELING-INDUCED SOIL MOVEMENTS AND PILE RESOPNSES

4.1 Introduction

As discussed in Chapter 2, only limited case histories and laboratory tests have been reported on the induced bending moment and axial load on the pile and pile movement due to tunnel construction. Therefore, centrifuge tests were performed in the present study to obtain a better understanding of tunnel excavation induced soil movements on adjacent piles in clay.

4.1.1 Test program

All the centrifuge tests were performed under 100g. Unless otherwise stated, the test configurations and results are presented in prototype scale hereinafter. The complete test program of seven tests for the present study is shown in Figure 4.1. In all the tests, the depth of clay layer and underlying sand layer is 25 m and 2 m, respectively. The tunnel cover C (distance from ground surface to tunnel crown) and tunnel diameter D are also kept constant as 12 m and 6 m, respectively. A pair of free-headed single piles are placed at equidistance at either side of the tunnel to measure the tunneling-induced bending moment and axial load on the piles, except for Test 5 which mainly focuses on the axial responses of very short piles.

In general, the 7 tests can be classified into 3 series, Test series 1 incorporates Tests 1, 2 and 3 conducted using a relatively stiff tunnel lining (EI = 4.88×10^8 kNm^2, equivalent to 30 mm thick steel-ring lining) to investigate the effect of distance of pile from tunnel under similar tunnel volume loss. Long piles with their tips below tunnel spring elevation are simulated in this test series. Test series 2 incorporates Tests 1, 4 and 5 to evaluate the effect of location of pile tip on pile responses under similar volume loss. Results of short piles with their tips at tunnel spring elevation and very short piles with their tips above the tunnel crown elevation are compared with those of long piles. Test series 3 incorporates Tests 1, 6 and 7 to study the effect of volume loss on the pile performances. Results of 3 tests with the same configuration but different volume loss are examined.

As the behaviour of clay is time-dependent, both short-term (immediately at the completion of tunnel excavation, approximately after 2 days of excavation in prototype time) and long-term pile responses were monitored regularly in all the tests.

4.1.2 Sign convention

The sign convention adopted in the present study refers to positive lateral soil movements as inwards towards the tunnel (i.e. contraction tunnel movement). Inward tunnel lining deflection is taken as positive, see Figure 4.2. The deflection of pile towards tunneling side is regarded as positive. The bending moment inducing pile shaft curvature towards the tunnel side is taken as positive. Compression axial load and downward pile vertical movement are regarded as positive.

4.2 Results of Test 1

Detail results of Test 1 are reported here as an illustrative example of a typical test results from the start to the end of a test. The configuration of Test 1 is given in Figure 4.1.

As shown in Figure 3.8, the soil was first consolidated to 90% degree of consolidation in the centrifuge. Owing to soil swelling in the process of tunnel installation at 1g, the soil sample was reconsolidated back to 90% degree of consolidation in the centrifuge before tunnel excavation. This would minimize the ground movement due to unfinished consolidation of the soil sample. The undrained soil shear strength obtained from T-bar tests is shown in Figure 3.9.

4.2.1 Deformation of tunnel lining

Figure 4.2 shows the tunnel crown, spring and invert deflections over time obtained from the image processing analysis of high resolution photographs taken during Test 1 using the procedure described in Chapter 3. At the completion of tunnel excavation (2 days), the tunnel crown settles by 66.1 mm, the invert heaves by 9.2 mm, and the spring protrudes 22.3 mm outwards. The tunnel volume loss based on the lining deformation is determined to be 1.96%. It should be noted that due to the very short model time period of tunnel excavation, no instrument readings can be taken during the process of tunnel excavation. At 720 days after tunnel excavation, the crown further settles by another 22.9 mm; the spring protrudes another 15.5 mm outwards; while the invert drops to 2.3 mm below its original elevation. The tunnel deformations remain fairly constant after 720 days of tunnel excavation.

Figure 4.3 shows the shape of the deformed tunnel lining over time for Test 1. It can be seen that the lining deforms into an oval shape with the tunnel spring lining protruding slightly outwards. This shows that the observed tunnel deformation in the present study resembles the case of tunnel ovalisation presented in Chapter 2.

It is evident from Figures 4.2 and 4.3 that the lining continues to deform over time with a similar ovalisation pattern. This is somewhat similar to the long-term lining deformation reported by Kongpathomporn (2002). The shape of the lining remains practically unchanged after 720 days of tunnel excavation, confirming the lining deformation has stabilized.

4.2.2 Tunnel induced soil movement

4.2.2.1 Subsurface soil movement

Subsurface soil movement was traced from high resolution photographs of the marker beads and analyzed using the computer program OPTIMUS as described in Chapter 3. Figure 4.4(a) shows the vector map of the subsurface soil movements at the end of tunnel excavation (2 days). It is noted that as the soil above the tunnel crown moves downwards, the soil between the tunnel crown and spring elevation gradually moves downwards and intensely away from the tunnel due to the spring line expansion. The soil beneath the tunnel spring line basically moves upwards towards the tunnel but with much smaller magnitudes. This subsurface soil movement pattern is very similar to that of a lined tunnel reported by Atkinson et al. (1975).

At the end of tunnel excavation, the largest soil movements (magnitudes>70% of maximum soil movement, shown in red color in Figure 4.4(a)) are spotted within 0.5

tunnel diameter at above and sides of the tunnel. At all elevations, the maximum soil settlement above the tunnel crown occurs at the tunnel vertical centre-line with the magnitude of settlement reducing from the tunnel crown elevation all the way up to the ground surface. In contrast, the soil movements diminish rather rapidly in the horizontal direction and become negligible (magnitudes<15% of maximum soil movement, shown in green color in Figure 4.4(a)) at an approximate distance of 1D from the tunnel circumference. It is interesting to note that almost all the significant soil movements (magnitudes>40% of the maximum soil movement, in red and blue colors) concentrate in a zone extending roughly from the tunnel spring line to a point on the surface with a offset of 15 m (2i) from the tunnel center, exhibiting a wedge shape.

Figure 4.4 (b) shows the vector map of the subsurface soil movements at 720 days after tunnel excavation. It is found that all the vertical soil movements are downwards whilst the lateral soil movements basically follow the same trend as those in the short-term. This is due to the dual effects of the progressive lining deformation and soil settlement in the long-term. Moreover, the size of the significant soil movement wedge is noted to be slightly wider than that in the short-term.

The measured subsurface soil movements can be transformed to shear strains (not engineering shear strain). Ou et al. (2000) presented the calculation procedure of the strains through soil movements, in which the shear strains were expressed as the half the sum of the angular distortions of soil elements. Figure 4.4 (c) and (d) display the derived shear strain contour for the subsurface soil movements at the end of excavation (2 days) and 720 days after tunnel excavation, respectively. It can be seen that the concentration area of large shear strains associated with tunneling appears to spread

from the tunnel spring line to a region within the upper soil layer. The maximum shear strain at the completion of tunnel excavation, which occurs at the tunnel spring line, is 2.41%. The shear strains outside the region are relatively small in magnitudes and in most cases, 40% less than of those in the region. The observed zone of large shear strains in the present study is wider as compared to the centrifuge test results reported by Kuwano et al. (1998) and finite element prediction by Grant et al. (1997), in which the shear zones were located only in the region of 30° and 60° extending from the tunnel spring line. This is probably attributed to the protrusion of the tunnel spring shearing the local soil as a result of the lining ovalisation. Nevertheless, similar shear band has also been observed in the preceding region in the contour, which is possibly because the soil above the tunnel moves towards the tunnel cavity as a whole block with local shear taking place in the above region, as discussed by Kuwano et al. (1998).

At 720 days after tunnel excavation, the large soil shear strain region extends to a depth of about 5 m above the tunnel crown and a width of about 3 m away from the tunnel spring. However, the maximum shear strain still occurs right aside the tunnel spring line and slightly increases to 3.4%.

Figure 4.5 compares the measured subsurface soil movements derived from the image processing results along the tunnel vertical centre-line with the predictions obtained from the empirical equation proposed by Mair et al (1993). Using Equation 2.4, the trough width factor at 6 different depths of z = 0 m, 4 m, 6 m, 8 m, 10 m and 12 m along the tunnel vertical centre-line is determined to be 6.2, 5.55, 4.9, 4.25 and 3.6, respectively. The corresponding settlements are respectively computed to be 37.5 mm, 41.9 mm, 47.4 mm, 54.7 mm and 64.5 mm, which are fairly close to the measured movements shown in Figure 4.5.

Figure 4.6 compares the measured and predicted (Mair et al, 1993) subsurface settlement troughs at the ground surface and at 4 m and 10 m depths below the ground surface. The propagation of the vertical soil movement trough appears to be an inverted 'half-ripple' shape. The lowest settlement trough, which has the largest magnitude of settlement and smallest trough width, is triggered off by the tunnel lining deformation directly. As reported earlier, the magnitude of soil movement increases with depth. It is postulated that the soil movement wedge above the tunnel crown behaves as an active zone during tunneling and it moves towards the void created by tunneling. The soil beyond the wedge acts like a passive zone as helps to support the wedge. However, the wedge does not settle as a rigid body since it is formed of clay. Thus, the soil in the wedge gradually deforms by arching and at the same time overcomes the resistance of the soil in the passive zone, which leads to the observed trough propagation pattern.

4.2.2.2 Surface soil movement

Figure 4.7 shows the measured surface settlement troughs at different times after tunnel excavation for Test 1. It is noted that the measured short-term surface settlement trough follows the Gaussian distribution curve fairly well. The trough width parameter i of Gaussian curve is determined to be 0.5. It is also noted that after the completion of tunnel excavation, the soil continues to settle with time and the rate of increase in settlement decreases with time. The incremental soil settlements become negligible after 720 days of tunnel excavation. However, Gaussian curve is found to be inappropriate to depict the measured long-term surface settlement troughs. The measured final trough (1080 days) has a somewhat wider parabolic shape than that of Gaussian curve with i = 0.5. Furthermore, Gaussian distribution curve largely

underestimates the measured settlement at the far end of the ground surface, showing that the spread of the surface settlement trough increases over time.

From the preceding comparisons, it is noted that the short-term surface and subsurface soil settlement troughs still follow the Gaussian curve distribution despite the tunnel spring line ovalises. This is consistent to the observation made by Verruijt (1998), as shown in Figure 2.29. For cases with relatively small tunnel ovalisation, the soil above the tunnel crown would settle through a similar vertical path as that for the tunnel contraction. As the tunnel ovalisation considerably increases upon tunnel excavation, the surface settlement trough would be narrower than the Gaussian curve as reported by Verruijt (1996 and 2000).

4.2.3 Pore water pressure

Pore water pressure changes during the tests were recorded by PPTs placed in the soil. In order to minimize the effects of reinforcement to the ground by PPTs, only 4 PPTs were used. The changes of excess pore water pressures for Tests 1, 2 and 3 are shown in Figure 4.8. As expected, most PPTs registered negative excess pore water pressures after tunnel excavation. This is in response to the unloading process of tunnel excavation. However, some positive excess pore water pressures are also registered in Test 3 (PPT 1, 2 and 3) where the PPTs are located very close to the tunnel periphery. It is noted that these PPTs are all in the zone of large shear strains described earlier. Therefore, it is quite likely that the positive excess pore water pressure zone is generated by the large undrained shearing of the clay in this zone. Similar observations were also reported by Schimdt (1989) and Kimura et al. (1994) for tunneling and excavation studies.

Both negative and positive excess pore pressures dissipate with time. The trends of excess pore pressure dissipation reveal that the ground water pressures stabilize at approximately 720 days after excavation. Some PPT readings do not return to the original levels because these PPTs may be dragged down by the soil movement in the long-term.

The above excess pore water pressure changes once again confirm that the behaviour of clay is time-dependent and the soil will continue to move with time as a result of dissipation of excess pore pressures.

4.2.4 Tunnel induced pile responses

Tunnel excavation would induce bending moment, axial force, deflection and vertical movement on the pile. The pile responses due to tunnel excavation induced soil movement for Test 1 are evaluated in this section.

4.2.4.1 Induced pile bending moment and deflection

Figures 4.9(a) and (b) show the development of induced maximum pile bending moment and pile head deflection with time, respectively. It should be noted that the pile head deflection is obtained by geometry from the two displacement readings of the non-contact laser transducers placed on the pile exposed portion. Both induced maximum bending moment and head deflection are noted to increase for some time after the completion of tunnel excavation. Both reach the respective peak values at about 720 days after tunnel excavation, after which they remain practically constant with time. This is consistent with the observed progressive lining deformation and soil movement profiles with time reported earlier.

Figures 4.9(c) and (d) show the induced pile bending moment and deflection profiles with time, respectively. It should be noted that the induced pile deflection profile is derived from the measured pile bending moment profile using the pile head deflection and rotation as the boundary conditions. The induced bending moment is noted to increase with depth and the maximum induced bending moment, which occurs approximately at the tunnel spring elevation, is negative (i.e. the pile bends away from the tunnel). The bending moments at the pile head and tip are zero as they have not been restrained. From the induced pile deflection profile, it can be seen that the pile head and tip move towards the tunnel while the pile waist moves away from the tunnel, forming a bow-shape. This is because the soil moves away from the tunnel at the tunnel spring elevation as a result of lining spring protrusion and hence pushes the pile shaft away from the tunnel. It is also noted that the shape of both bending moment and deflection profiles remain fairly constant over time.

Further evaluation of the pile responses can be obtained using the free-field soil movement at the pile location. Figure 4.10 shows the measured free-field lateral soil movement profiles at 6 m away from the tunnel vertical centre-line at different times. It is observed that the measured lateral soil movement at the pile head moves towards the side of tunnel and then gradually turns to move towards the other side below a depth of about 5 m. The maximum lateral movement occurs approximately at the elevation of the tunnel spring elevation after which the magnitude of movement decreases sharply all the way down to the pile tip. It is noted that the lateral soil movement profile follows roughly a similar trend as the pile deflection profile, showing that the pile basically deforms with the soil in the same manner. However, the magnitude of the pile deflection is much less than that of the soil and the pile deflection profile is also smoother than the soil movement profile due to the large pile

bending rigidity. The lateral soil movement continues to increase with time and reach the maximum values at approximate 720 days after tunnel excavation.

4.2.4.2 Induced pile axial force and pile vertical movement

Figure 4.11 shows the development of pile head settlement with time in Test 1. The pile continues to settle after the completion of tunnel excavation and stabilizes at about 720 days after tunnel excavation. As such, it is evident that the pile settlement is also time-dependent. It should be noted that the ground settlements also stabilize at the same time. Although the ultimate shaft friction may be fully mobilized before 720 days, the pile would keep on settling with the soil until the long-term equilibrium of the ground movement has been established, as postulated by Teh et al. (1995).

As the pile axial forces were measured by 'quarter bridge' strain gauge circuits due to the lack of space in the present study, the long-term strain gauge readings have a tendency to drift with time due to temperature changes. Therefore, the long-term pile axial forces could not be measured accurately and are hence not presented here.

Figure 4.12(a) shows the induced pile axial force profile at the end of excavation (2 days). It is noted that the induced axial load increases downwards from the pile head, and reaches its maximum value at approximate the tunnel spring elevation. Then the pile axial force gradually decreases to the pile tip. Figure 4.12(b) shows the pile settlement profile along the pile shaft at the end of excavation. It should be noted that the pile settlement profile is obtained by incorporating the measured pile head settlement with the elastic shortening of pile back-calculated from the pile axial force. It is noted that the tunnel excavation induced pile movement along the pile shaft is

practically the same as the elastic shortening of the pile is negligible. This is due to the much large axial stiffness of the pile relative to that of the clay. The implication of this phenomenon is that the pile settlement is mainly governed by the pile tip movement.

Figure 4.13 shows the measured free-field vertical soil movement profile at 6 m away from the tunnel vertical centre-line at the end of excavation. The vertical subsurface soil movement profile reveals that there is a neutral plane at about the depth of 15 m below the ground surface where the soil settlement is very close to the pile settlement. Above this plane the soil settles more than the pile, that is, the relative movement between the soil and the pile is downwards and hence the soil drags the pile down to impose negative skin friction on the pile. Below the neutral plane, the soil moves relatively upwards to the pile, which mobilizes positive skin friction along the pile shaft. As a result, negative skin friction is induced from the pile head till the neutral plane with the axial load reaching its maximum value. Below the neutral plane, positive skin friction is mobilized along the pile shaft.

4.3 Effects of pile-to-tunnel distance

Three tests (Tests 1, 2 and 3) were performed in Test series 1 to investigate the behavior of long pile (pile tip well below tunnel) having various pile-to-tunnel distances. The pile-to-tunnel distance is expressed as the ratio of the distance to tunnel diameter (D) hereinafter. Therefore, the pile-to-tunnel distance in Tests 1, 2 and 3 is 1D, 1.5D and 2D, respectively. Using the image processing technique, the tunnel volume loss for Tests 1, 2 and 3 is measured to be 2%, 1.86% and 1.4%, respectively. Other parameters of the three tests can be found in Figure 4.1.

4.3.1 Induced pile bending moment and deflection

Figures 4.14(a) and (b) show the development of maximum induced pile bending moment and pile head deflection with time for the three tests in series 1, respectively. As the tunnel volume loss is not identical in the 3 tests, the maximum pile bending moment and head deflection of Test 2 and 3 are linearly extrapolated to the corresponding values at ground loss of 2% for Test 1. The extrapolated values are also shown in Figure 4.14. Linear extrapolation of pile responses from centrifuge tests in proportion to ground surface volume loss from 1%-2.35% has been performed by Loganathan (1999 and 2000) who found such extrapolation still gave reasonable agreement with numerical predictions by Loganathan (2000). Both induced maximum bending moment and head deflection generally increase for some time after the completion of tunnel excavation in all the tests, exhibiting the time-dependent behaviors described earlier. The pile responses peak at 720 days after excavation. In general, the induced maximum pile bending moment and head deflection decrease with increasing pile-to-tunnel distance both in short-term and long-term.

Figure 4.15(a) and (b) show the normalized maximum pile bending moment and head deflection with pile-to-tunnel distance at various times in Test series 1. The extrapolated maximum pile bending moment and head deflection of the three tests are expressed as dimensionless ratios with those values of Test 1 as the benchmarks. It is noted that both maximum pile bending moment and head deflection drop sharply from 1D to 1.5D by almost 50%. In contrast, the reduction in pile responses becomes less significant from 1.5D to 2D. It appears that the pile lateral responses reduce exponentially with increasing pile-to-tunnel distance. In addition, this exponential

trend remains fairly constant with time, which is probably because the trend of long-term lateral soil movement is very similar to that in the short-term, as reported earlier. Figures 4.16(a) and (b) show the comparison of induced pile bending moment and lateral deflection profiles with time in the three tests. It should be noted that the values given in the figures are original values (i.e. without extrapolation). The pile bending moment profiles in the three tests basically follow a similar shape with maximum bending moments occurring at approximately tunnel spring elevation. This is consistent with the numerical predictions reported by Mroueh et al. (1999). However, it is noted that the profile obtained from Test 1 has a marked protuberance near the elevation of tunnel spring, showing an intense increase in bending moment. On the other hand, the profiles obtained from Test 2 and 3 are obviously 'smoother', showing a more gradual development of bending moment. Figure 4.16(b) reveals that the maximum pile deflection occurs at the pile head for all the three tests due to free-headed configuration.

Figure 4.17 shows the variations of free-field lateral soil movement profiles with time for the three tests. It is noted that the lateral soil movements in the three tests increase with time and decrease with increasing pile-to-tunnel distance. This is consistent with the variations of the observed pile bending moments and deflections in the three tests. Moreover, it can be seen that the lateral soil movement drops rapidly from 1D to 1.5D, while this tendency slows down sharply from 1.5D to 2D. The distinct trends can be related to the active and passive soil movement zones described earlier, as shown in Figure 4.4(a). The transition from the active soil movement zone to the passive soil movement zone takes place for pile-to-tunnel distance between 1D to 1.5D, where the magnitudes of the lateral soil movements decrease rapidly. On the contrary, the lateral soil movements in the passive zone decrease more gradually with increasing pile-to-

tunnel distance. The lateral pile responses, therefore, appear to be closely correlated with the soil movement trend, showing an exponential decrease in magnitude with increasing pile-to-tunnel distance.

4.3.2 Induced pile axial force and pile settlement

Figure 4.18 compares the induced axial load profiles at the end of tunnel excavation (2 days) for the three tests. Long-term pile axial forces are not presented due to the drifting of the long-term axial force gauges readings as presented in Section 4.2. All the induced axial load profiles are similar with the maximum values taking place approximately at the tunnel spring line. This implies that the axial load transfer patterns of the piles are essentially the same irrespective of the pile-to-tunnel distance for a long pile. Similar trend of axial load variation with pile-to-tunnel distance is also reported by Mroueh et al. (1999).

Figure 4.19 shows the development of original and extrapolated pile head settlements with time in the three tests. Once again, the pile head settlement exhibits time-dependent behaviour and reaches its respective peak value at 720 days after tunnel excavation. The magnitude of pile head settlement also decreases with increasing pile-to-tunnel distance.

Figures 4.20(a) and (b) and (c) show the variation of normalized maximum pile axial force, pile head settlement and pile base load (obtained from strain gauges at pile base) with pile-to-tunnel distance at the end of tunnel excavation. Again, an exponential decreasing trend of maximum pile axial force with increasing distance of pile to tunnel can be observed. On the other hand, the pile head settlement and base load appear to

follow a linear relationship with pile-to-tunnel distance. Skempton (1951) proposed a limiting value of $9C_uA_b$ (C_u = undrained soil shear strength at pile base, A_b = area of pile base) for the end-bearing capacity of a circular or square pile with length ≥ 4 diameters. As such, the estimated ultimate pile base resistance is 599 kN using the undrained soil shear strength profile shown in Figure 3.9. It can be found that the pile base loads in these three tests are substantially smaller than the estimated ultimate pile base loads. This indicates that only a small proportion of the base load has been utilized in these tests and hence an elastic deformation state for the soil at the pile base may be assumed. This assumption will be further evaluated in Chapter 5. In addition, both maximum pile axial force and settlement seem to be insignificant for pile-to-tunnel distance larger than 1.5D under a volume loss of around 2% in the present study.

Figure 4.21 shows the free-field vertical soil movement at respective pile locations at the end of excavation (2 days) for the three tests. Similar to the observed lateral soil movements, the vertical soil movements also decrease with increasing offset from the tunnel vertical centre-line and become more uniform further away from the tunnel. This is consistent with the observed variations of pile axial forces in the three tests. It is also noted that the neutral plane concept described earlier can be well-verified by the free-field vertical soil movements in the three tests as all the neutral planes are located approximately at the depth where soil settlement is close to the pile settlement. Moreover, these neutral planes all exist at about the tunnel spring elevation where the maximum pile axial force occurs. The results again confirm that the maximum pile axial force takes place at the neutral plane elevation located at about the tunnel spring elevation, irrespective of pile-to-tunnel distance.

4.4 Effects of location of pile tip

4.4.1 Short pile (Test 4) versus long pile (Test 1)

Test 4 was conducted using a short pile (pile tip located at tunnel spring elevation of 15 m) with the same pile-to-tunnel distance as the long pile (23.5 m) in Test 1 to study the effects of pile tip location relative to the tunnel. The tunnel volume loss for Test 1 and 4 is 2% and 1.23%, respectively. Detailed test parameters of Test 4 can be found in Figure 4.1.

4.4.1.1 Induced pile bending moment and deflection

Figures 4.22(a) and (b) show the induced pile bending moment and deflection profiles of Test 4 with time, respectively. It should be noted that the original values have been presented in the figure. The maximum bending moment of the short pile occurs at approximately 3 m above the elevation of the tunnel spring line instead of at the tunnel spring line as in the long pile case. The pile deflection profile of the short pile is marked different from that of the long pile. The short pile seems to have rotated. This is probably due to the large lateral soil movement (Figure 4.23) around the pile tip that pushes the lower half of the pile away from the tunnel and as a result, the upper half of the pile tilts toward the tunnel since the pile head is not restrained. In contrast, although the long pile experiences a similar large lateral soil movement around the tunnel spring elevation, the soil below the tunnel spring line hardly moves. Therefore, it can sufficiently 'lock' the pile tip in place so that the lower part of the long pile is bent back, forming a bow-shape.

Figures 4.24(a) and (b) show the development of induced maximum pile bending moment and pile head deflection with time in Tests 1 and 4, respectively. The

extrapolated values are also shown in Figure 4.24. It is evident that the maximum bending moment of the short pile is slightly less than that of the long pile. Similar findings were also reported by Chen (1999). In contrast, the deflection of the short pile head is significantly larger than that of the long pile. This implies that the short pile is more critical in term of lateral deformation than long pile upon tunnel excavation.

4.4.1.2 Induced pile axial force and pile vertical settlement

Figure 4.25 shows the induced pile axial force profile of Test 4 at the completion of tunnel excavation (2 days). It can be seen that negative skin friction has developed along the full shaft and reaches its maximum value at the pile base in the short pile case. It is noted that the maximum axial force of the short pile is less than that of the long pile (Figure 4.12(a)). Figure 4.26 shows the vertical soil movement at the completion of excavation at the pile location in Test 4. It is evident that the neutral plane does not exist in the short pile case as the soil settles more that the pile along the entire pile shaft. Therefore, the relative soil/pile movement is downwards and in turn drags down the entire pile shaft, imposing negative skin friction on the entire pile.

Figure 4.27 shows the development of pile head settlement with time in Test 1 and 4, respectively. It is evident that the pile head settlement of the short pile is significantly larger than that of the long pile. Moreover, the long-term settlement of the short pile is much larger than that of the long-pile. Thus, it is evident that the settlement of a short pile is more critical than a long pile associated with tunnel excavation in both short-term and long-term.

4.4.2 Very short pile in a large settlement zone

Jacobsz (2002) proposed a large settlement zone for piles at volume losses beyond 1.5% in sand. Similar large settlement zones were also observed in studies by Cording et al. (1975) and Morton et al. (1979) in sand. This zone is defined by a line extending upwards at an angle 45°+Ø/2 (Ø is the friction angle of sand) from the spring line of the excavated tunnel boundary to the ground surface. This zone was further sub-divided by Jacobsz (2002) according to the amount of settlement that the piles undergo at 1.5% volume loss as compared to the surface settlement. Piles with their bases installed in zone D settle less than the ground surface. Piles with their bases in zone B, settle more than the surface. In zones A and C, the pile and surface settlements are similar.

To examine the applicability of the above large settlement zone in clay, Test 5 was conducted to investigate the pile settlements inside and outside of the zone. Figure 4.28 illustrates the subdivided zones and respective pile locations in Test 5. For undrained cases in clay, the angle 45°+Ø/2 is 45° as Ø is zero. Therefore, the subdivided Zone C in sand is not appropriate to be included in the case of clay. Hence, the Zone B and C in sand are combined as Zone B in the clay case in Test 5. As such, only three zones (A, B and D) are to be studied in Test 5. Three piles (one instrumented and two dummy piles) are placed in Zone A, B and D, respectively in order to compare the pile settlements in these zones. The instrumented pile (pile A) is placed right above the tunnel crown (Zone A) to study the pile axial force in this region. The bending moment of pile A is not measured in this test as the pile is placed at the centre-ling of the tunnel and hence not expected to bend

Figure 4.29 shows the induced axial force profile of the instrumented pile for Test 5 at the end of tunnel excavation (2 days). It is noted that negative skin friction is

developed along the full shaft and the pile axial force reaches its maximum value at the pile base. This is very similar to the short pile case (Test 4) and also consistent with the vertical soil movement profile at the pile location where the soil settles more that the pile along the entire pile shaft.

Figure 4.30 shows the pile head settlement of the three piles in Test 5 with time. It is noted that the pile in zone D (see Figure 4.28) experiences negligible settlement compared with the two piles in Zones A and B. Moreover, both pile settlements in Zone A and B are significantly larger than the piles in Tests 1 to 4 whose tips are beyond the large settlement zone. These findings concur with the features of the large settlement zone described for sand by Jacobsz (2002). As such, it is evident that this large settlement zone may also be applicable for clay. However, as the trough width of clay is generally larger that of sand as reviewed in Chapter 2, the large settlement zone in clay is noted to be wider than that in sand.

The shape of the large settlement zone is essentially very similar as the soil wedge above the tunnel described earlier in this chapter. This wedge behaves like an active soil movement zone and the soil settlements in this block are relatively large. Therefore, piles whose tips are located in this zone would be dragged down by the large soil movements, resulting in large pile settlements. On the other hand, piles with their tips located out of the zone would experience smaller soil/pile interaction and hence less pile settlement as the soil movements beyond the large settlement zone are relatively small. It should be noted that the final two pile settlements in the large settlement zone are different and in excess of 40 mm, which could result in serious damages to the structures. The practical implication of the finding is to avoid tunneling excavation where the tip of existing pile foundations lies within the large settlement

zone. If such a scenario could not be avoided, special attention must be paid in the design stage.

Figure 4.31 shows the ratio of pile settlement versus surface settlement at pile location with time of the three piles in Test 5. It is noted that all the pile settlements are less than the surface settlements at their locations, which is different from the pile settlements in the subdivided zones described by Jacobsz (2002). This is probably because of the absence of working load on the piles in the present study. As the pile working load acts in the same direction as the tunneling-induced negative skin friction, it should increase the pile settlement by a certain extent. However, as the pile working load differs considerably in practice, it may not be practical to draw a general conclusion on the relation between pile settlement and surface settlement as attempted by Jacobsz (2002). Furthermore, the ratio of pile settlement/surface settlement in all three piles decreases and converges to a similar value with time. This suggests that this ratio is also time-dependent for clay and could not be simplified as that in sand.

From Figures 4.30 and 4.31, it is noted that both the pile settlement and ratio of pile settlement/surface settlement in Zone B are larger than those in Zone A. Similar observations are also reported by Jacobsz (2002) for sand. As the large settlement zone coincides with the active soil wedge as well as zone B is located near the edge of the wedge, this phenomena is somewhat related to the sliding plane of the soil wedge.

Figure 4.32 shows the comparison of the soil wedge in case of tunneling and excavation. It is noted that the soil wedge in tunneling is similar to the Rankine active sliding wedge in an excavation. In both cases, the angle of the sliding wedge is 45°+Ø/2 for sand and 45° for clay. Piles with their tips located near the sliding line, as

the pile in zone B, act like reinforcements to the wedge and prevent it from moving down. Therefore, significant loads can be attracted to these piles which could lead to intense soil/pile interactions and large pile settlements. This is similar to the soil nails reinforced across the sliding plane of slopes, whose loads and deformations are always of top concern.

However, it is also noted that the pile settlement in Zone B is significantly larger than that in Zone A in sand as reported by Jacobsz (2002), refer to Table 2.3, while in clay the pile settlement in Zone A is only marginally greater than that in Zone B. This is probably attributed to the dilation of sand caused by the soil shearing near the sliding plane. This dilation of sand can greatly reduce the sand stiffness and hence the pile base resistance, which is observed in Jacobsz's tests where the piles with their tips in zone B experience larger base load reductions than piles in zone A. However, as the soil used in this study is normally consolidated clay, the soil along the sliding plane is unlikely to dilate upon soil shearing. Therefore, the pile base resistance may not be affected as severely as that in sand and this results in a smaller differential pile settlements in Zone A and Zone B.

4.5 Effects of volume loss

Three tests (Tests 1, 6 and 7) are carried out using tunnel linings of different stiffness (see Table 4.1) in Test series 3 to investigate the behavior of long piles under various volume losses. The pile-to-tunnel distance and pile length are kept constant in the three tests as 6 m and 23.5 m, respectively. As the model tunnel collapsed after excavation in Test 7, only short-term tunnel induced ground and pile behaviours were studied in this test. This is because a tunnel collapse incident is always followed by immediate

ground treatments to minimize the adverse impacts on adjacent structures and consequently the pile responses in the long-term would be affected by these ground treatments, which have not been simulated in this test.

Table 4.1 Lining stiffness and volume loss (Test 1, 6 and 7)

Test No.	1	6	7
Stiffness of tunnel lining (EI) kNm^2	4.9×10^8	4.2×10^8	1.9×10^8
Tunnel volume loss	2%	4.2%	26.2% (collapse)

4.5.1 Deformation of tunnel lining

Figure 4.33 shows the tunnel lining deflection over time for Tests 1 and 6. It is noted that the tunnel linings in both tests deform in a similar ovalisation pattern over time (see Figure 4.3) but the magnitude of lining deflection of Test 6 is significantly larger than that of Test 1. Together with Table 4.1, it is evident that tunnel volume loss increases with decreasing lining stiffness in the present study.

To examine the deformation of collapsed tunnel lining in Test 7, the tunnel lining was carefully removed after the test. The periphery of the deformed lining was first traced on a graph paper. The software AutoCAD was then employed to reproduce the lining deformation as shown in Figure 4.34. The volume loss back-calculated from the lining deformation is 26.5%, which is slightly less than the measured ground surface volume loss of 28.2%. This indicates that the collapsed lining hardly rebounded after the centrifuge spun down and it can be used to depict the final in-flight lining deformation. It can be seen that the weak lining has been squeezed into a 'heart' shape with crown deeply caved in and spring shrank inwards. The maximum crown settlement and spring

shrinkage were 2.2 m and 0.36 m respectively. Similar failure mode of a lined tunnel in clay was also reported by Atkinson et al. (1975).

4.5.2 Tunnel induced soil movement

4.5.2.1 Subsurface soil movement

The subsurface soil movement profile of Test 6 essentially follows a similar pattern as that in Test 1, see Figures 4.4(a) and (b) and is hence not presented here. However, it is noted that the magnitude of subsurface soil movement in Test 6 is much larger than that in Test 1 as a result of the larger tunnel volume loss of Test 6.

On the other hand, as the large soil movement induced by the collapsed tunnel in Test 7, some of the marker beads are buried by the soil in this test. Therefore, accurate imaging processing analysis is not possible. However, the trend of the soil movement could still be observed by examining the exposed beads. It is found that the lateral soil movement in the vertical section near to the tunnel is basically towards the tunnel side (i.e. convergent movement). The vertical soil movement above the tunnel spring line is downwards, whereas the soil below that moves slightly upwards. This subsurface soil movement pattern is consistent with the lining deformation in this test. It should be noted that the induced lateral soil movements in the collapsed tunnel case is opposite to that of the stable lining. This is due to the lining spring shrinks inwards in case of tunnel collapse, while the lining spring expands outwards as a result of the ovalisation of the stable lining.

4.5.2.2 Surface soil movement

Figure 4.35 shows the surface settlement trough and the comparison with Gaussian curve at various times in Tests 1, 6 and 7. The long-term surface settlement trough of Test 7 is not shown here due to the reason stated earlier. It is noted that all the measured short-term surface settlement troughs for the three tests follow the Gaussian distribution curve reasonably with i = 0.5. This is somewhat similar to the observations of tunnel excavation in clay reported by Grant et al. (1998) where the form of surface settlement troughs and the trough widths do not change with volume loss up to 20%. However, it is also observed in Test 7 (collapsed case) that Gaussian curve significantly underestimates the measured surface settlement at the far end of the ground surface. This is probably due to the cave-in of the lining crown that widens the surface settlement trough. On the other hand, both the measured long-term surface settlement troughs in Tests 1 and 6 show a slightly wider parabolic shape than that of Gaussian curve as described in Section 4.2.2.2.

4.5.3 Induced pile bending moment and deflection

Figure 4.36(a) shows the induced pile bending moment profiles for Tests 1, 6 and 7. It is noted that Tests 1 and 6 share a similar bending moment profile with maximum bending moment being negative and at approximately the tunnel spring elevation. However, the bending moment of the collapsed case (Test 7) has a somewhat 'mirrored' profile as those of Test 1 and 6. The maximum induce pile bending moment of Test 7 is positive in sign although it still occurs at the depth of tunnel spring elevation. This is because the lateral soil moves in an opposite direction for stable and collapsed lining cases as described in Section 4.5.2.1. It is noted that all the maximum induced bending moments are below the pile bending moment capacity (3000 kNm).

Figure 4.36(b) shows the induced pile deflection profile for Tests 1, 6 and 7. The results again confirm that the pile is bent in opposite directions for the stable lining and collapsed lining conditions. Moreover, it is observed that the pile in Test 7 is not only bent but also translated toward the tunnel, whereas the piles do not translate in Tests 1 and 6. This phenomenon is related to the different lateral soil movement patterns for the two cases. In the collapsed case, all the lateral soil movement in the pile location is towards the tunnel due to the shrinkage of tunnel lining. The pile is therefore pushed by the soil towards the tunnel since it is not restrained at both ends. In contrast, the soil above and along the tunnel spring elevation in the stable lining case moves away from the tunnel as the tunnel lining ovalises, whilst the soil below moves towards the tunnel in response to ground unloading. As a result, the pile is bent back along the shaft below the tunnel spring elevation and hence 'locked' in place.

Figures 4.37(a) and (b) show the variation of maximum pile bending moment and head deflection with volume loss at the end of excavation (2 days) in Test series 3. As expected, both the maximum pile bending moment and head deflection increase with volume loss. However, it is noted that the rate of increasing decreases with increasing volume loss particularly from 4.2% to 28.2%. This is probably due to the fact that the soil has exhibited plastic behaviors under relatively large volume loss and the lateral soil pressure acting on the pile reaches the limiting value. Nevertheless, it should be noted that the maximum induced pile bending moment and head deflection in the tunnel collapsed test are significant and may threaten the structural integrity of the pile which is normally not designed to resist lateral load and deflection of such magnitude.

4.5.4 Induced pile axial force and vertical settlement

Figure 4.38 shows the induced pile axial force profile at the end of tunnel excavation (2 days) for Tests 1, 6 and 7. It is noted that the induced axial load in all three tests increases downwards from the pile head, and reaches their respective maximum value at approximate the tunnel spring elevation, revealing that the axial load transfer pattern along the pile is virtually the same for the three tests regardless of tunnel volume loss. All the measured maximum pile axial forces are well below the pile axial load capacity of 2500 kN.

Figure 4.39(a) shows the variation of maximum pile axial force with volume loss for Tests 1, 6 and 7. Again, an increasing trend of maximum pile axial force with tunnel volume loss can be observed and the rate of increase also decreases with increasing volume loss. This may be attributed to both soil plastic behaviour and pile/soil slip under relatively large volume loss. To further evaluate the pile axial force in the tunnel collapsed case, a method of determining the ultimate shaft friction P_{su} in clay proposed by Vijiayvergiya et al. (1972) is adopted here. The ultimate shaft friction P_{su} can be expressed as follow:

$$P_{su} = \lambda(\sigma_m^{'} + 2c_m)A_s \tag{4.1}$$

where

$\sigma_m^{'}$ = mean effective vertical stress between ground surface and pile tip;

c_m = average soil undrained shear strength along pile;

A_s = pile surface area;

λ = dimensionless coefficient.

As the axial force of the long pile in this test are subjected to both negative and positive skin friction due to tunnel excavation, $\sigma_m^{'}$ is determined to be the mean effective vertical stress between the ground surface and the point of maximum pile axial force to calculate the pile axial force at the location of the neutral plane. λ is determined to be 0.2 according to the λ versus pile penetration chart (Figure 4.40). $\sigma_m^{'}$ and c_m can be obtained from the soil density and the undrained shear strength profile. Therefore, the computed pile shaft resistance above the pile neutral plane is 1220 kN, which is fairly close to the measured pile maximum axial force of 1292 kN. This indicates that the ultimate pile shaft friction has been fully mobilized along the pile shaft. As such, it is evident that full pile/soil slip has occurred along the pile shaft above the neutral plane in the tunnel collapsed case. However, it should be noted that 28.2% is not necessary the volume loss for full pile/soil slip to occur as only three volume losses are investigated in the present study. Full pile/soil slip may occur at a smaller volume loss.

Figure 4.39(b) and (c) shows the variation of measured pile head settlement and base load with volume loss for Tests 1, 6 and 7. It is observed that both the pile head settlement and base load increase with volume loss. However, it is found that the rate of increase in pile head settlement increases with increasing volume loss. As the pile head settlement is governed by the pile base load as described earlier, it is noted that the increasing rate of pile head settlement is due to the soil plastic behaviors under large pile base load. The relation between pile settlement and base load will be further analyzed in Chapter 5. Moreover, it should be noted that for the tunnel collapsed case (Test 7), the pile base load (577 kN) is very close to the estimated ultimate pile base

resistance of 599 kN. The pile head settlement of 96 mm is also considerably large, revealing that the pile axial responses during tunnel collapse are critical as well.

<table>
<tr><th colspan="4">Test series 1 Effect of distance of pile from tunnel with similar volume loss</th></tr>
<tr><td>Test No.</td><td>Configuration</td><td>Common parameters</td><td>Individual parameters</td></tr>
<tr><td>1</td><td rowspan="3"> 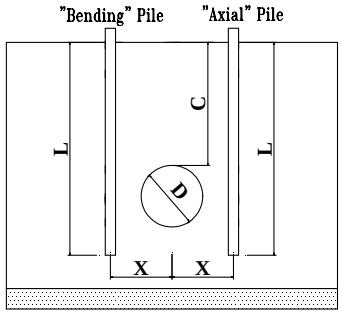
</td><td rowspan="3">C = 12 m
D = 6 m
L = 23.5 m</td><td>X = 6 m
Volume loss = 2.0 %</td></tr>
<tr><td>2</td><td>X = 9 m
Volume loss = 1.86%</td></tr>
<tr><td>3</td><td>X= 12 m
Volume loss = 1.4 %</td></tr>
<tr><th colspan="4">Test series 2 Effect of location of pile tip with similar volume loss</th></tr>
<tr><td>Test No.</td><td>Configuration</td><td>Common parameters</td><td>Individual parameters</td></tr>
<tr><td>1</td><td rowspan="3"> 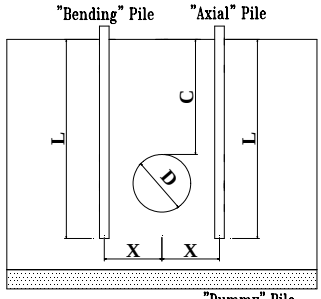

 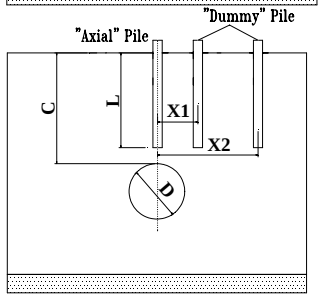
</td><td rowspan="3">C = 12 m
D = 6 m</td><td>X = 6 m
L = 23.5 m
Volume loss = 2.0 %</td></tr>
<tr><td>4</td><td>X = 6 m
L = 15 m
Volume loss =1.23 %</td></tr>
<tr><td>5</td><td>X1 = 5 m
X2 = 17 m
L = 10 m
Volume loss = 1.76 %</td></tr>
<tr><th colspan="4">Test series 3 Effect of volume loss</th></tr>
<tr><td>Test No.</td><td>Configuration</td><td>Common parameters</td><td>Individual parameters</td></tr>
<tr><td>1</td><td rowspan="3"> 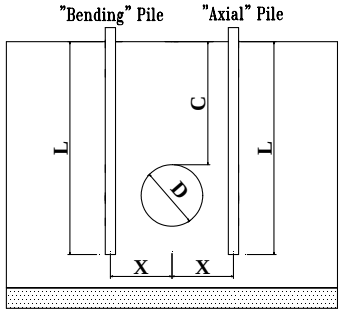
</td><td rowspan="3">C = 12 m
D = 6 m
L = 23.5 m
X = 6 m</td><td>Volume loss = 2.0 %</td></tr>
<tr><td>6</td><td>Volume loss = 4.2%</td></tr>
<tr><td>7</td><td>Volume loss = 28.2 %</td></tr>
</table>

Figure 4.1 Test program and parameters

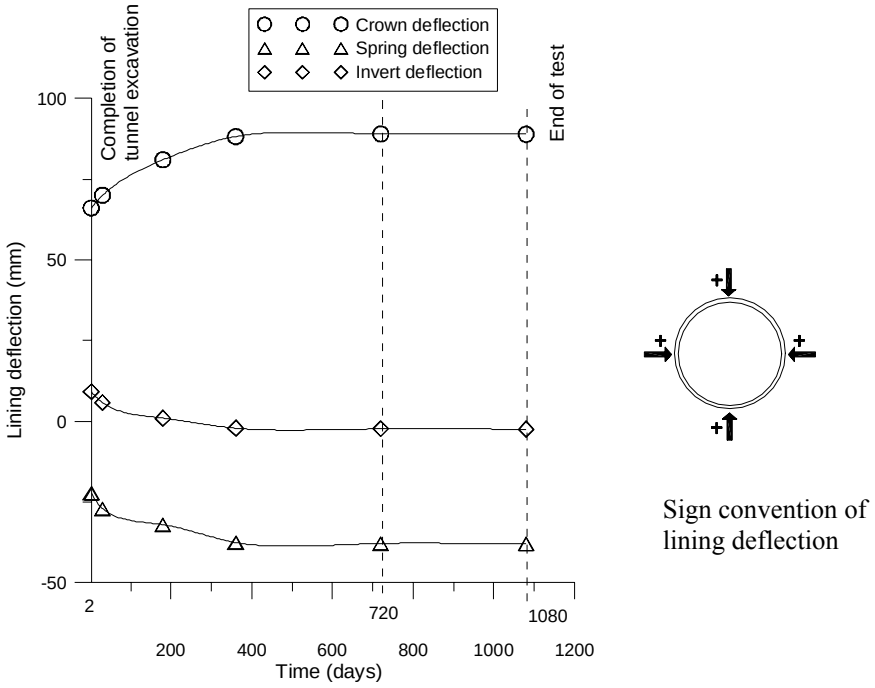

Figure 4.2 Tunnel lining deflection (Test 1)

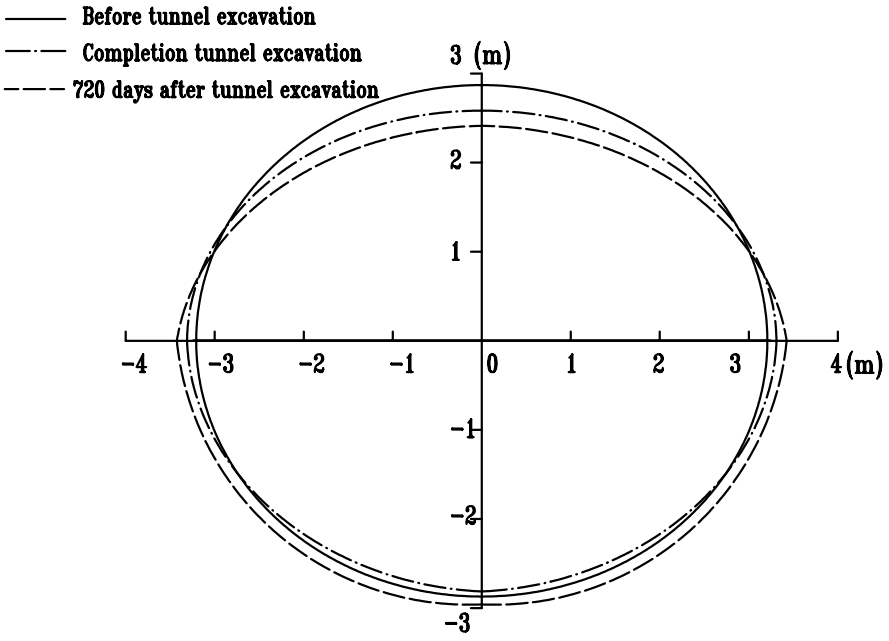

Figure 4.3 Simplified tunnel lining deformation with time for Test 1 (not to scale)

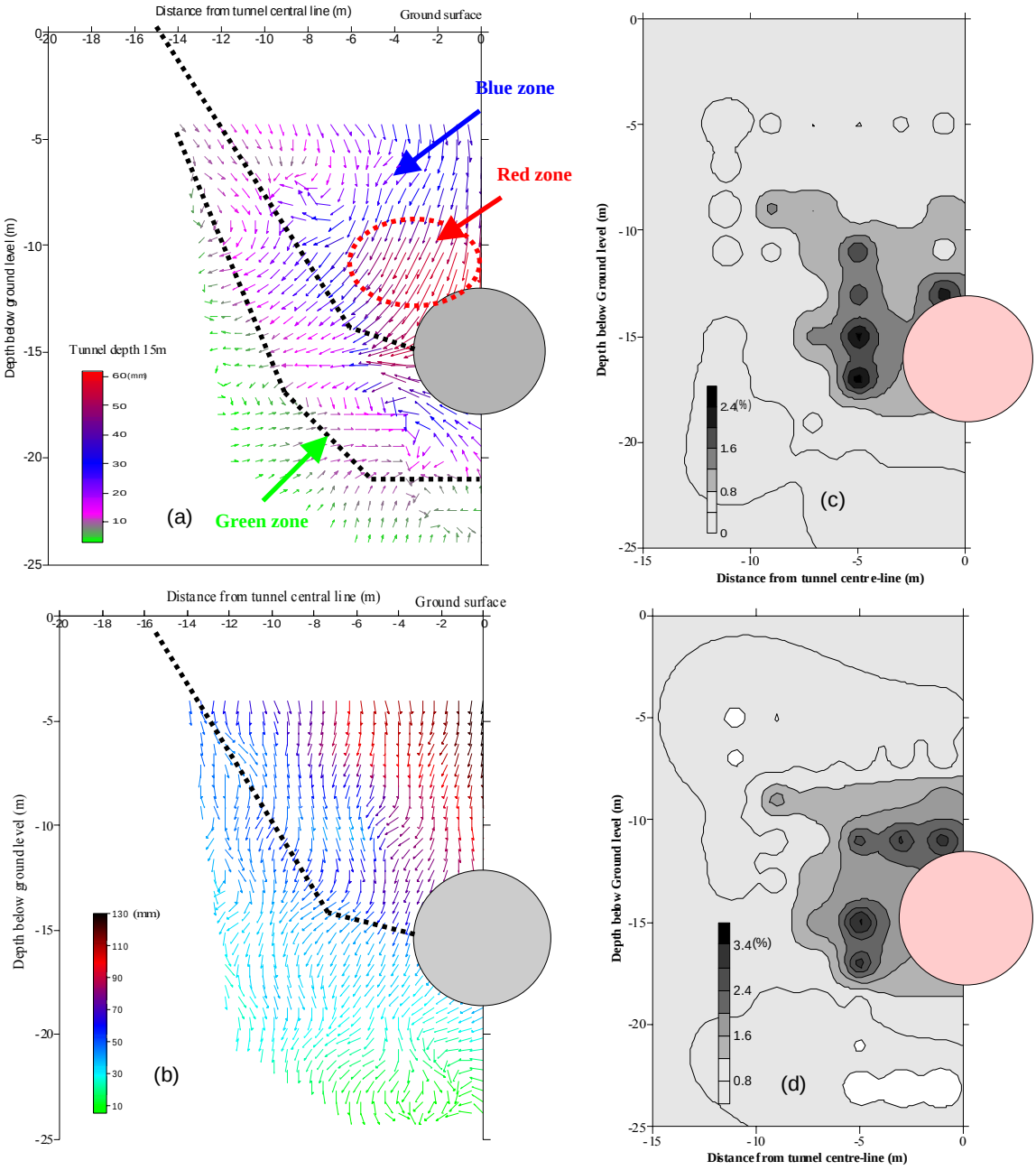

Figure 4.4 Development of subsurface soil movements at (a) 2 days and (b) 720 days after tunnel excavation. Shear strains at (c) 2 days and (d) 720days after tunnel excavation. (Test 1)

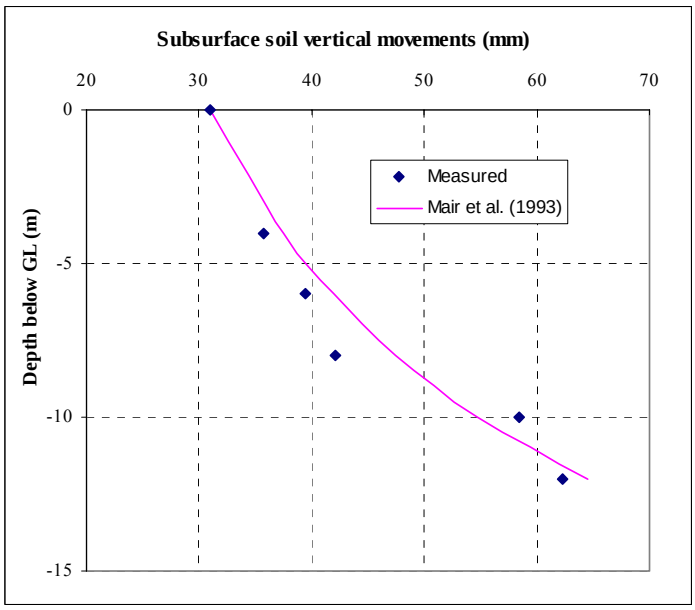

Figure 4.5 Comparison of predicted and measured soil vertical settlement along tunnel vertical centre-line (Test 1)

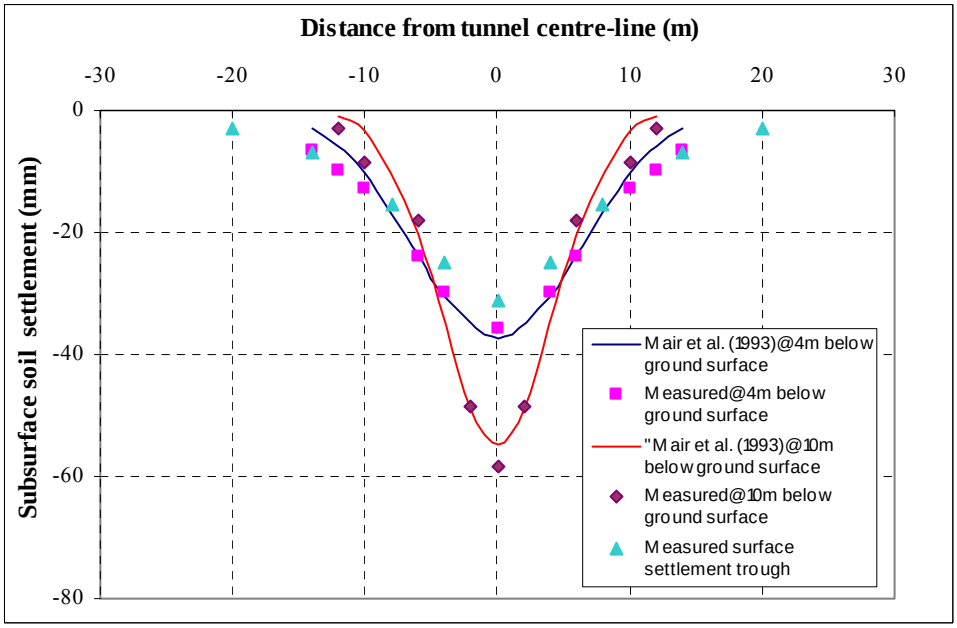

Figure 4.6 Comparison of predicted and measured subsurface soil settlement troughs (Test 1)

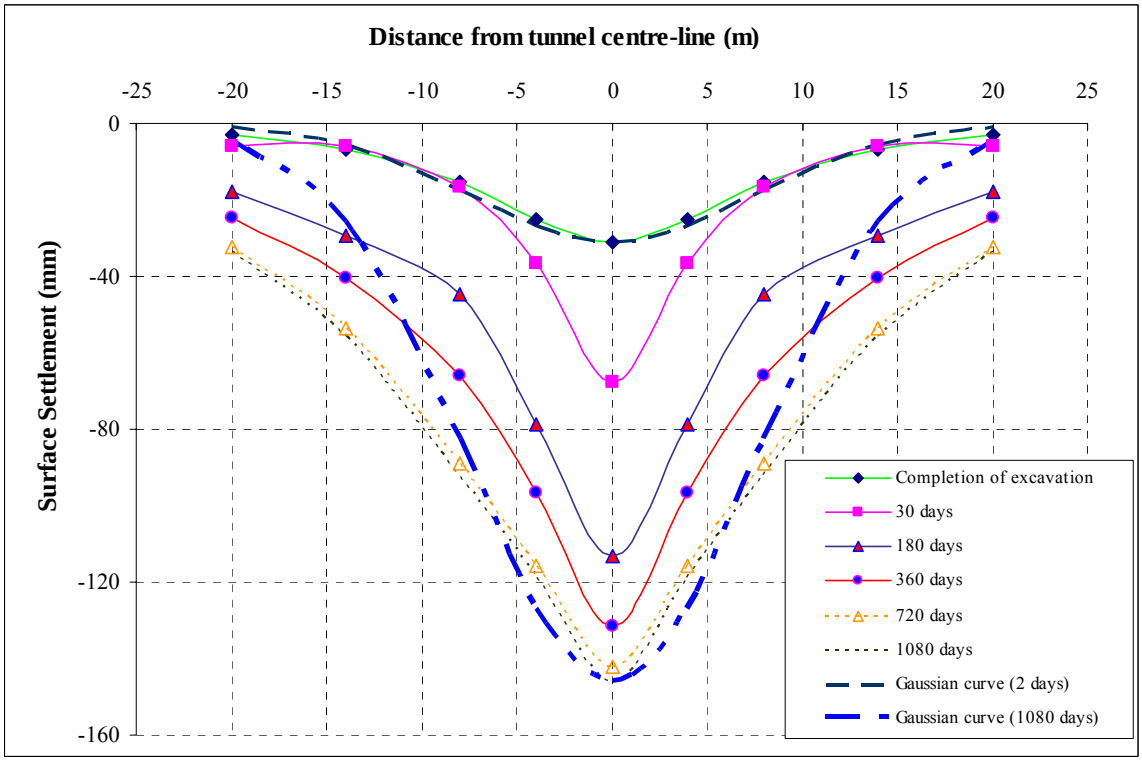

Figure 4.7 Ground surface settlement trough over time (Test 1)

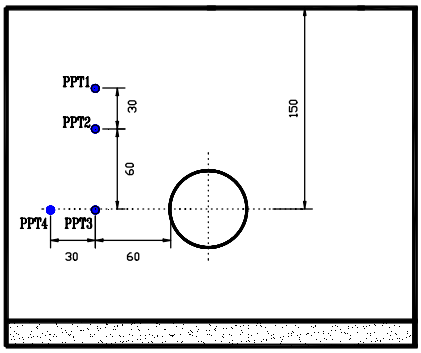

Test 1 Locations of PPTs

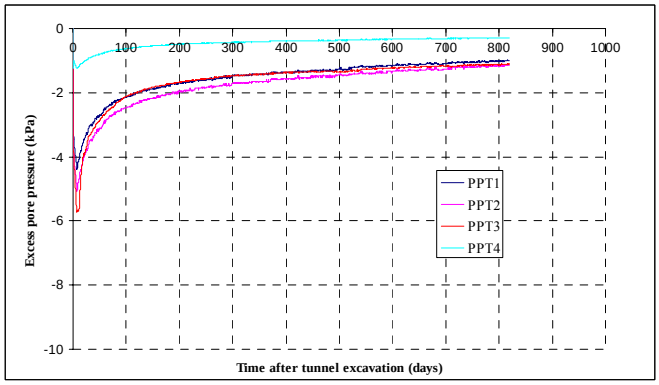

Pore pressure dissipation over time in Test 1

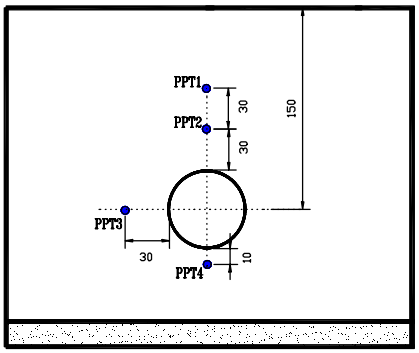

Test 2 Locations of PPTs

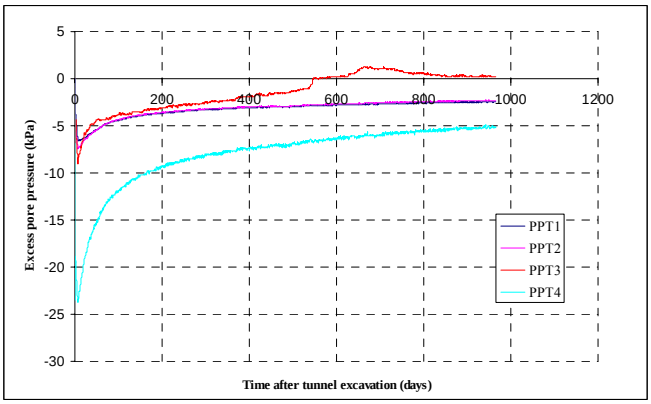

Pore pressure dissipation over time in Test 2

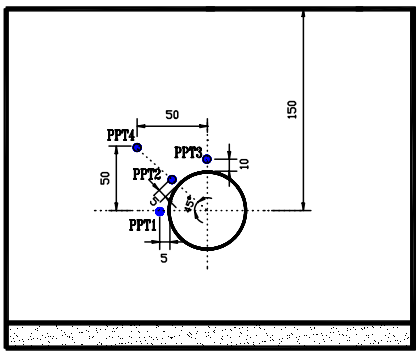

Test 3 Locations of PPTs

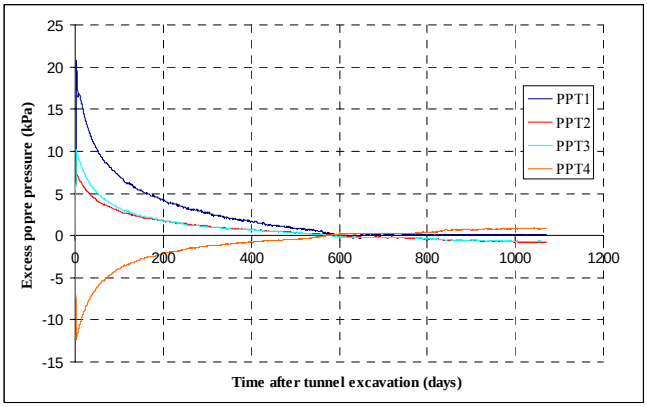

Pore pressure dissipation over time in Test 3

Figure 4.8 Comparisons of excess pore water pressure variations in Tests 1, 2, 3 (Dimension in mm)

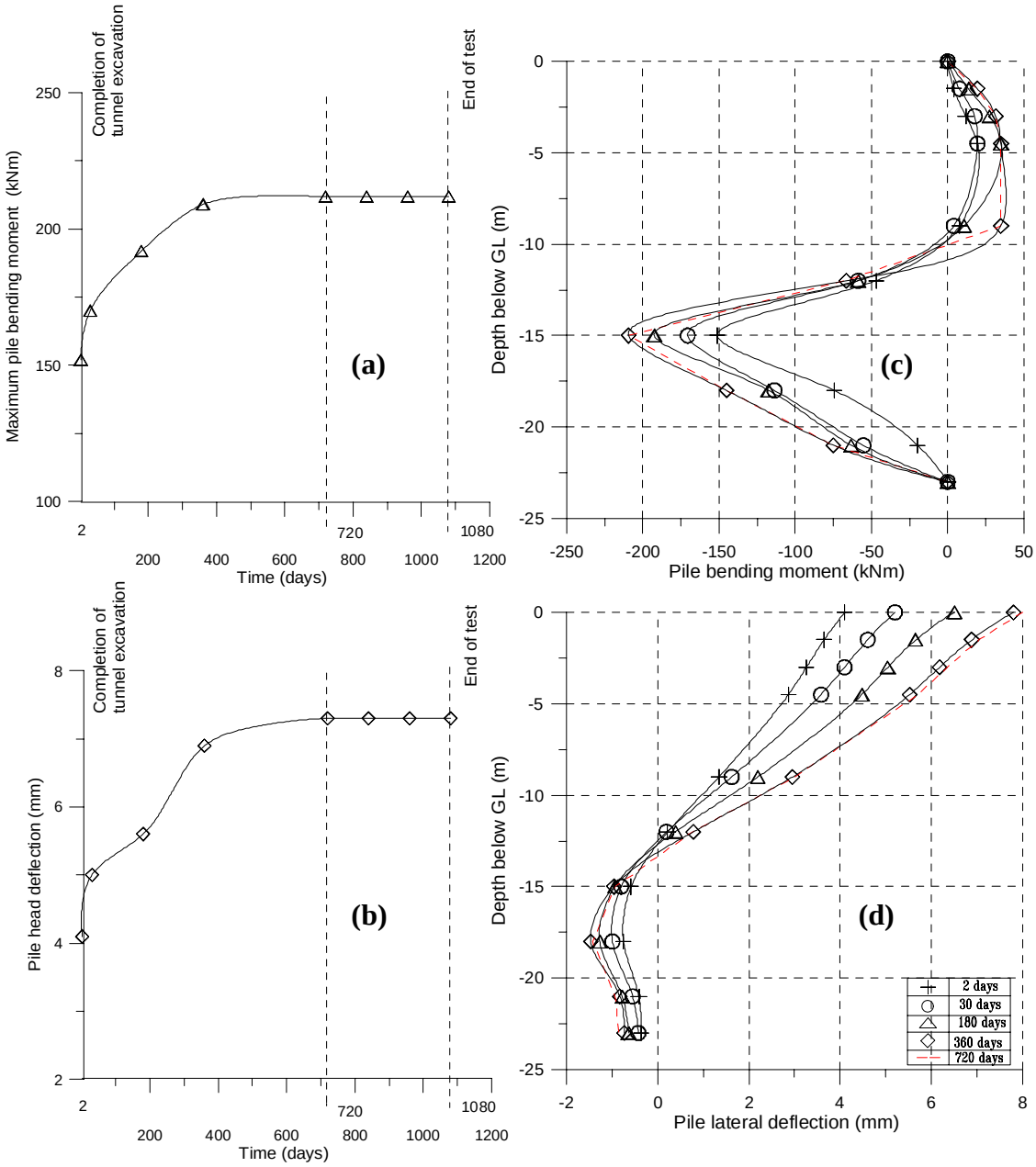

Figure 4.9 Variations of (a) induced maximum pile bending moment, (b) induced pile head deflection, (c) induced pile bending moment profiles and (d) induced pile lateral deflection profiles with time. (Test 1)

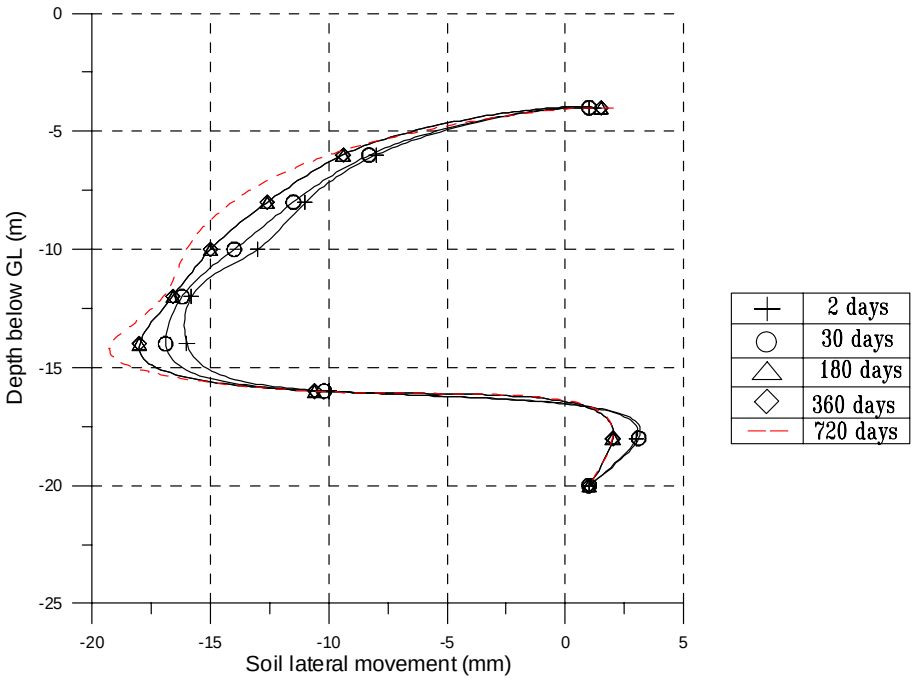

Figure 4.10 Variations of the measured free-field lateral soil movement profile at 6 m away from the tunnel vertical centre-line with time (Test 1)

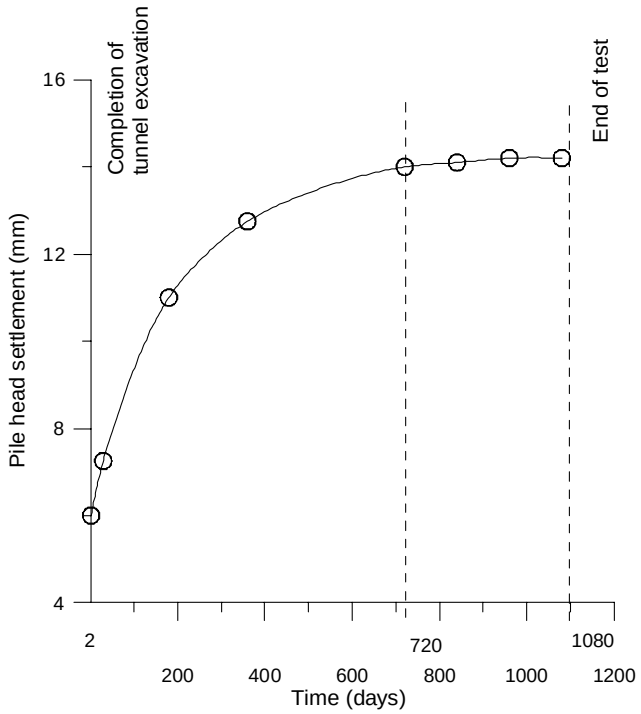

Figure 4.11 Variation of pile head settlement with time (Test 1)

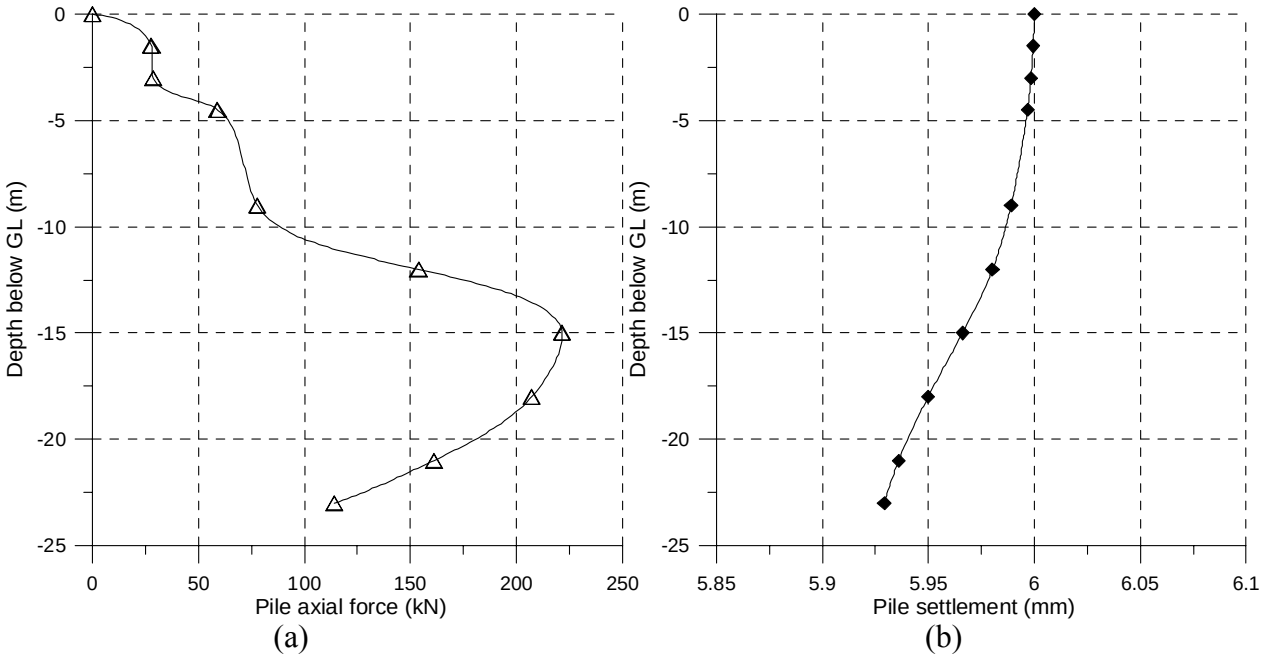

Figure 4.12 (a) Induced pile axial force profile and (b) pile settlement profile at 2 days (Test 1)

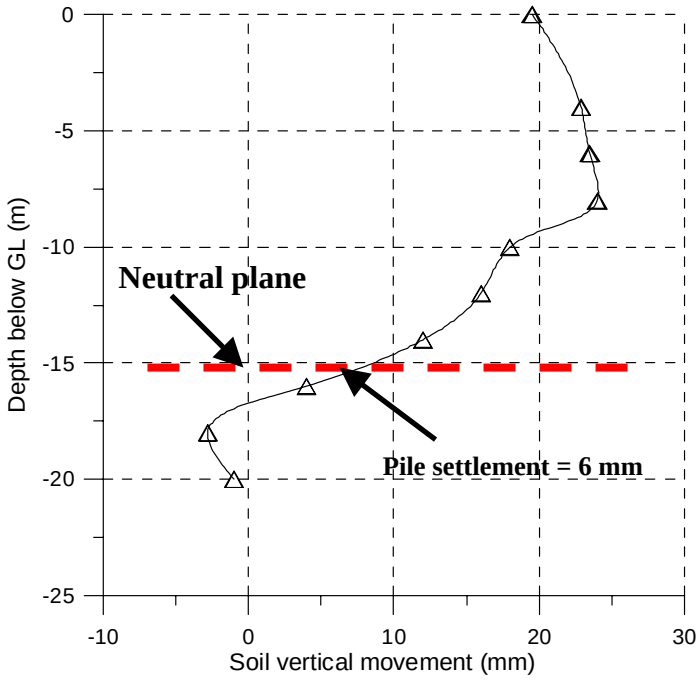

Figure 4.13 Measured free-field vertical soil movement profile at 6 m away from the tunnel vertical centre-line at 2 days (Test 1)

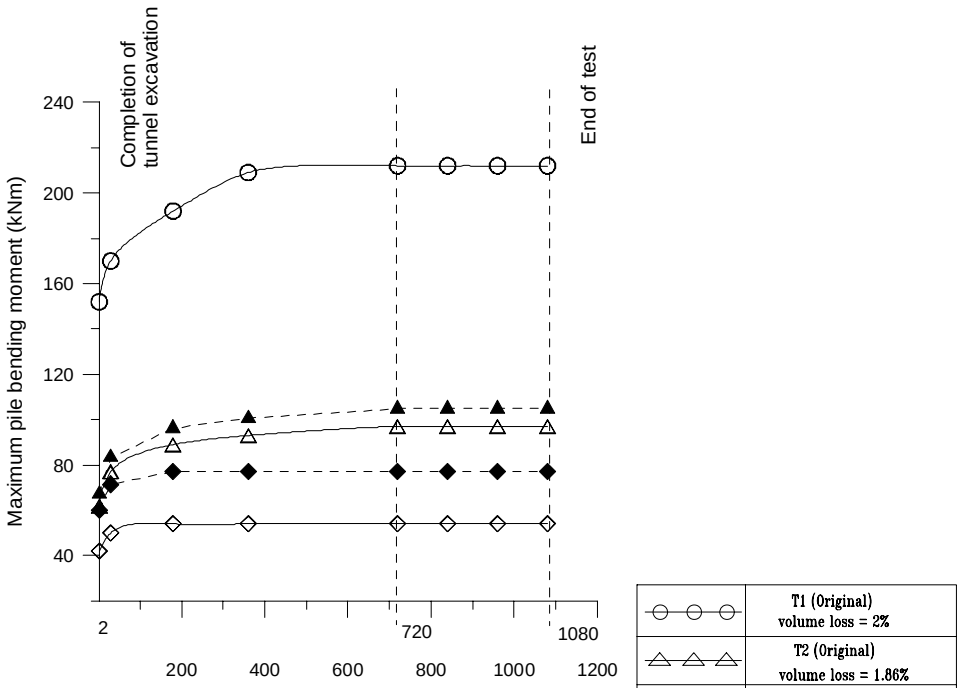

(a)

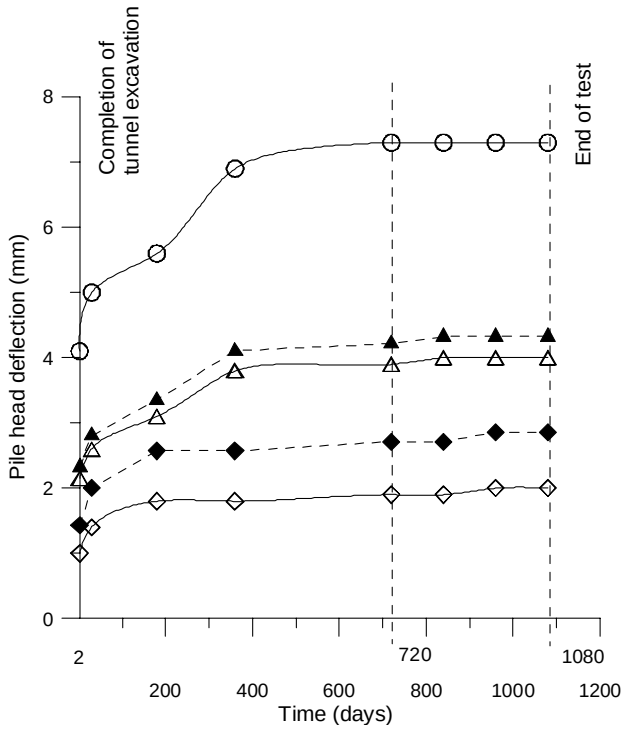

(b)

Figure 4.14 Variations of (a) induced maximum pile bending moment and (b) induced pile head deflection with time. (Tests 1, 2, and 3)

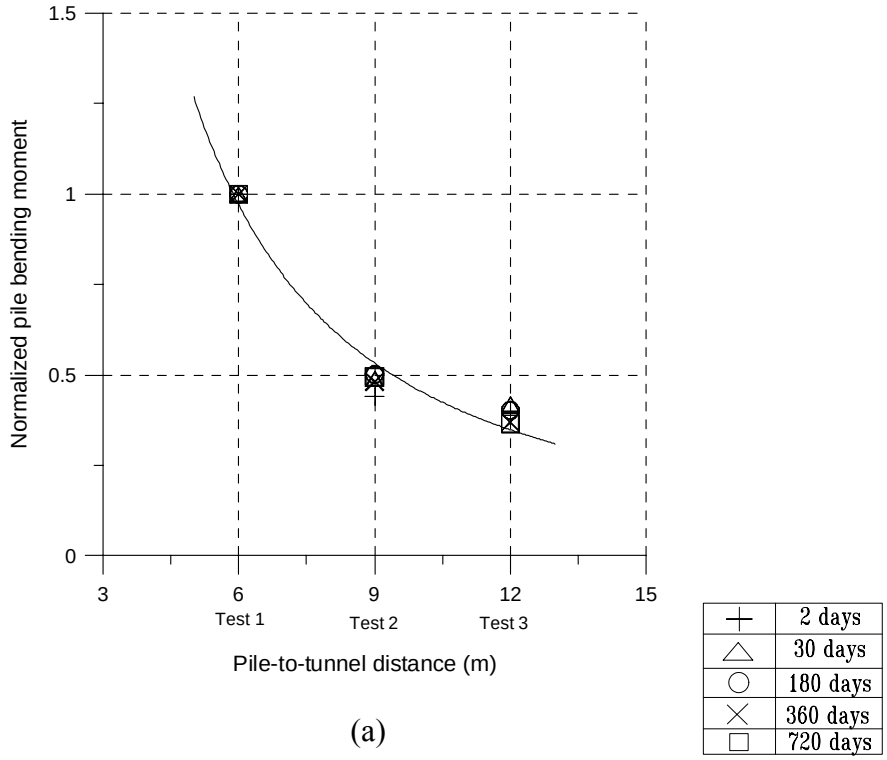

(a)

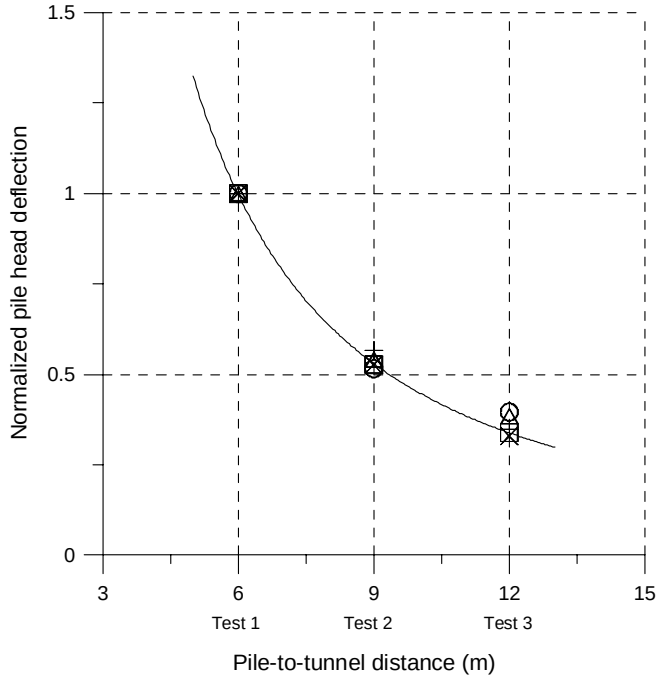

(b)

Figure 4.15 Variations of normalized (a) induced maximum pile bending moment and (b) normalized induced pile head deflection with pile-to-tunnel distance. (Tests 1, 2, and 3)

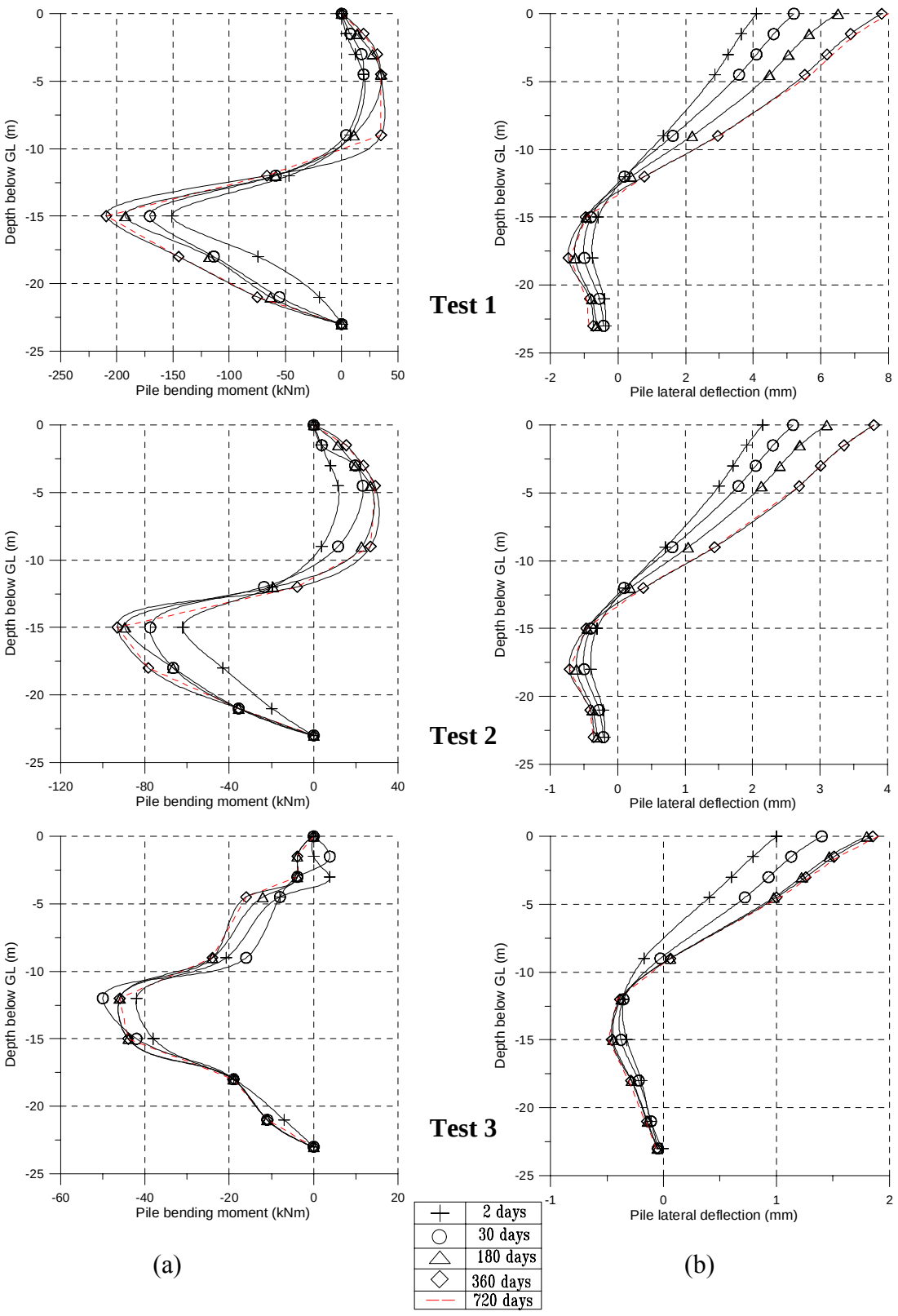

Figure 4.16 Variations of (a) pile bending moment profiles and (b) pile lateral deflection profiles with time. (Tests 1, 2 and 3)

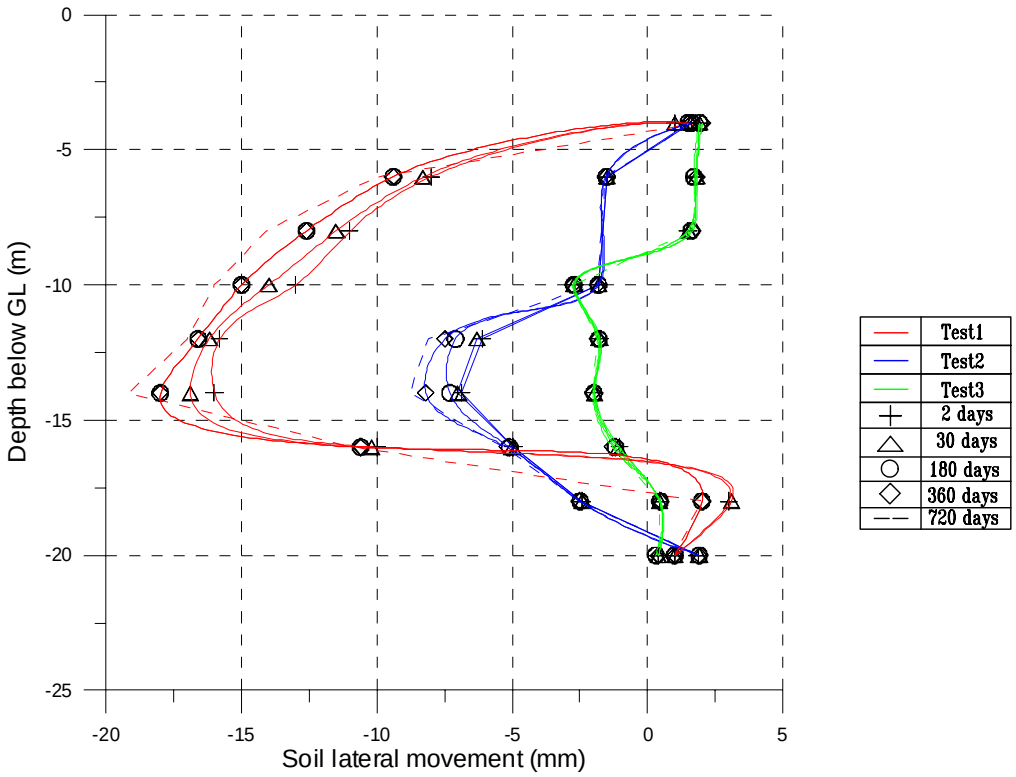

Figure 4.17 Variations of free-field lateral soil movement at pile locations with time (Tests 1, 2 and 3)

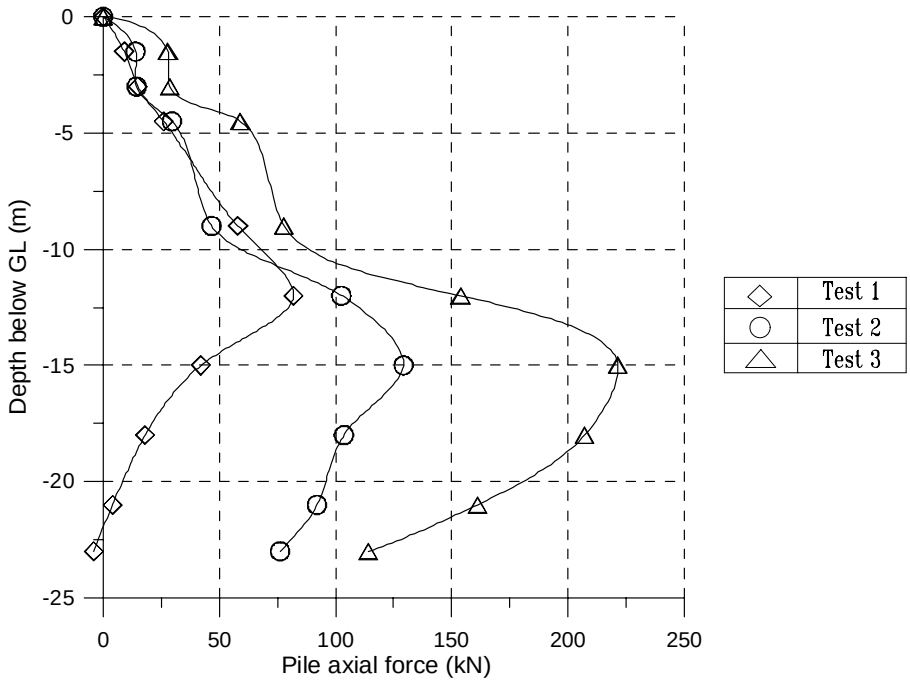

Figure 4.18 Pile axial force profiles at 2 days (Tests 1, 2 and 3)

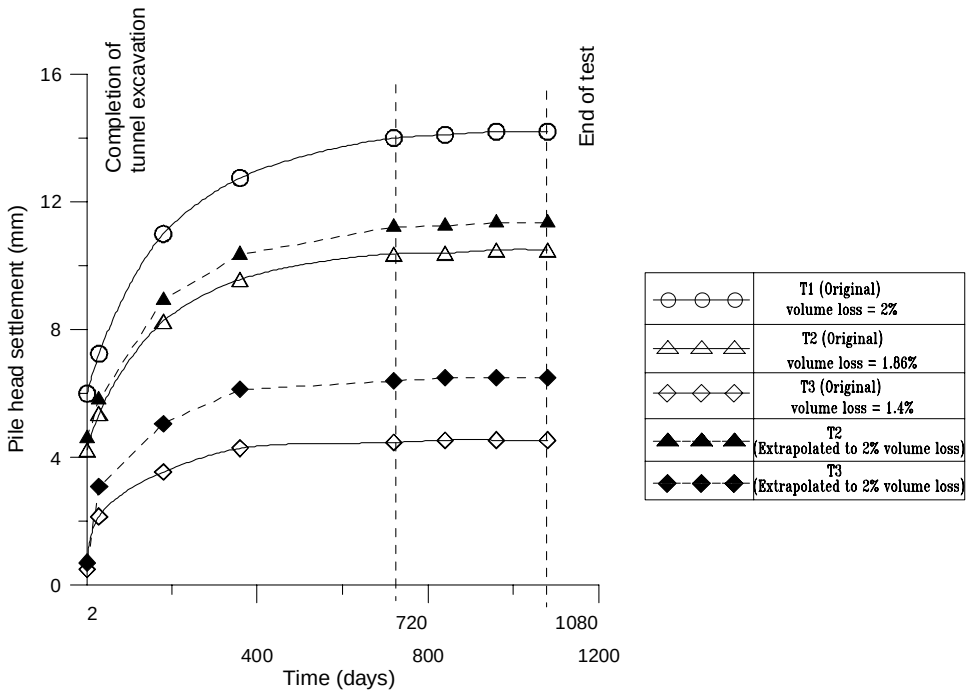

Figure 4.19 Variations of pile head settlement with time (Tests 1, 2 and 3)

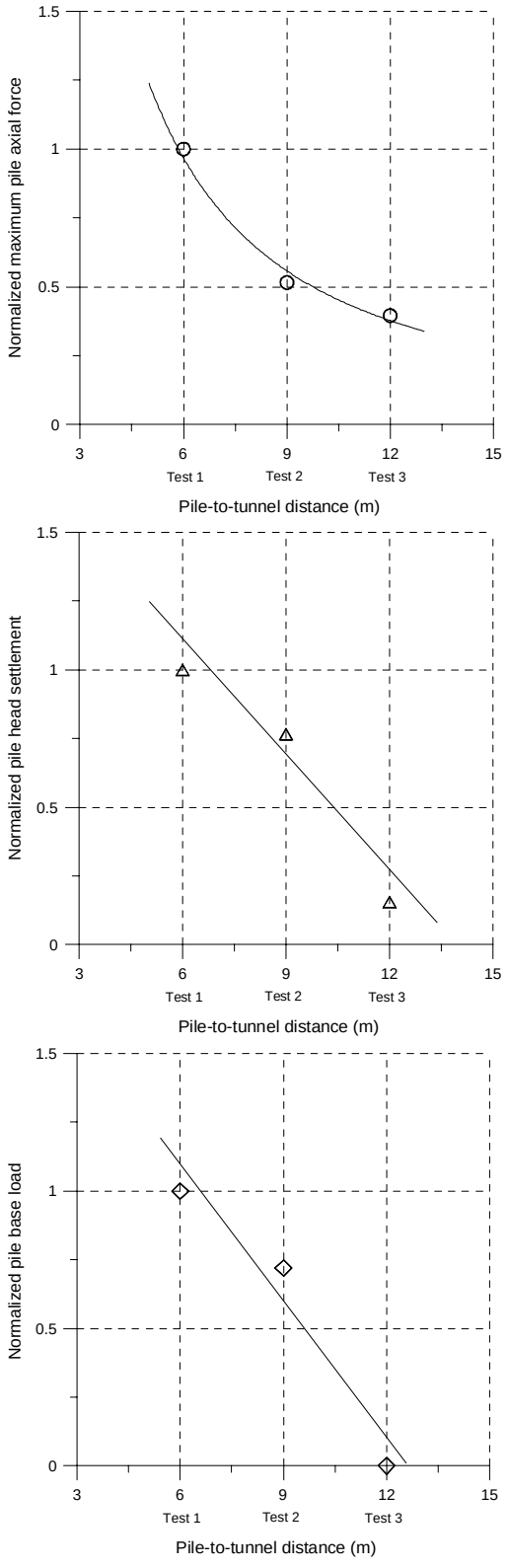

Figure 4.20 Variations of normalized (a) maximum pile axial force, (b) pile head settlement and (c) pile base load with pile-to-tunnel distance. (Tests 1, 2, and 3)

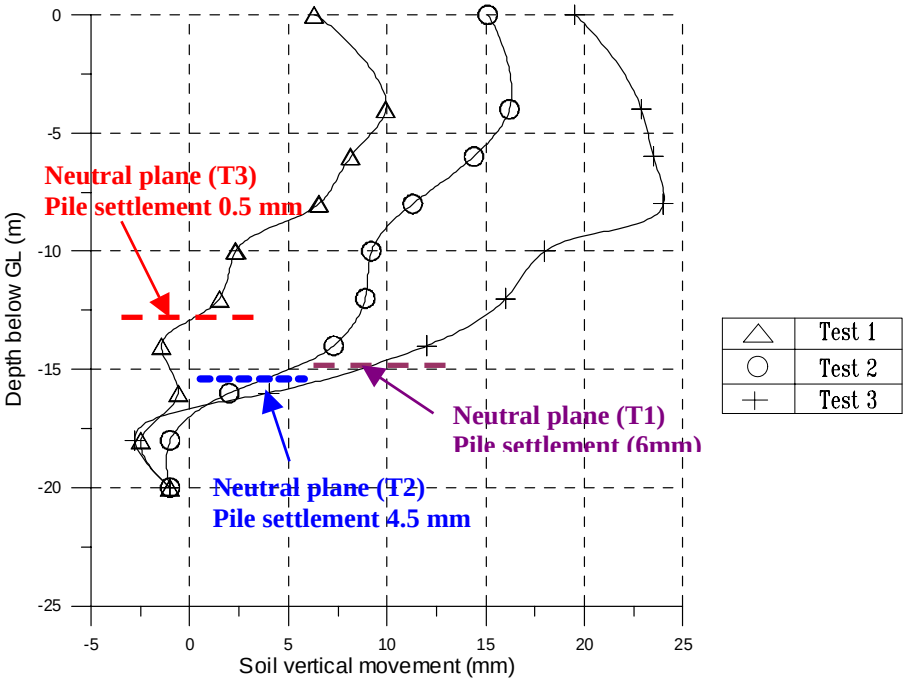

Figure 4.21 Variations of free-field vertical soil movement at pile locations at 2 days (Tests 1, 2 and 3)

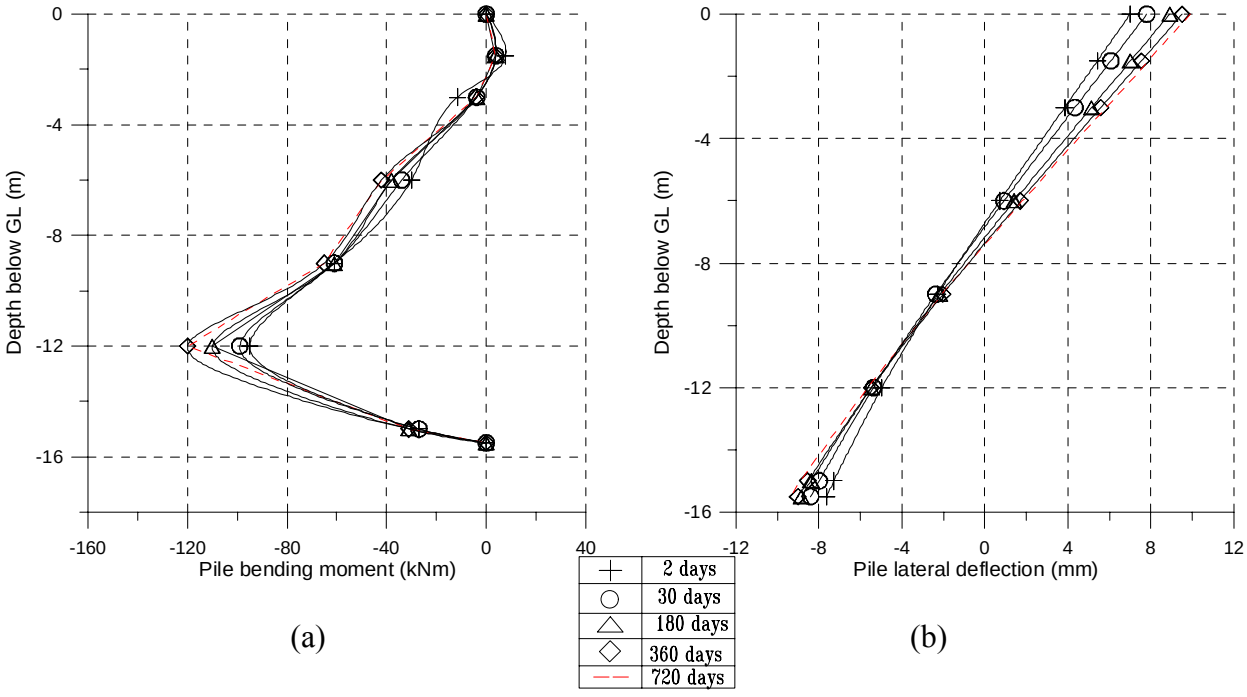

Figure 4.22 Variations of (a) pile bending moment profile and (b) pile lateral deflection profile with time. (Test 4)

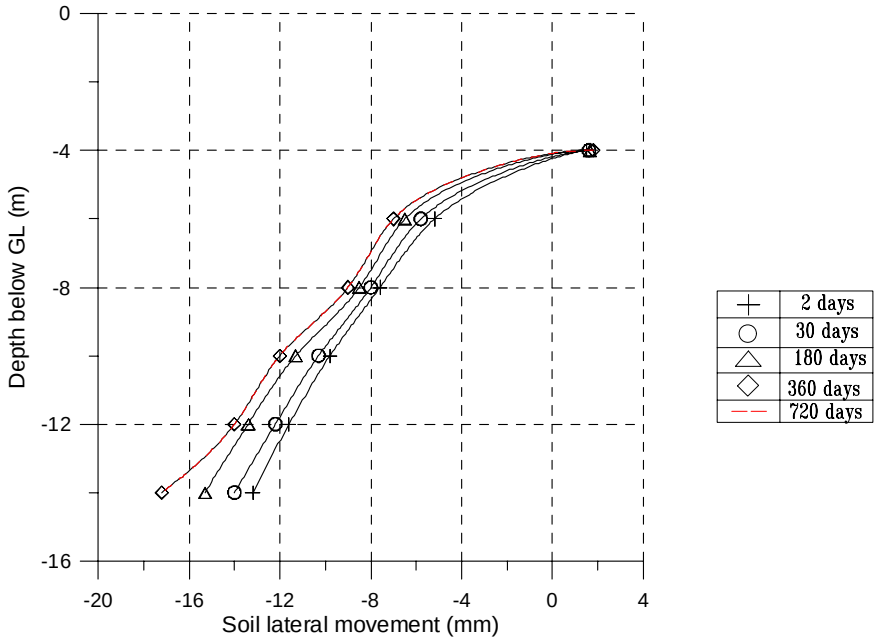

Figure 4.23 Variations of the measured free-field lateral soil movement profile at pile location with time (Test 4)

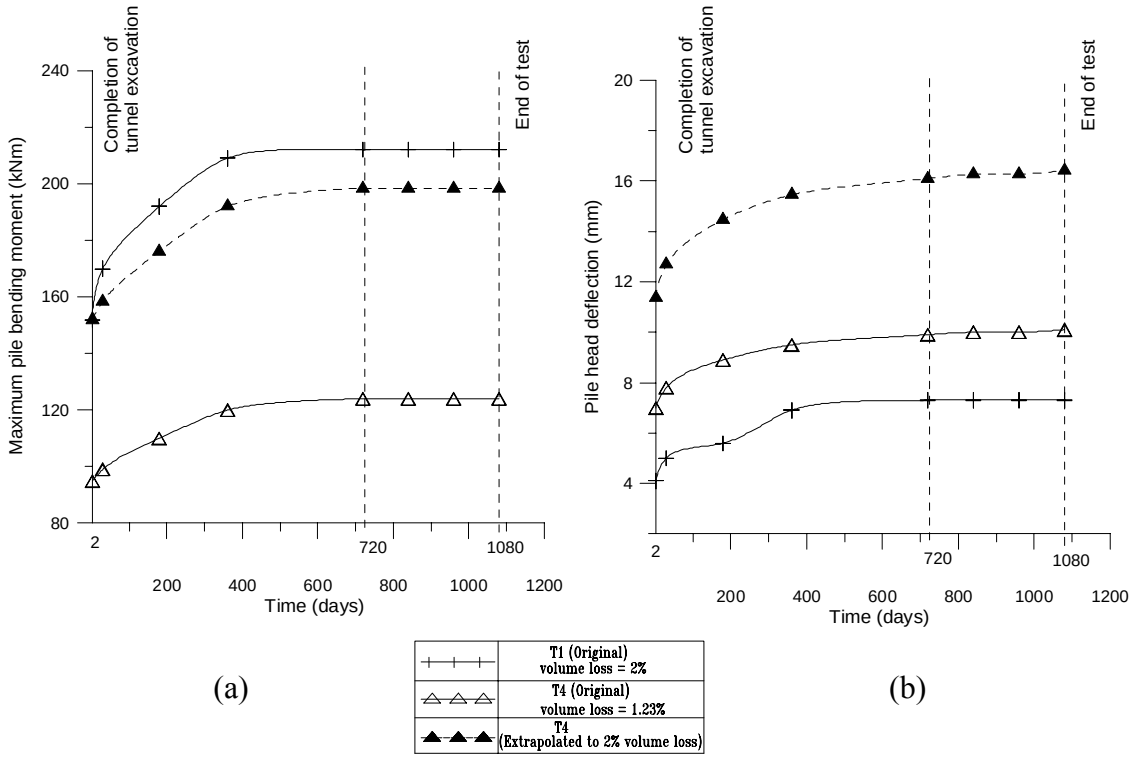

Figure 4.24 Variations of (a) pile bending moment profiles and (b) pile lateral deflection profiles with time. (Tests 1 and 4)

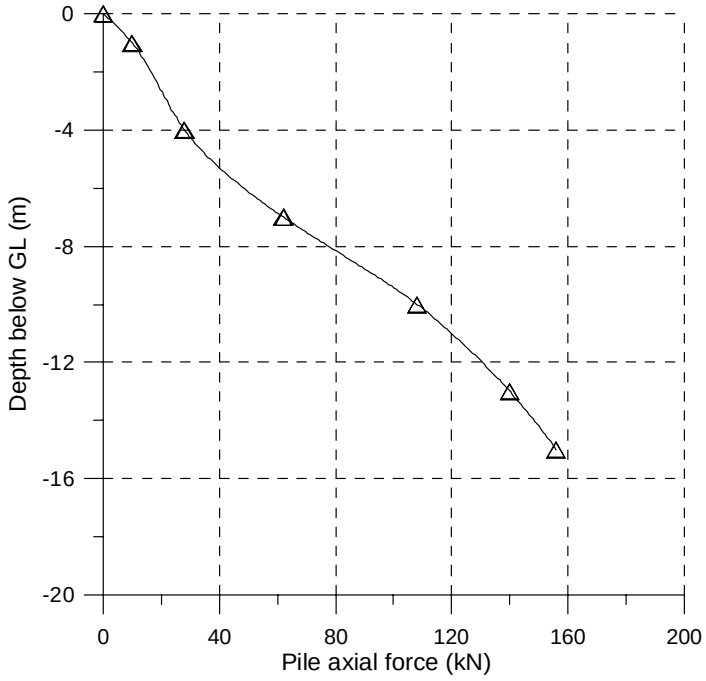

Figure 4.25 Pile axial force profiles at 2 days (Test 4)

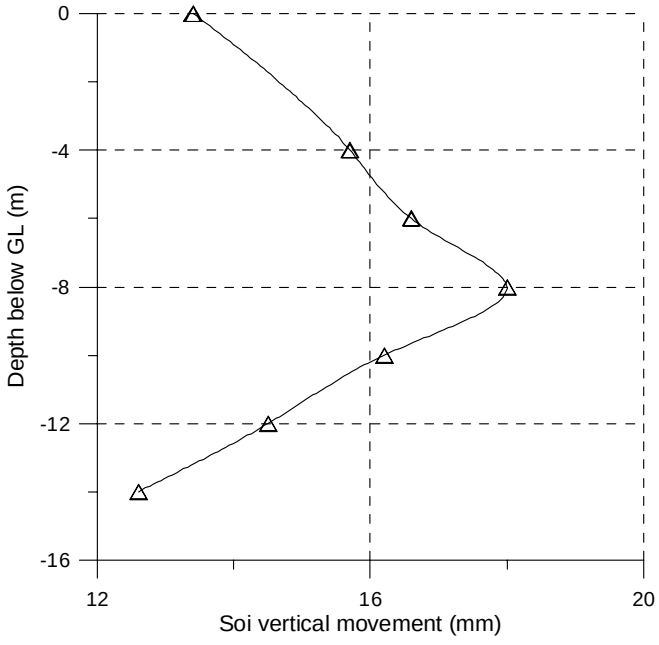

Figure 4.26 Measured free-field vertical soil movement profile at 6m away from tunnel vertical centre-line (Test 4)

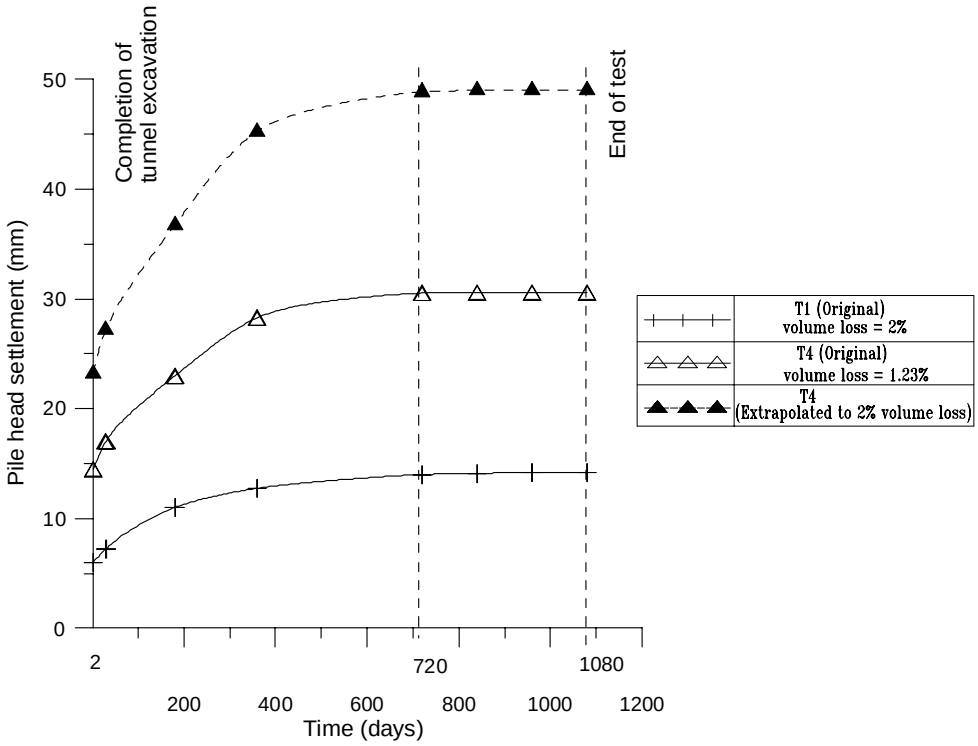

Figure 4.27 Variations of pile head settlement with time (Tests 1 and 4)

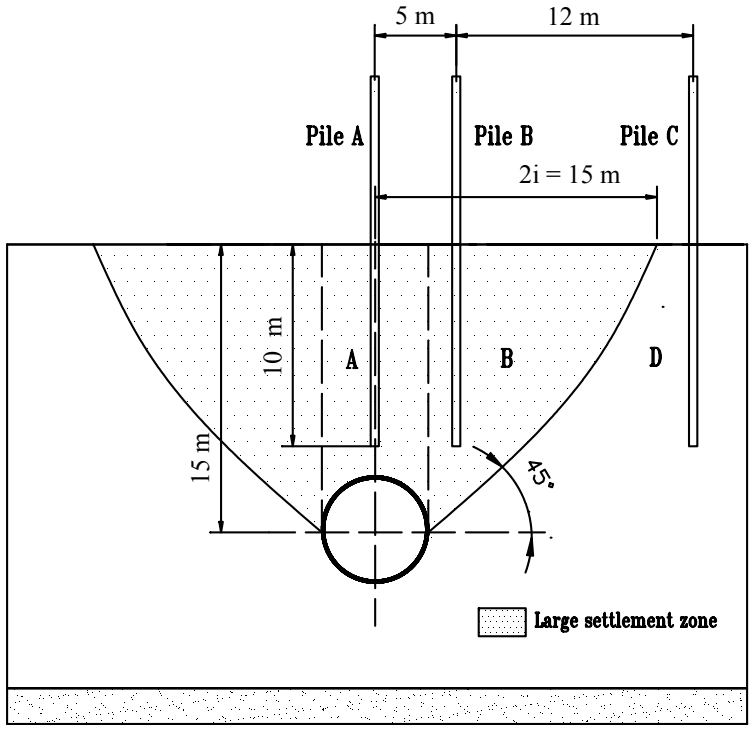

Figure 4.28 Large settlement zone and pile locations in clay (Test 5)

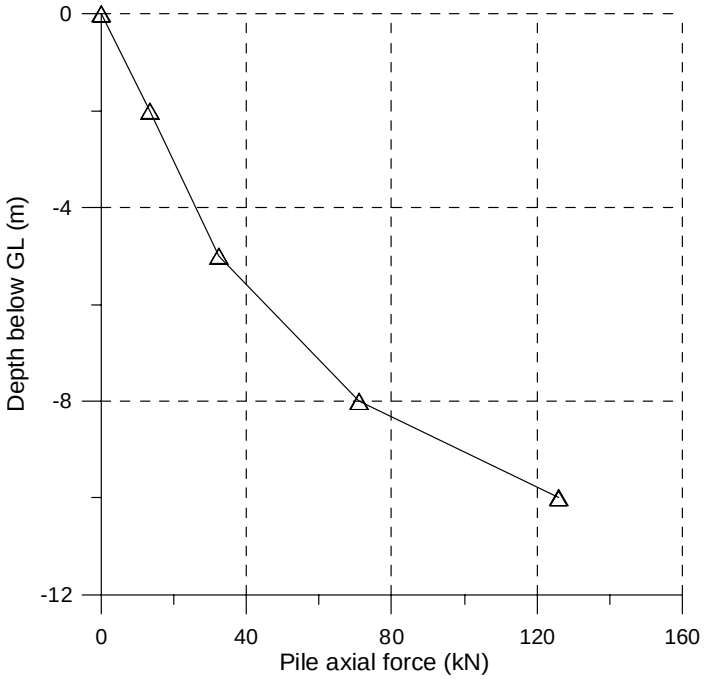

Figure 4.29 Pile axial force profiles at 2 days (Test 5)

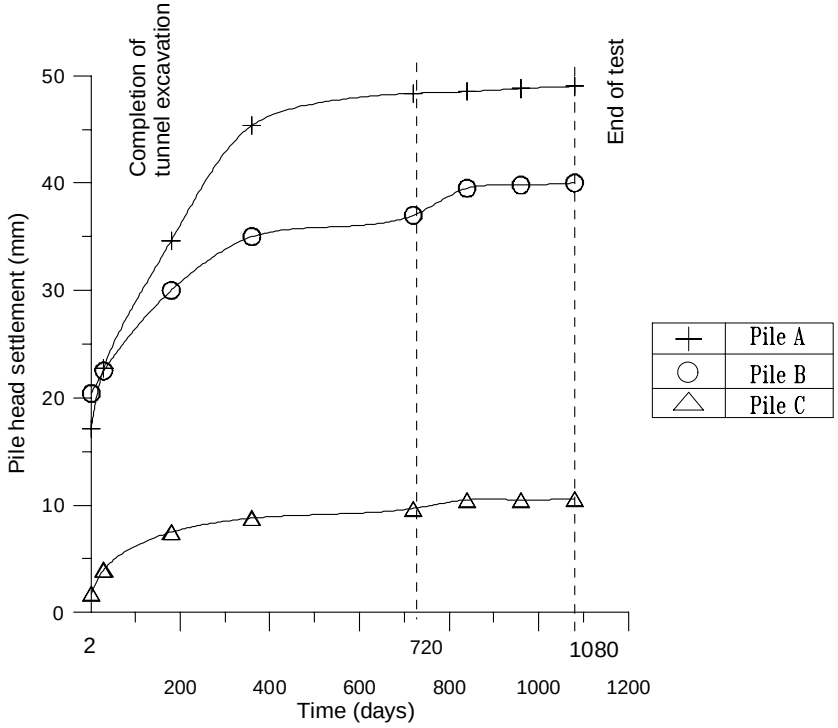

Figure 4.30 Variations of pile head settlement with time (Test 5)

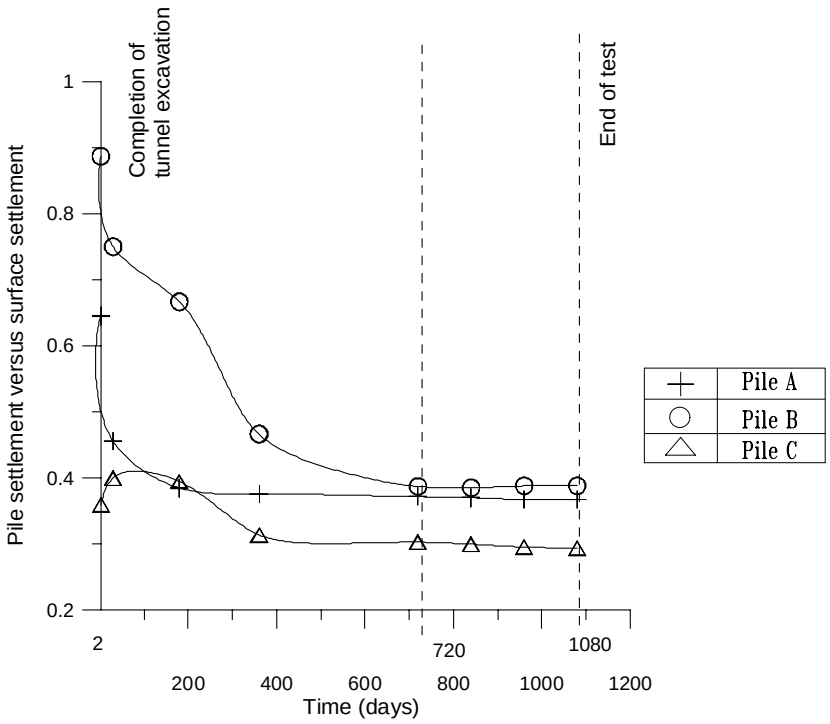

Figure 4.31 Variations of pile settlement versus surface settlement with time (Test 5)

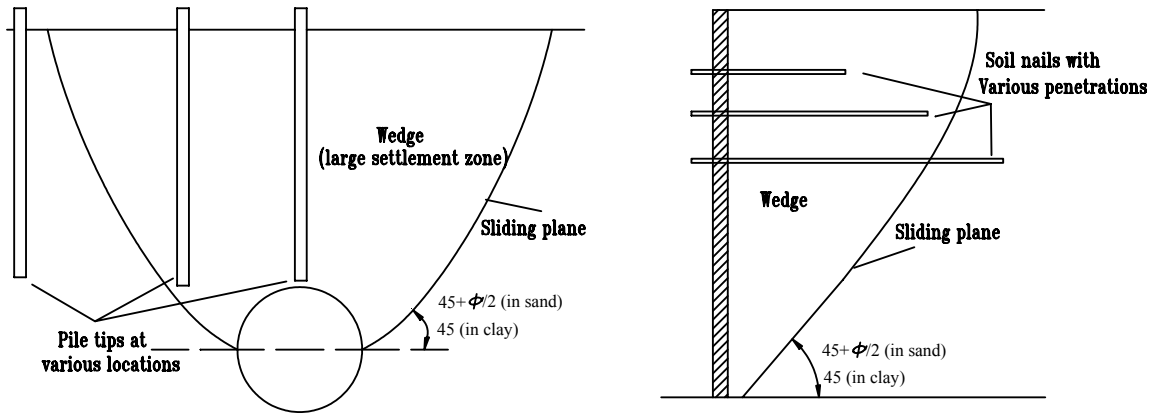

Figure 4.32 Comparison of sliding wedges of tunneling and excavation

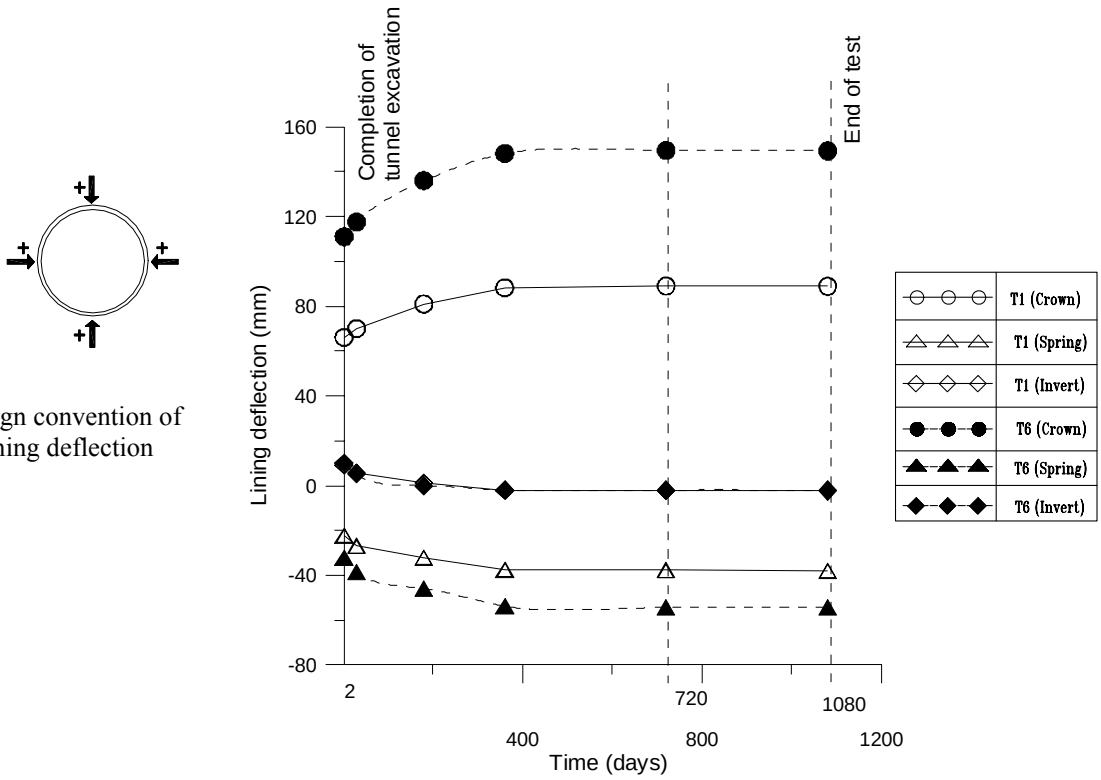

Figure 4.33 Tunnel lining deflection (Tests 1 and 6)

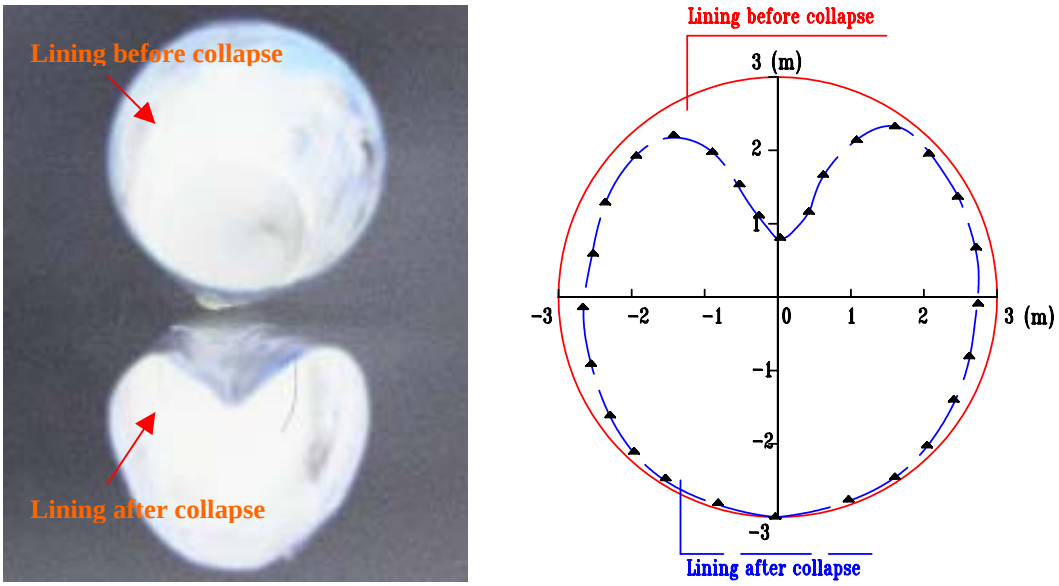

Figure 4.34 Photograph and lining deformation of the collapsed tunnel lining (Test 7)

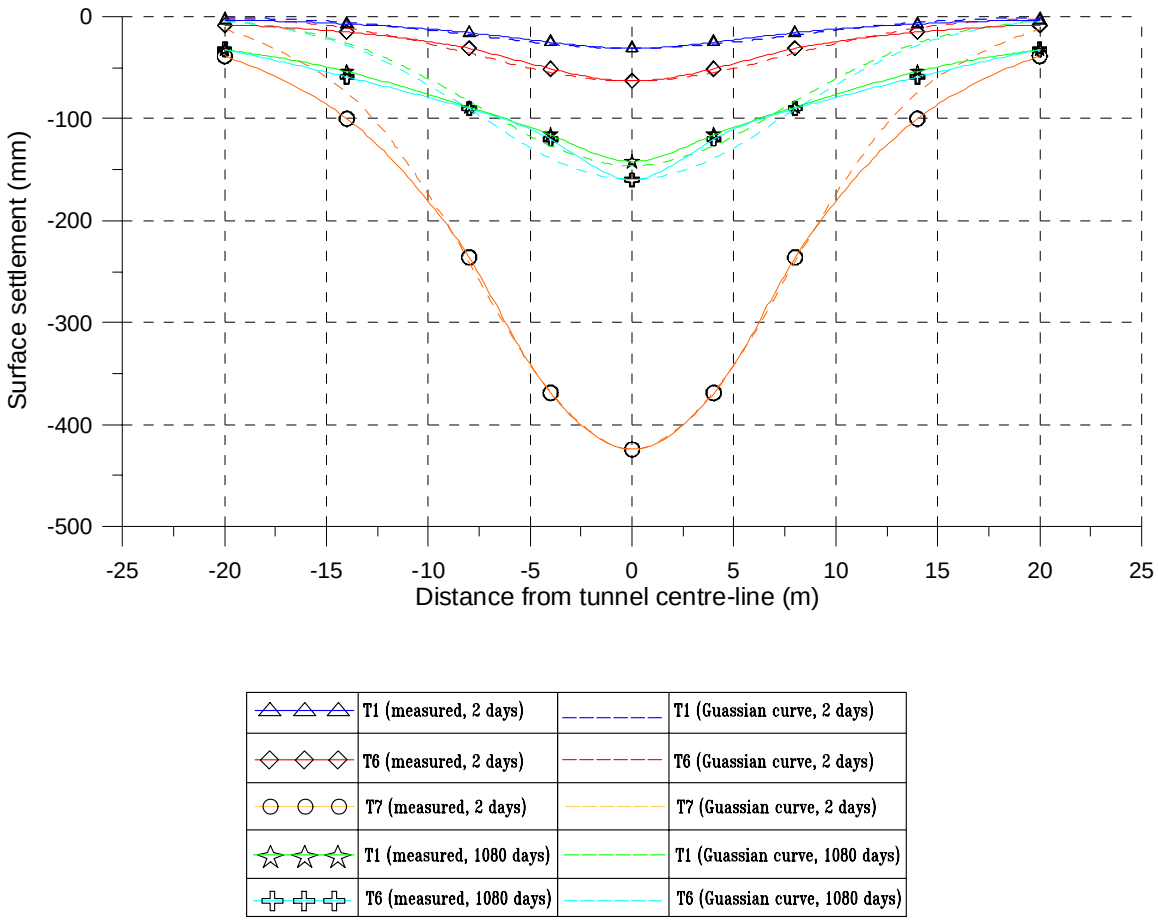

Figure 4.35 Measured surface settlement trough and comparison with Gaussian curve at the end of tunnel excavation (2 days) (Tests 1, 6 and 7)

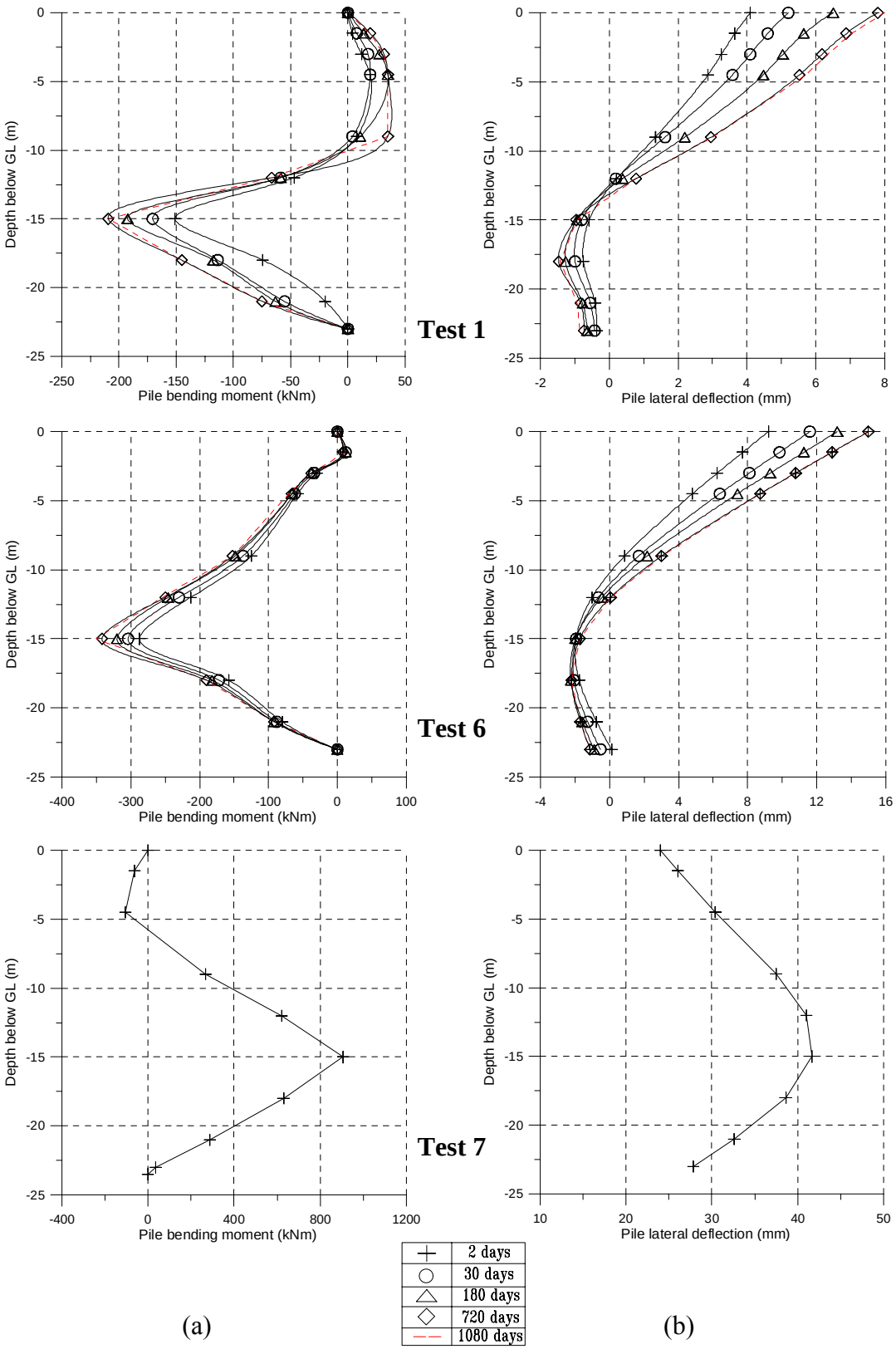

Figure 4.36 Variations of (a) pile bending moment profiles and (b) pile lateral deflection profiles with time. (Tests 1, 6 and 7)

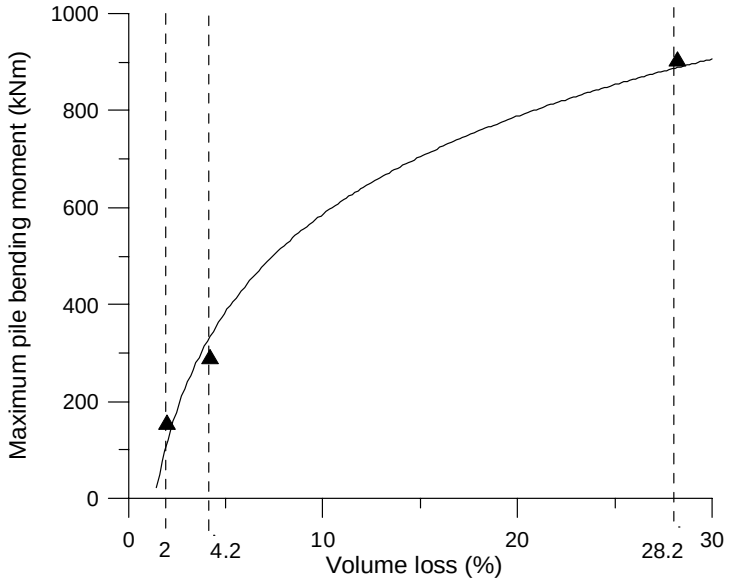

(a)

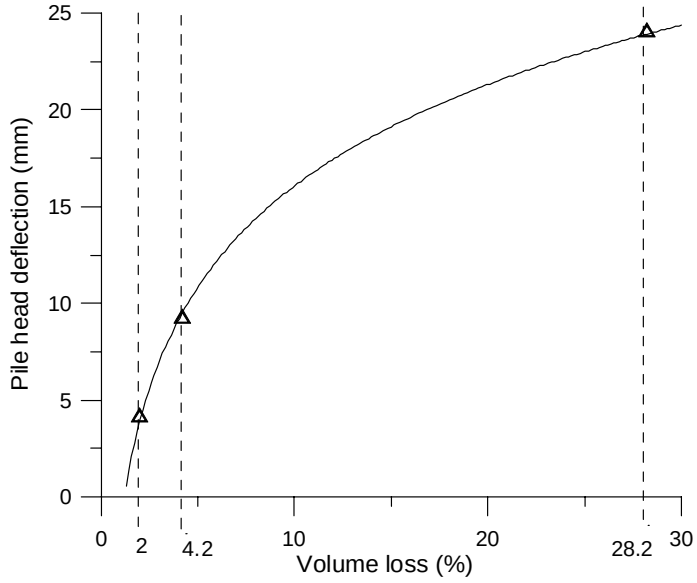

(b)

Figure 4.37 Variations of (a) induced maximum pile bending moment and (b) induced pile head deflection with volume loss at the end of tunnel excavation. (Tests 1, 6 and 7)

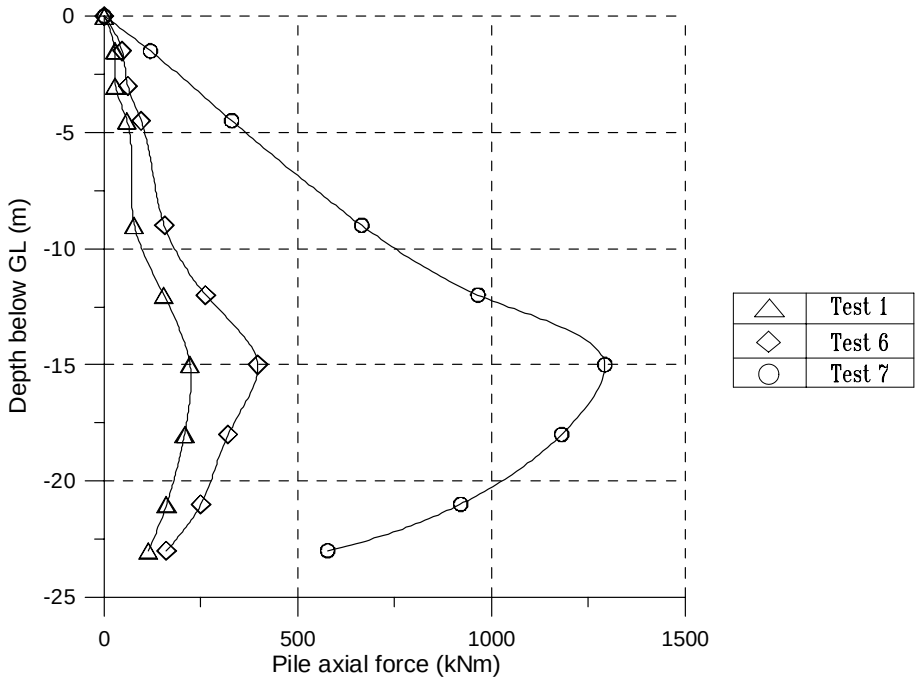

Figure 4.38 Induced pile axial force profile (Tests 1, 6 and 7)

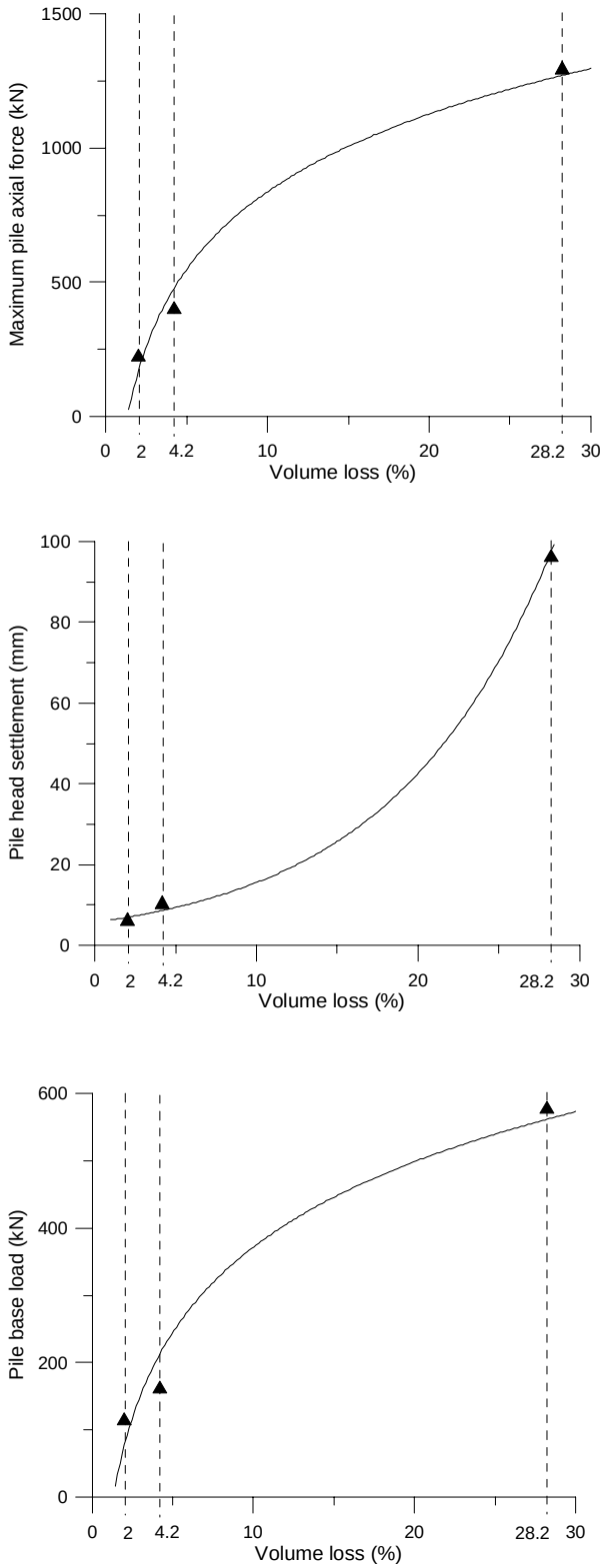

Figure 4.39 Variations of (a) maximum pile axial force, (b) pile head settlement and (c) pile base load with volume loss. (Tests 1, 6 and 7)

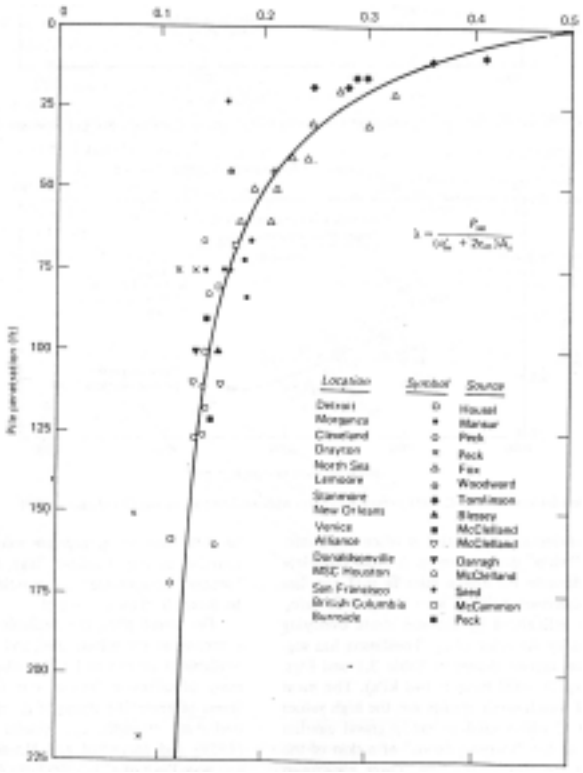

Figure 4.40 Friction capacity coefficient λ vs. pile penetration (After Vijiayvergiya et al, 1972)

CHAPTER FIVE

COMPARISONS OF TEST RESULTS IN SAND AND THEORETICAL PREDICTIONS

5.1 Introduction

In the first part of this chapter, the test results in clay presented in Chapter 4 is compared with those results of tests in sand carried out by Feng (2003). The lining stiffness versus volume loss in the two types of soils is first compared, followed by the evaluation of lining deformations. Comparisons of the induced ground movements are then made. The similarities and differences in pile responses between clay and sand are then elaborated.

In the second half of this chapter, the lateral pile responses obtained in the present study will be compared with the predictions of a numerical method developed in the NUS. The measured pile settlements will also be compared with an analytical solution proposed by Poulos (1980).

5.2 Description of tests in sand

Feng (2003) reported the results of centrifuge model tests on free-headed single piles due to nearby tunnel excavation in sand in 100g. The same simulation method of tunnel excavation proposed by Sharma et al. (2001) was adopted in the tests. A 25 m deep dry sand bed with specific gravity of 2.65 and relative density of 81% was used as the model ground. The tunnel diameter (6 m) and tunnel depth (16 m) were kept

constant in all tests and very similar with those in the present study. Two instrumented hollow square aluminum model piles similar to those in the present study were used to measure the induced pile bending moment and axial force.

Two major series of tests were conducted to investigate the effects of stiffness of tunnel lining and pile-to-tunnel distance as well as effects of pile tip location relative to tunnel on pile responses. It is observed that the measured ground surface settlement and subsurface settlement troughs due to tunneling generally follow the classical Gaussian distribution. Feng established that for a long pile with its tip located below the tunnel, both induced maximum pile bending moment and axial force occur at the elevation of tunnel spring line. However, short piles behave markedly different from long piles with the maximum induced bending moments occurring slightly above the pile tip and the induced axial force increasing linearly down the pile shaft.

5.3 Comparisons of lining stiffness and deformation in clay and sand

5.3.1 Tunnel lining stiffness

Table 5.1 compares the volume loss associated against tunnel lining stiffness of in sand and clay. As the overburden pressures at the tunnel crown level are quite similar for both cases (200 kPa in sand and 245 kPa in clay), it is evident that the tunnel lining stiffness required to prevent the collapse of tunnel in clay is much larger than that in sand. Similar phenomena were also found in many field measurements (Ward et al., 1981). Zhou et al. (1998) concluded that the low supporting pressure for the stability of sand around a tunnel is mainly due to the arching effect. Evidence of soil arching, however, was also observed for tunneling in clay as the magnitude of soil settlement

decreases from the tunnel crown level to the ground surface. Therefore, it might be deduced that sandy soils have a much stronger arching effect than clay, which in turn results in a lower stress acting around the tunnel. This is again confirmed in the stable lining cases that a stiffer tunnel lining in clay deforms considerably more than a less stiff lining in sand.

Table 5.1 Comparison of volume loss versus lining stiffness in sand and clay

	Linings in sand (after Feng, 2003)		Linings in clay (this study)	
EI (kNm^2)	4.67×10^7	1.46×10^8	1.85×10^8	4.9×10^8
Ground volume loss	33% (collapsed case)	1.02% (stable lining)	28.2% (collapsed case)	2.0% (stable lining)

5.3.2 Ling deformation

Figure 5.1 shows the tunnel lining deformation in sand. It is noted that the lining deformation pattern in sand is similar to that in clay. Both linings experience a phenomenon of horizontal ovalisation with the tunnel crown settles, spring expands, and invert heaves. This is probably due to the tunnel linings that are 'ready-in-place' in this simulation method. As the brass foil lining is rigid along its circumference, it is essentially not compressible by hoop thrust. Therefore, the lining spring line has to protrude outside in order to accommodate the tunnel crown settlement and hence the tunnel lining deforms into a horizontal ovalised shape as a whole. However, it should be noted that the model brass lining used in the present study is mainly a means to introduce an ovalised tunnel deformation and evaluate its effects on adjacent pile foundations. In the sense, it does not represent the scenario where very rigid linings (such as very thick permanent tunnel linings) with good workmanship are installed in

the field as ground movement would largely be prohibited upon the installation of these linings. It is also noted that the tunnel lining would continue to deform over time in clay, whereas in sand the lining deformation remains essentially unchanged soon after tunnel excavation, as established by Feng (2003).

5.4 Tunneling-induced soil movement

Figure 5.2 displays the subsurface soil movement vectors at the completion of tunnel excavation in sand. The subsurface soil movements in sand were measured by small beads embedded into the front surface of the sand whose movements were monitored and calculated using the PIV technique. It is noted that the trend of the subsurface soil movements in sand is very similar as that in clay due to the similar ovalised tunnel deformation. The soil above the tunnel moves down. The soil around the tunnel gradually moves downwards and at the same time moves away from the tunnel due to enlarging of the lining spring. However, it is noted that the subsurface soil movement in sand decrease more rapidly in the horizontal direction than that in clay.

Figure 5.3 shows the surface settlement troughs under similar volume loss in clay and sand. Both the measured settlement troughs follow Gaussian curve well. However, it is evident that the settlement trough in clay is markedly different from that in sand as e the sand settlement trough is much narrower than that of clay. This is consistent with many field observations as reviewed in Chapter 2. The difference in the width of the surface settlement trough is likely due to the different soil movement propagation mechanisms between clay and sand. In clay, the deformation of the soil propagates 'gradually' upwards and outwards from the tunnel cavity to the ground surface. However, the deformation in sand propagates sharply and almost vertically from the

tunnel to the ground surface. This is due to the fact that the dense sand used by Feng (2003) is much stiffer than the soft clay used in the present study. Therefore, the soil settlement trough attenuates more rapidly in the horizontal direction in sand than in clay. In addition, the different mechanisms suggest that the ground deformation in sand may cause more severe damages to the ground surface or structures above and nearby the tunnel; while in clay, it can cause differential settlement spreading a wider range. This may explain why sinkholes on the ground surface associated with tunneling are mainly spotted in competent soils like sand in the field; while such drastic settlements are less common in clay.

5.5 Pile responses

Similarities:

For long piles with tips well beneath the tunnel, the location of induced maximum pile bending moment and axial force is approximately at the tunnel spring elevation for both clay and sand. The induced maximum pile bending moment and axial force reduce exponentially with increasing pile-to-tunnel distances in both clay and sand.

For short piles with tips at or above the tunnel, the induced maximum bending moment occurs slightly above the pile tip and the induced axial force increase almost linearly along the pile shaft for both clay and sand.

Differences:

The most distinct difference of single pile behaviour in the case of a stable tunnel is that for clay, the induced pile responses would gradually increase over time, whereas

for sand, the pile bending moments remain essentially unchanged after the completion of excavation, as established by Feng (2003). This is due to the fact that for sand, essentially most of the excess pore water pressures generated during excavation would have completely dissipated soon after the completion of the excavation and hence, there is insignificant time-dependent pile behaviour. Time-dependent pile behaviour in clay could be seen as the effect caused by the progressive tunnel lining and soil deformations over time due to dissipation of excess pore pressure.

In order to compare the magnitudes of the pile responses in clay and sand, two sets of tests in the cases of collapsed tunnel and stable tunnel with similar volume loss and pile-to-tunnel distance are selected. Figure 5.4 shows the layout and volume loss for the two sets of tests. Figure 5.5 shows the comparisons of induced maximum pile bending moment, head deflection and maximum axial force, respectively. As the pile behavior in sand does not change over time, only short-term pile responses are presented in Figure 5.5. It is evident that the induced pile responses in sand are larger than those in clay. This appears to show that the impact of tunnel excavation on piles in sand is more severe than that in clay under similar volume loss and pile-to-tunnel distance in the short-term. This is contrast to the general belief that the pile behaviour in clay should be more severe as it is considerably weaker than sand. Clearly more studies are needed to evaluate the test observations.

5.6 Comparisons with theoretical predictions

5.6.1 Comparison with numerical predictions on pile lateral responses

The numerical method developed by Chow et al. (1996) is used to back-analyze the lateral responses of single piles due to tunnel induced lateral soil movement obtained

from the centrifuge tests. This numerical method has been used successfully by Leung et al. (2000) and Ong et al. (2003) to back-analyze excavation-induced single pile behaviour in sand and clay. The concept of analysis is based on finite element method where the pile is represented by beam elements and the soil is idealized using the modulus of subgrade reaction. The non-linearity of the soil behaviour can be incorporated to an extent by limiting the soil pressure that can act on the pile. The numerical analysis requires the knowledge of the pile bending rigidity (EI), the distribution of lateral soil stiffness (K_h) with depth, the limiting soil pressure (p_y) that acts on the pile and the lateral soil movements. This approach is used in the present study to predict the pile responses in clay.

For clay, the distribution of the lateral soil stiffness with depth, K_h is assumed to be related to the Young's modulus of the soil, E_s, as follow (Chow and Yong, 1996):

$$K_h \cong E_s \tag{5.1}$$

For clay, the Young's modulus of soil can be correlated to the undrained shear strength C_u.

$$E_s = \beta C_u \tag{5.2}$$

where β usually falls in the range between 150 and 300 according to Poulos and Davis (1980). β is adopted as 150 in the present study.

To account for the nonlinear behaviors of soils, for pile in clay, a simplified distribution of soil resistance or limiting pressure, p_y, with a maximum value of $9c_u$ is suggested:

$$p_y = 2(1+z/d)c_u \leq 9c_u \quad (5.3)$$

where z is depth and d is pile diameter.

It has been established from the earlier sections that the pile lateral response is time dependent. Therefore in the numerical back analysis, the measured lateral soil movement profiles corresponding to the short-term (2 days) and long-term (720 days) pile bending moment profiles are both used as the inputs. As the predicted profiles in the long pile tests are essentially very similar, only one long pile test (Test 3) and one short pile test (Test 4) are presented here. Figures 5.6(a) and (b) show the measured free-field lateral soil movement profiles and the comparison between the measured and predicted bending moment and deflection profiles of the pile for Tests 3 and 4, respectively. It is noted that the measured and predicted pile bending moment and deflection profiles for both cases reveal fair agreement. However, for the short pile case (Test 4), the predicted maximum bending moment occurs at 10 m below the ground surface, which is about 2 m higher than that of the measured one. This is probably due to the two strain gauges in this region are attached at 9 m and 12 m along the pile and hence the pile bending moment at 10 m could not be captured.

In practice, the maximum pile bending moment and deflection are the most important concerns on the pile responses. This is so because excessive induced bending moment can cause structural failure of a pile while large pile deflection can threaten its serviceability. A comparison of the predicted and measured induced maximum pile bending moment and lateral deflection is summarized in Table 5.2. Results of Tests 5 and 7 are not presented in the table as the reasons mentioned earlier. Again, there is reasonably good agreement between the predicted and measured values. However, it is

noted that the numerical program generally overpredicts the magnitudes of the pile bending moment and deflection although no limiting soil/pile pressure is observed to be exceeded in all predictions. Apart from the precision of measured test data, the reason may be due to the input soil strength values are based on the measured soil strength profile prior to tunnel excavation. Ong et al. (2004) reported that soil strength would be weakened upon stress relief caused by excavation and this resulted in reduced soil pressures acting on adjacent piles. As the ground unloading and large soil movement during tunnel excavation also cause stress relief in the soil, it is very likely that the soil at the pile location also experiences strength reduction to a certain extent and in turn results in smaller pile lateral responses. Nevertheless, from the above comparisons, it is evident that this reduction is not significant in the present study as the over-predictions are generally in the order of 10%.

Table 5.2 Measured and predicted maximum pile bending moment and deflection

Test No.		Maximum bending moment (2 days)	Maximum lateral deflection (2 days)	Maximum bending moment (720 days)	Maximum lateral deflection (720 days)
1	Measured	152 kNm	4.1 mm	213 kNm	8 mm
	Predicted	186 kNm	4.7 mm	241 kNm	6.1 mm
2	Measured	62 kNm	2 mm	93 kNm	3.9 mm
	Predicted	86 kNm	3.1 mm	116 kNm	3.7 mm
3	Measured	42 kNm	1 mm	46 kNm	1.9 mm
	Predicted	53 kNm	2.3 mm	60 kNm	2.5 mm
4	Measured	95 kNm	7 mm	124 kNm	10 mm
	Predicted	94 kNm	10.4 mm	129 kNm	12.5 mm
6	Measured	287 kNm	9.2 mm	350 kNm	16 mm
	Predicted	320 kNm	10 mm	385 kNm	12.5 mm

5.6.2 Pile settlement analysis

Poulos and Davis (1980) proposed an analytic solution for predicting pile settlement. The pile is considered to be a cylinder, of length L, shaft diameter d, and base diameter d_b. The soil is considered as an isotropic elastic half-space, having elastic parameter E_s and ν_s that are not influenced by the presence of the pile.

Only the pile base settlement analysis in this solution is adopted because the elastic shortening of piles in the present study is negligible, and the base loads can be measured in the tests. Therefore, by assuming the pile base is acted upon by a uniform vertical stress, the pile settlement due to elastic base soil deformation is expressed as:

$$\rho = \frac{PI}{E_s d_b} \tag{5.4}$$

where P = Applied load;

$I = I_0 R_k R_h R_{v;}$

I_0 = Settlement-influence factor;

R_k = Correction factor for pile compressibility;

R_v = Correction factor for soil Poisson's ratio;

R_h = Correction factor for finite depth of layer on a rigid base;

E_s = Young's modulus of soil;

d_b = Diameter of pile base.

As the short-term base load in the present study can be measured, $I_0 R_k R_v$ equals to 1, i.e. $PI_0 R_k R_v$ equals to the pile base load. However, as the clay boundary is very close to the rigid container base, the effect of finite depth of layer on a rigid base is considered based on the design charts (Figure 5.7) proposed by Poulos and Davis (1980). The

estimation of the Young's modulus of soil is identical to that described in Section 5.6.1. The d_b of the model square pile is determined to be 1.48 after being converted to the diameter of a circular pile with the equivalent base area.

The base load versus pile settlement derived from the above equation is plotted in Figure 5.8. It is noted that the measured pile settlement for Tests 1 to 6 generally agrees with the gradient of the predicted base load/settlement line. However, it is observed that the pile settlement in the tunnel collapsed case (Test 7) is almost 3 times of the predicted value. This is due to the fact that the ultimate pile base resistance ($9C_uA_b$ = 599 kN) has almost been fully mobilized in Test 7 as mentioned earlier. Therefore, the pile tip sinks deeply into the soil in order to mobilize this large base resistance. Moreover, as both the pile settlement and base load are significantly large in this test, the soil at the pile base is likely to be under a plastic or yield state, causing the large pile settlement.

On the other hand, it is noted that the base load/settlement line underestimates the pile settlement when the pile tip is located right above the tunnel crown. This is probably due to the base load has reached 42% of the estimated ultimate base load at the pile tip, whereby the base soil may exhibit some plastic behaviour at this stage, which leads to higher pile settlement than the elastic prediction. As such, it is noted that an elastic analysis may be adequate in analyzing the pile settlement in the present study when pile tips are embedded below or at the tunnel spring level under volume loss less than 4.2%, whereas when the pile tips are above tunnel spring level, an elastic solution may underestimate the pile settlement.

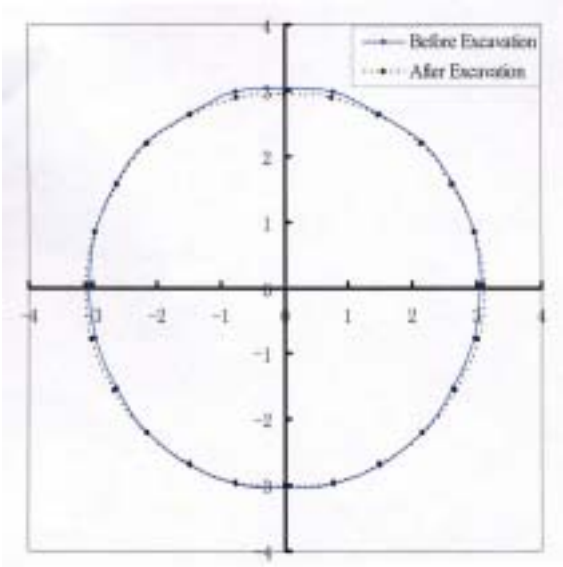

Figure 5.1 Lining deformation in sand (volume loss 3.53%, after Feng 2003)

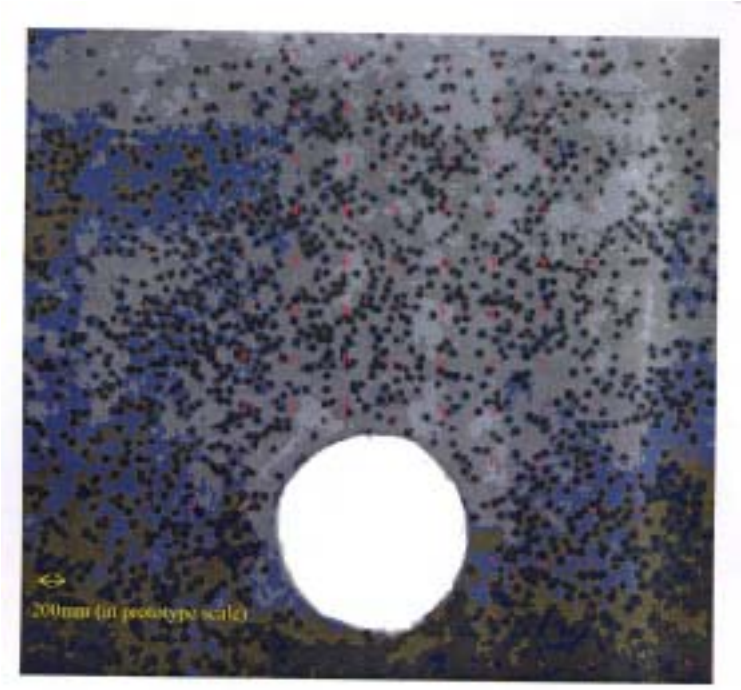

Figure 5.2 Subsurface soil movement in sand (after Feng 2003)

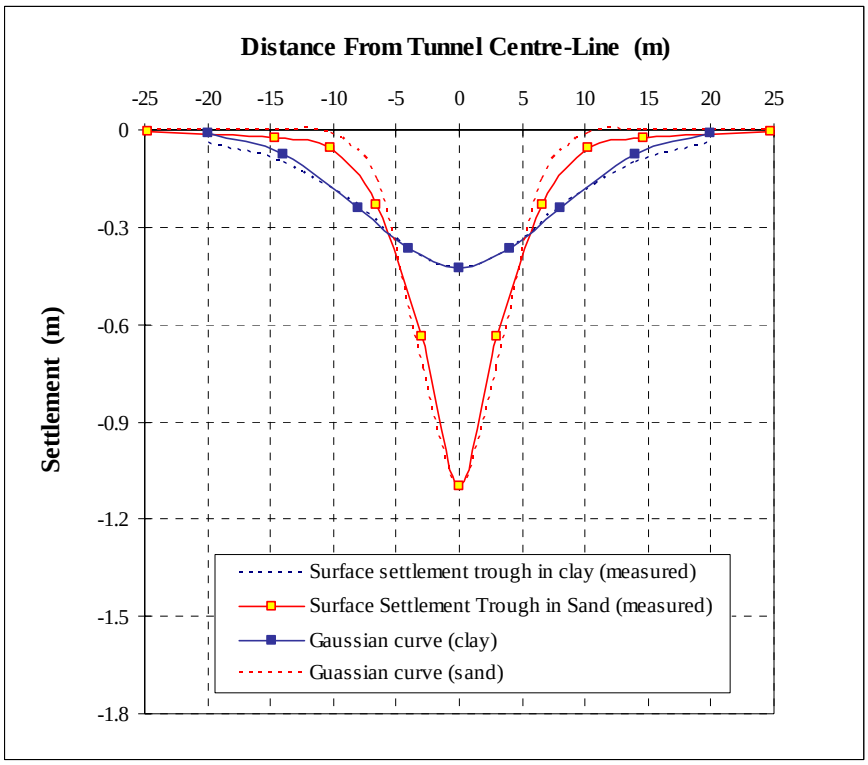

Figure 5.3 Comparisons of surface settlement troughs in sand and clay (Volume loss: sand 33%, clay 28.6% (Test 7))

Test	Test Layout	Parameters	Volume loss	Test	Test Layout	Parameters	Volume loss
Sand (collapse)	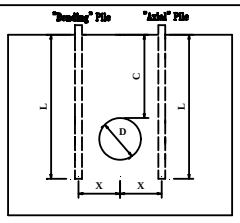	D = 6 m C = 13 m L = 25 m X = 5 m	33%	Sand (stable)	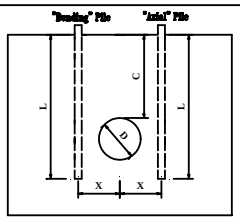	D = 6 m C = 13 m L = 25 m X = 9 m	1.02%
Clay (collapse)	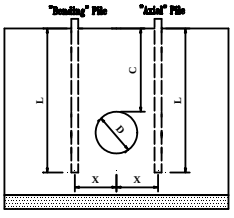	D = 6 m C = 12 m L = 23 m X =6 m	28.6%	Clay (stable)	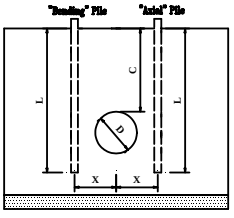	D = 6 m C = 12 m L = 23 m X = 9 m	1.86%

Figure 5.4 Configurations of the tests in Feng (2003) and the present study

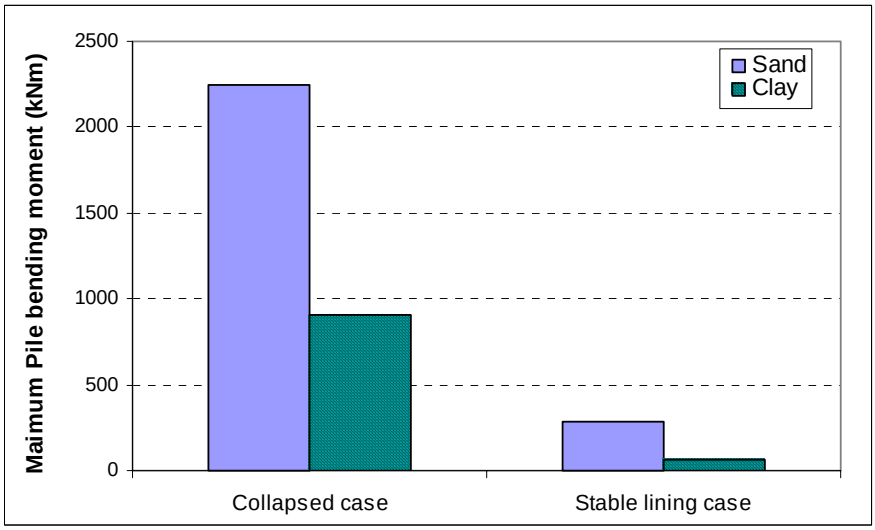

(a)

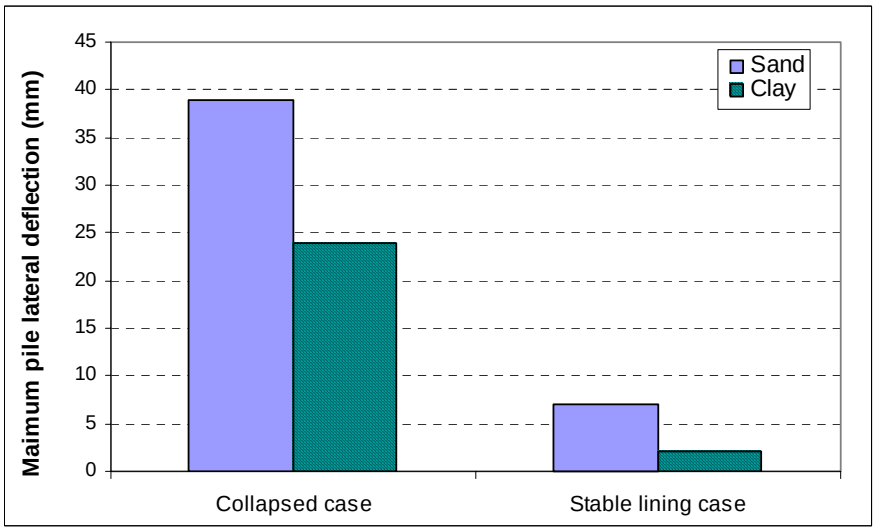

(b)

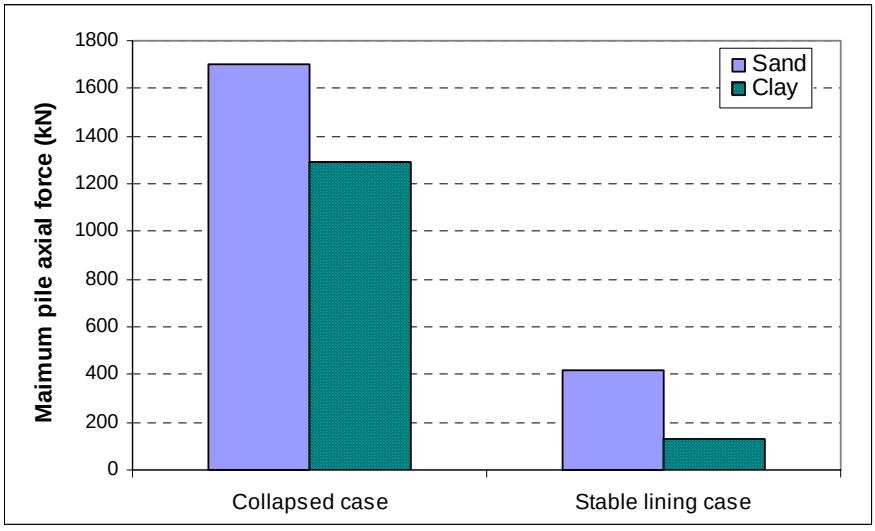

(c)

Figure 5.5 Comparisons of (a) maximum pile bending moment, (b) pile head deflection and (c) maximum pile axial force in sand and clay

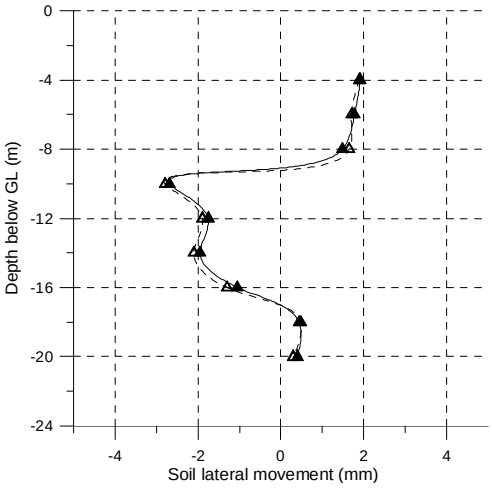

(Test 3)

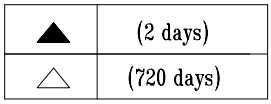

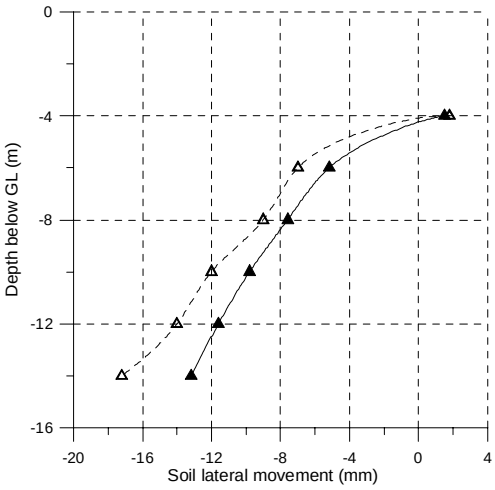

(Test 4)

(a)

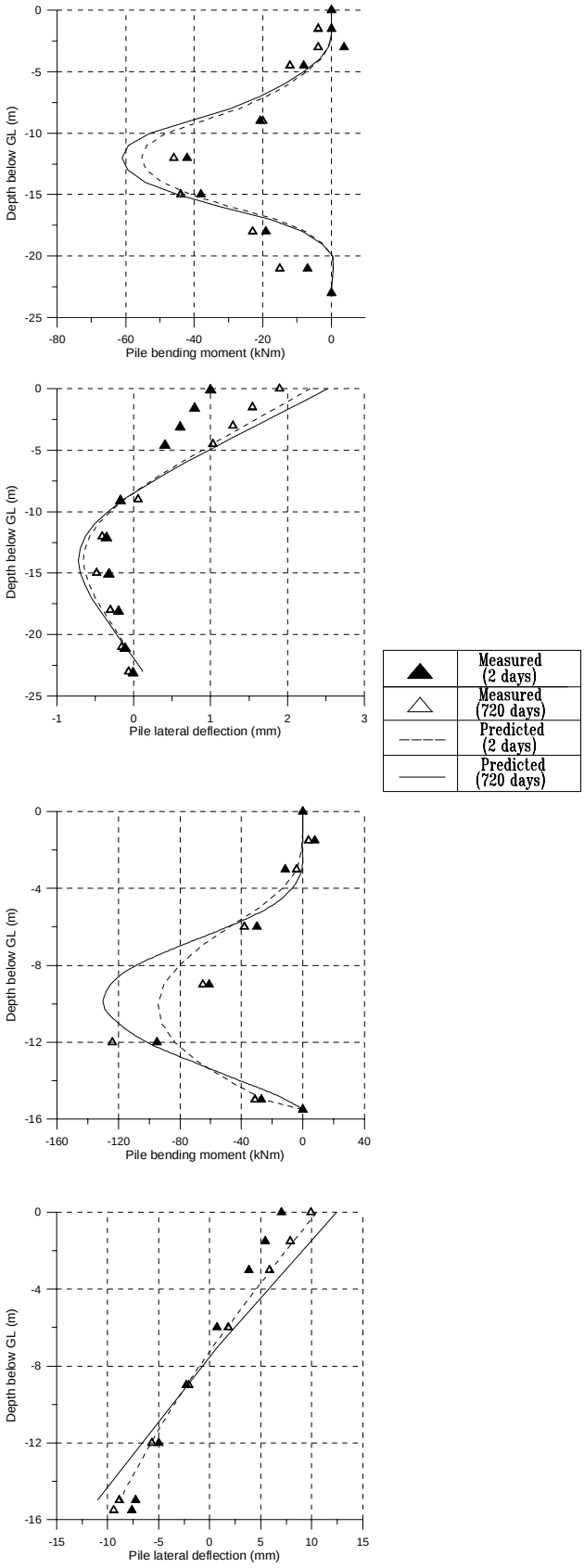

(b)

Figure 5.6 (a) Measured free-field soil lateral movement, (b) comparisons of measured and predicted pile bending moment and lateral deflection profiles (Tests 3 and 4)

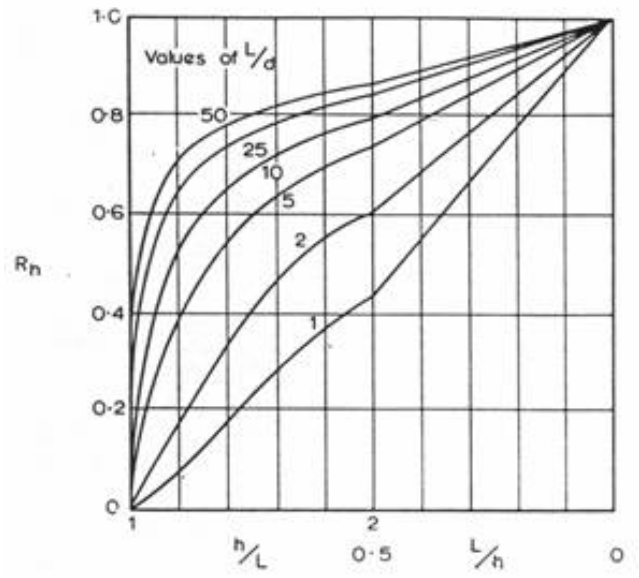

Figure 5.7 Correction factor R_h for finite depth of layer on a rigid base (Poulos and Davis, 1980)

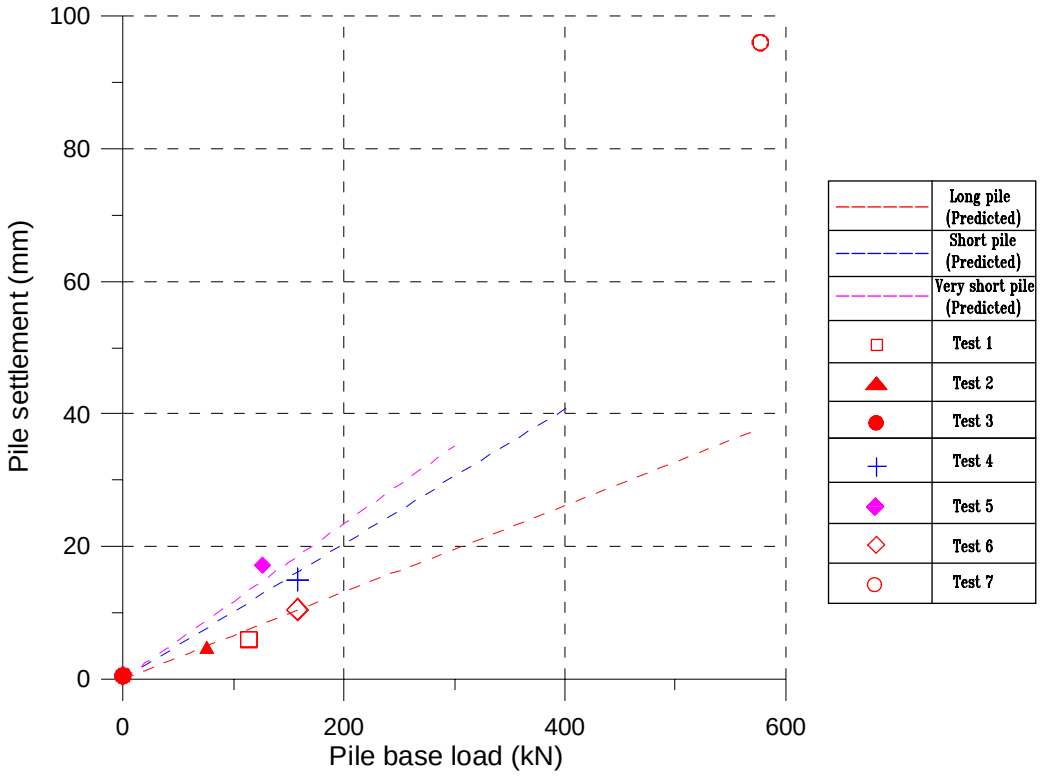

Figure 5.8 Measured pile settlement versus analytical prediction (Test 1 to 7)

CHAPTER SIX

CONCLUSIONS

Centrifuge model tests have been carried out to investigate tunnel excavation induced ground movements and its influence on an adjacent free-headed single pile in clay. Three test series have been performed in the present study to evaluate the effects of distance of pile from tunnel, pile length and ground loss on pile responses due to tunnel excavation. Test results in clay are then compared with previous tests done in sand using the same simulation technique of tunnel excavation. The measured pile lateral and axial responses due to tunnel excavation in the present study are back analyzed using an existing finite element program developed by Chow et al. (1996) and an analytical solution derived by Poulos and Davis (1980), respectively.

6.1 Concluding remarks

6.1.1 Tunnel excavation induced soil movement

Soil movement due to tunnel excavation in both stable tunnel lining and collapsed tunnel lining cases has been investigated. It is observed that for the tests with relatively stable tunnel lining, the tunnel crown settles, the spring expands, and the invert slightly heaves. As such, the tunnel deformation in the present study resembles the case of tunnel ovalisation reviewed in Chapter 2. Owing to the tunnel ovalisation, the soil near the tunnel spring moves away from the tunnel. Both the measured surface and subsurface soil settlement troughs can be reasonably represented by the classic Gaussian distribution. Furthermore, a wedge of active soil movement zone enveloped

by these settlement troughs above the tunnel crown can be identified and is consistent with the derived shear strain distribution in the soil. In the post-excavation period, both the subsurface and surface soil settlements continue to increase with time as a result of progressive lining deformation and dissipation of excess pore water pressure generated upon tunnel excavation. For the collapsed tunnel case, the tunnel lining deforms into a 'heart' shape which in turn results in a convergent soil movement profile towards the tunnel.

6.1.2 Long pile and short pile responses under a stable tunnel

The behaviours of a long pile and short pile under a stable tunnel have been studied. The test results reveal that both the maximum pile bending moment and axial force occur approximately at the tunnel spring elevation for long piles with tips below the tunnel. The pile lateral deflection profile exhibits a bow-shape with the largest deflection occurring at the pile head. The shape of pile lateral deflection is somewhat similar to the lateral soil movement profile at the pile location, revealing that the pile basically deforms together with the soil. A neutral plane at the tunnel spring level is noted. Above the neutral plane, the soil settles more than the pile and hence imposing negative skin friction. It is established that the development of induced pile lateral and vertical responses is time-dependent due to the progressive tunnel deformation and soil movements after tunnel excavation.

On the other hand, the test results reveal that the maximum bending moment of a short pile (tip at or above the tunnel spring) occurs slightly above the pile tip, while the axial force increases almost linearly along the pile shaft. Both induced maximum bending moment and axial force of a short pile are slightly lower than those of a long pile with

the same pile-to-tunnel distance. On the contrary, the lateral deflection and vertical settlement of a short pile are much more severe than those of a long pile.

6.1.3 Effect of pile-to-tunnel distance

Pile behaviours with pile-to-tunnel distance of 6m, 9m and 12m have been evaluated in the 1st series of tests. It is observed that the shape of the induced pile bending moment, lateral deflection and axial force profiles remains fairly constant for piles at various distances from the tunnel, showing the development of bending moment along the pile during tunnel excavation is similar irregardless of the distance. However, the pile bending moment, head deflection and axial force decrease exponentially with increasing pile-to-tunnel distance, while the pile vertical settlement and base load decrease almost linearly with the distance of pile from the tunnel. The induced pile responses are found to be insignificant when the pile-to-tunnel distance is larger than 1.5D at a volume loss of around 2% in the present study.

6.1.4 Effect of volume loss

Pile behaviours under three different tunnel volume losses (2%, 4.2% and 28.2%) have been studied. It is observed that the pile bends in opposite direction in the stable and collapsed lining cases due to the different lateral soil movement patterns in the two cases. However, the pile axial load profiles are found to be similar irrespective of volume loss. As expected, the induced pile responses increase with volume loss. The rates of increase in maximum pile bending moment, head deflection and axial force decreases with increasing volume loss, whereas the rate of increase in pile vertical settlement increases with increasing volume loss.

For the pile in collapsed tunnel case, the test results reveal that significant load and deformation can be imposed on the pile by the large soil movement induced by tunnel collapse. Both the induced shaft friction and base resistance of the pile are noted to be almost fully mobilized, while the induced maximum pile bending moment is critical and may cause structural failure of the piles.

6.1.5 Comparison with test results in sand

The test results in the present study have been compared with previous test results done in sand using the same simulation method of tunnel excavation. It is established that the lining stiffness required for the stability of sand around a tunnel is much lower than in clay probably due to the stronger arching effect of sand according to Zhou et al. (1998). Both lining deformations in sand and clay exhibit a horizontal ovalised shape. However, tunnel lining deformation is observed to be time-dependent in clay, whereas in sand the lining deformation remains essentially unchanged soon after tunnel excavation. The settlement troughs in sand and clay follows Gaussian distribution curve reasonably well. However, it is found the settlement trough in sand is considerably narrower than that in clay.

6.1.6 Comparisons with theoretical predictions

The experimental results have been back-analyzed with an existing finite element program and an analytical solution. It is found that the pile bending moment and lateral deflection profiles can be predicted reasonably well using the existing finite element program developed at the National University of Singapore. The pile settlement is back-analyzed using an analytical elastic solution proposed by Poulos and Davis (1980). It is found that the measured long pile and short pile settlements under

relatively small tunnel volume loss (less than 4.2%) basically agree with the elastic predictions. The measured settlement of a very short pile is slightly larger than the predicted value due to the soil plastic behavior under relatively large pile base load. The measured pile settlement in the tunnel collapsed case is almost 3 times of the predicted value because the pile base load has almost reached the ultimate base resistance and hence results in significant soil plastic behavior.

6.2 Recommendations for future study

As the present study is intended to investigate the soil movement and pile responses caused by an ovalised tunnel in clay and only free-headed single pile is studied due to the limited M.ENG. candidature period, recommendations for future research work are described below.

6.2.1 Modeling of tunnel excavation in the centrifuge

1. As the tunnel operation is virtually a 3-D problem, it would be highly desirable to develop a reliable 3-D modeling technique in the centrifuge to simulate progressive tunnel advancement and its effects on soil movement and pile responses.

2. As the tunnel contraction and ovalisation are the two basic forms of tunnel deformation and often coexist in the field, it would be desirable to compare the effects the two deformation patterns. This requires another tunnel modeling method to simulate tunnel contraction deformation patterns.

6.2.2 Model ground

As the normally consolidated clay used in the present study is relatively soft, it would be interesting to carry out tests with stiff clays to evaluate the effects of soil strength on tunnel induced soil movement and pile responses.

6.2.3 Pile conditions

1. As many pile heads are more or less restrained, it would be interesting to evaluate the behavior of a pile with pinned or fixed pile head.

2. As most pile foundations in service are subjected to axial loads transferred from superstructures, future study on behavior of a pile with working load would be desirable.

3. It would be useful to investigate the responses of pile groups due to tunnel excavation.

REFERENCES

Atkinson J.H., Orr T.L.L. and Potts D.M. (1975). Research studies into the behaviour of tunnels and tunnel linings in soft ground. A report to transport and road research laboratory department of the environment.

Attewell, P. B., Glossop, N. H. and Farmer, I. W. (1978). Ground deformations caused by tunneling in a silty alluvial clay. Ground Engineering, Vol. 11, No. 8, pp. 32-41.

Chen, L. T., Poulos, H. G. and Loganathan, N. (1999). Pile responses caused by tunneling. Journal of Geotechnical and Geoenvironmental Engineering, Vol. 125, No. 3, pp. 207-215

Cheng, C. Y. (2003). Finite element study of tunnel-soil-pile interaction. M Eng thesis submitted for examination, National University of Singapore.

Chow, Y. K. and Yong, K. Y. (1996). “Analysis of piles subject to lateral soil movements.” Journal of The Institution of Engineers, Singapore, Vol. 36, No. 2, pp. 43-49.

Clough, G. W. and Schmidt, B. (1981). Design and performance of excavations and tunnels in soft clay. In Soft Clay Engineering, Elsevier. Pp. 569-634.

Clough, G. W. and Leca, E. (1989). With focus on use of finite element methods for soft ground tunneling. Review paper in Tunnels et Micro-Tunnels en Terrain Meuble-

du Chantier à la Théorie. Presse de l'Ecole Nationale des Ponts et Chaussées, Paris, pp. 531-573.

Coutts, D. R. and Wang, J. (2000). Monitoring of reinforced concrete piles under horizontal and vertical loads due to tunneling. Tunnels and Underground Structures (eds. Zhao, Shirlaw & Krishnan), Balkema. pp. 465-473.

Dasari (2002) Analysis and ground movements due to tunneling, Tunneling workshop 2002, National University of Singapore

Doran S. R., Wood T., Tham S. K., Copsey J. P., J.N. Shirlaw and Wen D. (2000) The assessment of limits for the movement of subway tunnels and trackwork due to adjacent construction. Tunnels and Underground Structures, Zhao, Shirlaw & Krishnan (eds), 2000 Balkema, pp.495-500.

Dyer, M. R., Hutchinson, M. T. and Evans, N. (1996). Sudden Valley Sewer: a case history. Proc. Int. Symposium on Geotechnical Aspects of Underground Construction in Soft Ground, London (eds. R. J. Mair and R. N. Taylor), Balkema, pp. 671-676.

Feng, S. H. (2003). Centrifuge modeling of tunnel-pile interaction. M Eng thesis submitted for examination, National University of Singapore.

George (1981). Lost-ground subsidence in two shallow tunnels, Soft-Ground Tunneling, Failures and Displacement.

Grant, R. J. and Taylor, R. N. (2000). Tunneling-induced ground movements in clay. Geotechnical Engineering, Proc. Institutions of Civil Engineers, Vol. 143, No. 1, pp. 43-55.

Gunn, M. J. (1993). The prediction of surface settlement profiles due to tunneling. Predictive Soil Mechanics, Proc. Wroth Memorial Symposium, Oxford 1992, Thomas Telford, pp. 304-316.

Hegarden, H. J. A. M., van der Poel, T. J. and van der Schrier, J. S. (1996). Ground movements due to tunneling: influence on pile foundations. Proc. Int. Symposium on Geotechnical Aspects of Underground Construction in Soft Ground, London (eds. R. J. Mair and R. N. Taylor), Balkema, pp. 519-524.

Jacobsz, S. W., Standing, J. R., Mair, R. J., Soga, K., Hagiwara, T. and Sugiyama, T. (2001). The effects of tunneling near single driven piles in dry sand. Proc. of Asian Regional Conf. on Geotechnical Aspects of Underground Construction in Soft Ground, Tongji University Press, Shanghai, pp. 29-35.

Kuwano J., Taylor R. N. and Grant R. J. (1998). Modeling of deformations around tunnels in clay reinforced by soil nails. Proceeding of Centrifuge 98, 1998, Rotterdam.

Kongpathomporn. C (2002). Long-term Behavior of Flexible Tunnel due to Downward Hydraulic Gradient in Clay. Master thesis, Tokyo Institute of Technology.

Lake, L. M., Rankin, W. J. and Hawley, J. (1992). Prediction and effects of ground movements caused by tunneling in soft ground beneath urban areas. CIRIA Project Report 30, Construction Industry Research and Information Association, London.

Lee, K. M., Rowe, R. K. and Lo, K. Y. (1992). Subsidence due to tunneling: Part I – Estimating the gap parameter. Canadian Geotechnical Journal, Vol. 29, No. 5, pp. 929-940.

Lee, R. G., Turner, A. J. and Whitworth, L. J. (1994). Deformations cased by tunneling beneath a piled structure. Proc. XIII Int. Conf. Soil Mechanics and Foundation Engineering., New Delhi, Vol. 2, pp.873-878.

Lee, S. W. (2002). The use of compensation grouting in tunneling: a case study. Geotechnical Engineering, Vol. 155, Issue 2, pp. 101-109.

Loganathan, N. and Poulos, H. G. (1998). Analytical prediction for tunneling-induced ground movements in clays. Journal of Geotechnical and Geoenviromental Engineering, Vol. 124, No. 9, pp. 846-856.

Loganathan, N. (1999). The effect of tunneling-induced soil movements on pile foundation. PhD Thesis, University of Western Australia.

Loganathan, N., Poulos, H. G. and Stewart, D. P. (2000). Centrifuge model testing of tunneling induced ground and pile deformations. Geotechnique, Vol. 50, No. 3, 283-294.

Mair, R. J. (1979). Centrifugal modeling of tunneling construction in soft clay. PhD Thesis, University of Cambridge.

Mair, R. J. (1992). Developments in geotechnical engineering research: application to tunnels and deep excavation, Unwin Memorial Lecture 1992. Proc. Institution of Civil Engineers and Civil Engineering, Vol. 93, pp. 27-41.

Mair, R. J., Taylor, R. N. and Bracegirdle, A. (1993). Subsurface settlement profiles above tunnels in clay. Geotechnique, Vol. 43, No. 2, pp. 315-320.

Mair, R.J. and Taylor R.N. (1997). Bored tunnelling in the urban environment. State-of-the-art Report and Theme Lecture, Proceedings of 14th International Conference on Soil Mechanics and Foundation Engineering, Hamburg, Balkema, Vol.4., 2353-2385

Moh, Z-C., Ju, D. H. and Hwang, R. N. (1996). Ground movements around tunnels in soft ground. Proc. Int. Symposium on Geotechnical Aspects of Underground Construction in Soft Ground, London (eds. R. J. Mair and R. N. Taylor), Balkema, pp. 725-730.

Morton, J. D. and King, K. H., (1979). Effect of tunneling on the bearing capacity of and settlement of piled foundations. Proc. Tunneling ’79, (ed. M. J. Jones), pp. 57-58. London: IMM

Mroueh, H. and Shahrour, I. (2002). Three-dimensional finite element analysis of the interaction between tunneling and pile foundations. Int. Journal for Numerical and Analytical Methods in Geomechanics., Vol. 26, pp. 217-230.

O'Reilly, M. P. and New, B.M. (1982). Settlements above tunnels in the United Kindom – their magnitude and prediction. Tunneling 82, London, IMM, pp 173-181.

Ou, C. Y., Liao, J. T. and Cheng, W. L. (2000). "Building response and ground movements induced by a deep excavation". Geotechnique, Vol. 50, No. 3, pp 209-220.

Poulos, H. G. and Davis E. H. (1980). Pile foundation analysis and design. John Wiley & Sons.

Panet, M. and Guenot, A., (1982). Analysis of convergence behind the face of a tunnel. Proc. Tunnelling 82, Institution of Mining and Metallurgy, London, pp. 197-204.

Peck, R. B. (1969). Deep excavations and tunneling in soft ground. Proc. 7th International Conference Soil Mechanics and Foundation Engineering, Mexico City, State of the Art Volume, pp. 225-290.

Potts, D. M. (1976). Behaviour of lined and unlined tunnels in sand. phD Thesis, University of Cambridge.

Rankin, W. J. (1988). Ground movements resulting from urban tunneling; prediction and effects. Conference on Engineering Geology of Underground Movements, Nottingham. BGS.

Rowe, R. K. and Lee, J. M. (1992). Subsidence due to tunneling: Part II – evaluation of a prediction technique. Canadian Geotechnical Journal, Vol. 29, No. 5, pp. 941-954.

Rowe, R. K., Lo, K. Y. and Kack, G. J. (1983). A method of estimating surface settlement above tunnels constructed in soft ground. Canadian Geotechnical Journal, Vol. 20, No. 8, pp. 11-22.

Schmidt, B. (1989). Consolidation settlements due to soft ground tunneling, 12th International Conference on Soil Mechanics and Foundation Engineering, Rio. Vol. 2, pp. 797-800.

Sharma, J. S., Bolton, M. D. and Boyle. R. E. (2001). A new technique for simulation of tunnel excavation in a centrifuge. Geotechnical Testing Journal, Vol. 24, No. 4, pp. 343-349.

Shirlaw, J. N. (1995) Observed and calculated pore pressures and deformations induced by an earth pressure balance shield: Discussion. Canadian Geotechinical Journal. Vol. 32, pp. 181-189.

Skempton, A. W. (1951). The bearing capacity of clays. Building. Res. Congress, London. Inst. Civ. Engrs., div. I: 180.

Simpson, B., O, Riordan, N. J. and Croft, D. D. (1979). A computer model for the analysis of ground movements in London clay. Geotechnique, Vol. 29, No. 2, pp 149-175.

Simpson, B., Atkinson, J. H. and Jovicic, V. (1996). The influence of anisotropy on calculations of ground settlements above tunnels. Proc. Int. Symposium on Geotechnical Aspects of Underground Construction in Soft Ground, London (eds. R. J. Mair and R. N. Taylor), Balkema, pp. 591-594.

Strack, O.E. and Verruijt A. A complex variable solution for the ovalization of a circular tunnel in an elastic half-plane. GeoEng 2000: An International Conference on Geotechnical & Geological Engineering, November 19-24, 2000, Melbourne Australia.

Taylor, R. N. (1995). Tunneling in soft ground in the UK. Underground Construction in Soft Ground (eds. K. Fujita and O. Kusakabe), Balkema, pp. 123-126.

Teh, C. I. and Wong, K. S. (1995). Analysis of downdrag on pile groups. Geotechnique, Vol. 45, No. 2, pp. 191-207.

Teunissen, E. A. H. and Hutteman, M. (1998). Pile and surface settlements at full scale tests North/South metro line Amsterdam. Tunnels and Metropolises (eds. Negro Jr. and Ferreira), Balkema, Rotterdam.

Tham, K. S. and Deutscher, M. S. (2000). Tunnelling under Woodleigh Workers' Quarters on Contract 705. Tunnels and Underground Structures (eds. Zhao, Shirlaw and Krishnan), Balkema.

Verrujit, A. and Booker, J. R. (1996). Surface settlements due to deformation of a tunnel in an elastic half plane. Geotechnique, Vol. 46, No. 4, pp. 753-756.

Verrujit, A. and Booker, J. R. (1998). Discussion: Surface settlements due to deformation of a tunnel in an elastic half plane. Geotechnique, Vol. 48, No. 5, pp. 709-713.

Verrujit, A. and Booker, J. R. (2000). Complex variable analysis of Mindlin's tunnel problem. Proceedings of the Developments in Theoretical Geomechanics, 2000, pp. 3-22.

Vijiayvergiya, V. N., Focht, J. A. Jr. (1972). A new way to predict the capacity of piles in clay. 4th Annual Offshore Tech. Conf., Houston, Vol. 2: 865-874.

Yann Leblais and Alain Bochon (1991). Villejust Tunnel: Slurry shield effects on soil and lining behaviour and comments on monitoring requirement. Tunneling' 91, 1991.

Yashuhiro Katoh, Michio Miyake and Masato Wada (1998). Ground deformation around shield tunnel. Proceeding of Centrifuge 98, 1998, Rotterdam.